Elsevier Editorial System(tm) for Energy Conversion and Management

Manuscript Draft

Manuscript Number: ECM-D-18-03419R1

Title: Valve Timing Optimisation of a Spark Ignition Engine with Skip Cycle Strategy

Article Type: Original research paper

Section/Category: 5. Fuels, Combustion, and Chemical Processes

Keywords: skip cycle, variable valve timing, fuel economy, unburned hydrocarbon, nitrogen oxide.

Corresponding Author: Dr. Ranga Dinesh,

Corresponding Author's Institution: University of Southampton

First Author: B Dogru

Order of Authors: B Dogru; R Lot; Ranga Dinesh

Abstract: Skip cycle strategy (SCS) is a stroke volume modulation method leading to reduction in pumping loss through deactivation of engine valves under part-load conditions. Although SCS achieves a significant fuel economy, it increases regulated pollutant emissions such as nitrogen oxide and unburned hydrocarbon in comparison to normal 4-cycle engine operation. This paper investigated normal cycle strategy, skip cycle strategy as well as combination of skip cycle strategy and variable valve timing strategy for a spark-ignition engine using one-dimensional numerical model. The skip cycle engine was modelled at several steady-state operation points and then optimised at best ignition timing providing maximum brake torque at each simulation case. The numerical results obtained for both normal cycle and skip cycle have been validated against the experimental data. After completing the validation of numerical results with engine test bench data for both normal and skip cycle operations, optimisation of intake and exhaust valve timing profiles have been carried out regarding advancing or retarding camshaft relatively to the crankshaft position. In case of SCS and variable valve timing application together, NOx concentration was reduced by 35.1%, 39.4%, 26.8% and HC emission was reduced by 54.9%, 49.3% and 47.4% on average for brake mean effective pressure load levels of 1, 2 and 3 bar respectively at all among engine speed ranges between 1200 and 1800 rpm compared to stand alone SCS strategy. Furthermore, no remarkable additional brake specific fuel consumption was observed for SCS plus variable valve timing strategy compared to stand alone SCS.

Cover letter

Dr. K. K. J. Ranga Dinesh

Energy Technology Research Group

Faculty of Engineering and the Environment

University of Southampton

Southampton, SO17 1BJ, UK.

Dear Editor,

Please find enclosed the Revised Paper, titled **"Valve Timing Optimisation of a Spark Ignition Engine with Skip Cycle Strategy"** by B. Dogru, R. Lot and K.K.J. Ranga Dinesh. This paper is an original research paper based on the work carried out by the first author leading to investigate **performance and emissions of spark ignition engines** and it has not been submitted to other journals.

Sincerely,

K.K.J. Ranga Dinesh

July 2018

Highlights

- SI engine emissions issue of skip cycle strategy is investigated.
- 1-D numerical results are validated with the experimental data.
- Two variable valve timing strategies are proposed.
- Optimal intake and exhaust valve timings are integrated into the skip cycle model.
- VVT and SCS combination offers significant reduction of NOx and HC.

Valve Timing Optimisation of a Spark Ignition Engine with Skip Cycle Strategy

B. Dogru, R. Lot, K.K.J. Ranga Dinesh*

*Corresponding Author, Energy Technology Research group, Faculty of Engineering and the Environment, University of Southampton, Southampton, SO17 1BJ, UK.

Phone: +44 (0)23 8059 2872, email: dinesh.kahanda-koralage@soton.ac.uk

Abstract

Skip cycle strategy (SCS) is a stroke volume modulation method leading to reduction in pumping loss through deactivation of engine valves under part-load conditions. Although SCS achieves a significant fuel economy, it increases regulated pollutant emissions such as nitrogen oxide and unburned hydrocarbon in comparison to normal 4-cycle engine operation. This paper investigated normal cycle strategy, skip cycle strategy as well as combination of skip cycle strategy and variable valve timing strategy for a spark-ignition engine using one-dimensional numerical model. The skip cycle engine was modelled at several steady-state operation points and then optimised at best ignition timing providing maximum brake torque at each simulation case. The numerical results obtained for both normal cycle and skip cycle have been validated against the experimental data. After completing the validation of numerical results with engine test bench data for both normal and skip cycle operations, optimisation of intake and exhaust valve timing profiles have been carried out regarding advancing or retarding camshaft relatively to the crankshaft position. In case of SCS and variable valve timing application together, NO_x concentration was reduced by 35.1%, 39.4%, 26.8% and HC emission was reduced by 54.9%, 49.3% and 47.4% on average for brake mean effective pressure load levels of 1, 2 and 3 bar respectively at all among engine speed ranges between 1200 and 1800 rpm

compared to stand alone SCS strategy. Furthermore, no remarkable additional brake specific fuel consumption was observed for SCS plus variable valve timing strategy compared to stand alone SCS.

Keywords: skip cycle, variable valve timing, fuel economy, unburned hydrocarbon, nitrogen oxide.

1. Introduction

High gas exchange losses and low volumetric efficiency are the main problems effective on fuel consumption and pollutant emissions under urban traffic conditions of spark ignition (SI) engines in which load is conventionally controlled by throttle valve employed between air filter and intake manifold. Due to less fresh charge requirement and the airflow restriction by closer throttle valve position, SI engines are forced to do much more gas exchange work in addition to less power production under part-load conditions [1]. This issue causes poor combustion quality, insufficient combustion speed, and also unexpected further fuel consumption with regards to excessive low indicated efficiency during power cycle at part-load condtions compared to high-lead conditions [2]. In addition, road transport emissions are shown the main source of air pollution and aimed to keep under control by several legislations, policies and regulations [3] (e.g. European Union Directives and Regulations on Motor Vehicles) to ensure a high level environmental protection. In order for adaptation of Euro 6 emission standards to passenger cars and light commercial vehicles in a real driving emission (RDE) test procedure, a new regulation [4] has been reported recently to reflect vehicle emissions along a total trip including urban, rural and motorway route segments better than laboratory testing.

Since all reasons described above, instead of conventional load control based on just throttle valve position, alternative SI engine load control technologies such as variable valve timing (VVT), variable valve lift (VVL), camless engine valve control (CEVC), fuel stratification, turbocharging (or supercharging) and stroke volume modulation strategies have been investigated for two decades to manufacture environment friendly vehicles with a better fuel economy [5]. Thanks to electronic engine control management (EECM) systems which have recently become an essential factor for gasoline engines to perform high engine efficiency and low exhaust emissions while satisfying in driving comfort and road holding issues, these high technology and complex engine solutions are widely used in most of the gasoline engine market [6].

Variable valve timing options such as earlier or later valve opening-closing than default valve profile in terms of rotating camshaft back or forward relatively to the crankshaft, shifting valve duration or valve lifting are very effective on fuel consumption over reducing pumping losses and pollutant emissions over changing in-cylinder states such as pressure and averaged temperature [7-15].

The opinion of camless engines in terms of eliminating camshaft and timing belt allowing valve control by electromagnetic or pneumatic actuators has been afforded for a short time past [16-18]. In this camless concept, an electronically controlled solenoid system allows a fully flexible valve actuation, valve duration shifting and lift adjustment depending on cyclic load and crankshaft speed levels. Although a few engine research and development companies have been working on camless engine prototype experimentation on test bench [19-21], no mass car production has been

presented into market yet due to lack of expected valve activation sensitivity, noise and electrical safety problems.

Fuel stratification method enables a wider throttle valve area and less fuel consumption by supplying a rich mixture near spark plug and a very lean mixture at other regions of combustion chamber [22-26]. Turbocharging and supercharging meet same power requirement with a smaller engine displacement (i.e. engine downsizing) so it offers a better fuel economy and reduced friction losses [27-32]. Stroke volume modulation strategy can be categorised into three groups such as cylinder deactivation (cylinder cut-off), skip fire and skip cycle strategies. Cylinder deactivation can be applied for a cylinder or a group of cylinders permanently during desired operation conditions either by deactivation of intake and exhaust valves to reduce the active stroke volume allowing a reduction in pumping losses as well as heat transfer losses under part-load conditions [33]. A few recent studies have also been reported deactivating a cylinder by means of valve deactivation and combination of spark cut-off and fuel cut-off [34-37]. Skip fire strategy is based on just cutting spark fire in order to deactivate a cylinder depending on driver torque demand [38-39] or skip a power cycle with both ignition and injection disabling [40-42].

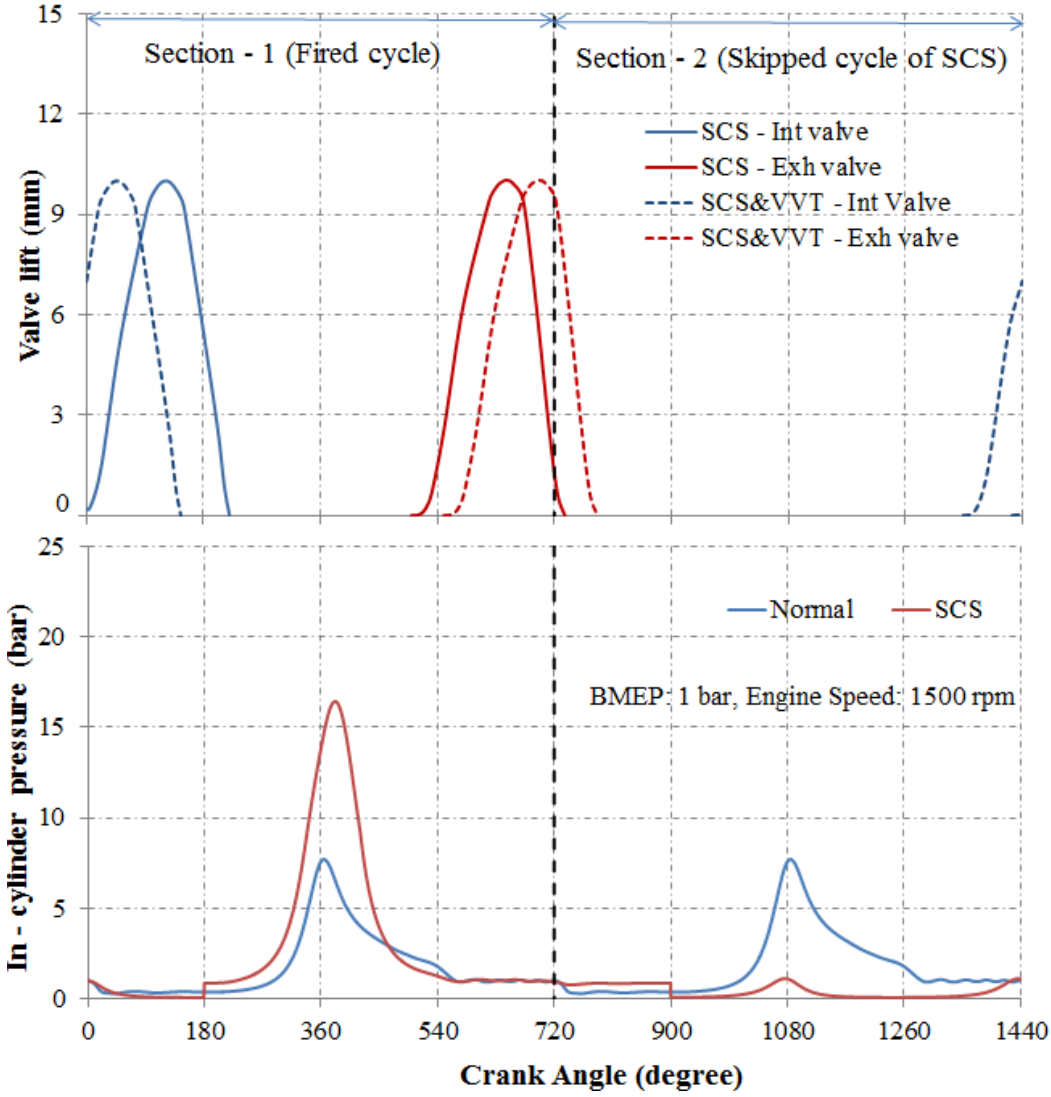

Figure 1. Representation of SCS and proposed further VVT strategies at BMEP: 1 bar and 1500 rpm

Skip cycle strategy (SCS) is another type of stroke volume modulation strategy to vary the power frequency of SI engines under part-load operation conditions [43]. This technique is based on a principle in which valve engagement, fuel supply and spark arc are disabled in several cycles to reduce pumping (throttling) losses therefore to achieve an equivalent power level. In this technique, the fresh charge is increased in sequential cycle as seen in fired cycle section of Fig. 1. However, in contrast to part-load conditions, SCS is not expected to play a major role on fuel

economy at full-load conditions due to lower pumping losses and higher volumetric efficiency as a result of wide open throttle (WOT).

Possible combination selections from among the methods mentioned above could present various advantages in order to overcome efficiency problem of SI engines. The one possible combination studied in the literature was VVT and supercharging combination [44-46]. A few studies were also reported for VVT and cylinder deactivation combination [47, 48]. Other combinations investigated were: supercharging with stratified charge mixture [49]; supercharging with VVT and VVL [50]; cylinder deactivation, VVT and VVL with stratified charge [51]. A recent study reported a camless fully flexible electromagnetic valve train system (without a mechanical valve deactivation) combined with a skip cycle approach with optimum valve timing and lift adjustments to reduce pumping losses [52].

However, combined effect of mechanical skip cycle and variable valve actuation on SI engine performance and emissions has not been investigated so far. Previously, the authors have presented a self-developed novel skip cycle mechanism which has been manufactured to engage or disengage the intake and exhaust poppet valves [53]. Despite achieving significant fuel saving under part-load operation conditions in this experimental SCS investigation, nitrogen oxide (NO_x) concentration could increase due to higher fresh charge and averaged cylinder temperature rise as observed in [54-56], hydrocarbon (HC) emissions in terms of incomplete combustion products could also increase due to undesired oil suction from crankcase to cylinder as mentioned in [57-60], flame quenching on cylinder wall as discussed in [61-63], and deposit of unburned mixtures in crevice cylinder volumes such as piston liner,

valve seat and spark plug thread as discussed in [64-66] in comparison to normal (N) 4-cycle engine operation.

The objective of the present study is to mitigate the unfavourable exhaust gas emissions of a skip cycle SI engine under part-load conditions. Two variable valve timing strategies (EIVO: early intake valve opening, LEVO: late exhaust valve opening) along with skip cycle strategy are investigated for an SI engine using a one-dimensional simulation model. Firstly, the skip cycle strategy was modelled and ignition timing was optimised based on minimum spark advance for maximum brake torque (MBT) at 15 steady-state simulation points including low load (break mean effective pressure, BMEP: 1-2-3 bar) and low engine speed (1200-1350-1500-1650-1800 rpm) ranges. Secondly, the simulation results for both normal engine and SCS were verified with the experimental data for a four cylinder water-cooled naturally aspirated SI engine with 1.8 litre stroke volume and stoichiometric air-fuel ratio (AFR=14.6) in which SCS was carried out. Then intake valve timing and exhaust valve timing were optimised and integrated into the model in a way that the valve duration and the valve lift are kept default in the engine configuration. The comparative results regarding engine performance and engine-out emissions will be presented for normal operation, SCS and SCS with variable valve timing (SCS&VVT) strategies. The findings of this study will help to identify the advantage of combining skip cycle strategy with variable valve timing in achieving lower engine exhaust emissions with better fuel economy.

2. Numerical model architecture

Simulation of normal engine operation and proposed skip cycle strategy was carried out using a one dimensional Ricardo Wave gas dynamics analysis software. Software library is based on physical principles of “Mean Value Model” which assumes all processes and effects are spread out over the engine cycle, all boundary conditions at the beginning of an engine cycle are fixed and the same initial starting conditions are exposed [67]. In order to build up base engine model, predictive engine parameters such as throttle valve position, burning duration (BDUR) and 50% fuel mass burned (CA50) are used to estimate the engine performance at several low BMEP load levels and engine speed ranges. BDUR is rapid burning angle as a crank interval required to burn the bulk of mixture charge and CA50 corresponds to crankshaft angle where half of fuel heat is released due to the combustion. Both are very important for representing combustion curve characteristics [1]. The pre-validation process showed that predicted CA50, BDUR and throttle valve angles using for combustion model calculation are very compatible to experimental test bench data. The nominal engine features at full load condition are given in Table 1.

Table 1. Nominal engine specifications at full load condition

Feature	Value
Displacement	1820 cc
Number of cylinders	4 (in-line)
Bore×Stroke	85×80 mm
Compression ratio	9:1
AFR (Air-fuel ratio)	14.6

Power	27.3 kW@2400 rpm
Torque	108.7 Nm@1600 rpm
BMEP	7.5 bar
Timing of IVO (intake valve opening)	16°CA BTDC
Timing of EVO (exhaust valve opening)	40°CA BBDC
Valve duration	236°CA (for both intake and exhaust)

Modelling of skip cycle strategy needs a full valve deactivation for the skipped cycle and higher fresh mixture for the fired cycle of two sequential cycles (Fig. 1). In this study, a new approach consisting of a fired (F) cycle and a skipped cycle (S) is applied into the simulation model to reflect a “Net Power Cycle” definition derived from these two cycles in order to allow an equivalent power level with a normal (N) operation cycle. Since more fresh charge is inducted to the engine in fired section of two sequential cycles, throttle valve must be opened wider and spark timing must be adjusted closer to compression top dead centre (TDC) due to having a higher cylinder compression pressure and a better flame development. A wider throttle valve position provides a decrease in pumping losses and fuel consumption. In calculation of net power cycle, net cycle power is obtained with extraction of fired cycle power from skipped cycle power (Eq.1). The indicating parameters such as GMEP (gross mean effective pressure) and IMEP (indicated mean effective pressure) are calculated as an average cycle value (Eq. 2 and Eq. 3) to represent a virtual cycle giving target power demand. The net power cycle concept is also referred in experimental data calculations. The equations used for a “Net Power Cycle” are described as following (Eq.1-6):

$$Power_{net} = Power_{cycle-F} - Power_{cycle-S} \quad (1)$$

$$GMEP_{net} = \left(GMEP_{cycle-F} - GMEP_{cycle-S}\right)/2 \quad (2)$$

$$IMEP_{net} = \left(IMEP_{cycle-F} - IMEP_{cycle-S}\right)/2 \quad (3)$$

$$PMEP_{net} = GMEP_{net} - IMEP_{net} \quad (4)$$

$$BMEP_{net} = \frac{1200 \times Power_{net}}{V_h \times n} \quad (5)$$

$$FMEP_{net} = BMEP_{net} - IMEP_{net} \quad (6)$$

where $GMEP_{net}$ (bar) is net gross mean effective pressure, $IMEP_{net}$ (bar) is net indicated mean effective pressure, $PMEP_{net}$ (bar) is net pumping mean effective pressure, V_h (litre) cylinder displacement, n (1/sec) is crankshaft revolution per minute and $FMEP_{net}$ (bar) is net frictional mean effective pressure.

The modelling framework consists of time-dependent governing equations involving the simultaneous of the flow in a duct configuration. By assuming flow varies only in stream wise direction (x-direction), the governing conversation equations of mass (Eq.7), energy (Eq.8) and momentum (Eq.9) of unsteady compressible fluid motion can be written as follows [68]:

$$\frac{\partial \rho}{\partial t} + \frac{\partial}{\partial x}(\rho u_x) = 0 \quad (7)$$

$$\frac{\partial}{\partial t}[\rho h] + \frac{\partial}{\partial x}[\rho u_x h] = \frac{\partial p}{\partial t} + u_x \frac{\partial p}{\partial x} + \tau_{xx} \frac{\partial u_x}{\partial x} - \frac{\partial q_x}{\partial x} + \dot{Q} + \dot{W}_{ext} \quad (8)$$

$$u_x \frac{\partial}{\partial x}[\rho u_x] + \frac{\partial}{\partial t}[\rho u_x] = -\frac{\partial p}{\partial x} + \frac{2}{3}\mu\left(2\frac{\partial^2 u_x}{\partial x^2}\right) \quad (9)$$

where ρ (kg/m^3) is fluid density, t (sec) is time, u_x (m/s) is averaged axial velocity, h (J/kg) is enthalpy, p (N/m^2) is pressure, τ_{xx} (N/m^2) is viscous shear stress, q_x (J/m^{2}s) is heat flux, $\dot{Q}$ (J/s) is heat source, $\dot{W_{ext}}$ (J/s) is external work and μ (kg/ms) is dynamic viscosity.

The equations are spatially discretised using a second order finite difference method and the time integration is based on the first order explicit method. The mass equation accounts for changes of in-cylinder mass due to flow through valves and due to fuel injection. The energy equation is based on the first law of thermodynamics and equates the change of internal energy of in-cylinder gases to the sum of enthalpy fluxes in and out of the chamber, heat transfer, and piston work [69].

Since combustion occurs through a flame propagation process, the changes in gas temperature, pressure and density require a separated gas approach in the combustion chamber as burned and unburned regions [1]. The two-zone model is used to capture more details about the chemical processes taking place during the combustion period. Hence, all the sub-models (combustion model, heat transfer model and emission models) are performed by two zones assumption which the mixture is conceptually divided into burned and unburned zones.

Based on mean value model approach, Net Power Cycle definition, time dependent fluid governing equations and separated two-zones gas approach described above , each engine component is modelled by simulation elements such as orifices (joints linking two ducts), throttle valve, ambient (flow termination for intake and exhaust), engine valves, engine cylinders, ducts (connecting orifices or junctions) and Y–junctions (using for modelling spherical volumes representing a compatible geometry with original engine dimensions and configuration). In the proposed simulation; 75 ducts, 38 orifices and 23 Y-junctions are used to discretize large single volume geometry into sub-volumes to show the pulsed characteristics of fluid propagation better than constant as in mean value models [70]. Moreover, 4 injectors, 8 engine

valves, 1 throttle valve, 2 ambients and 4 engine cylinders are integrated into the model (Fig. 2).

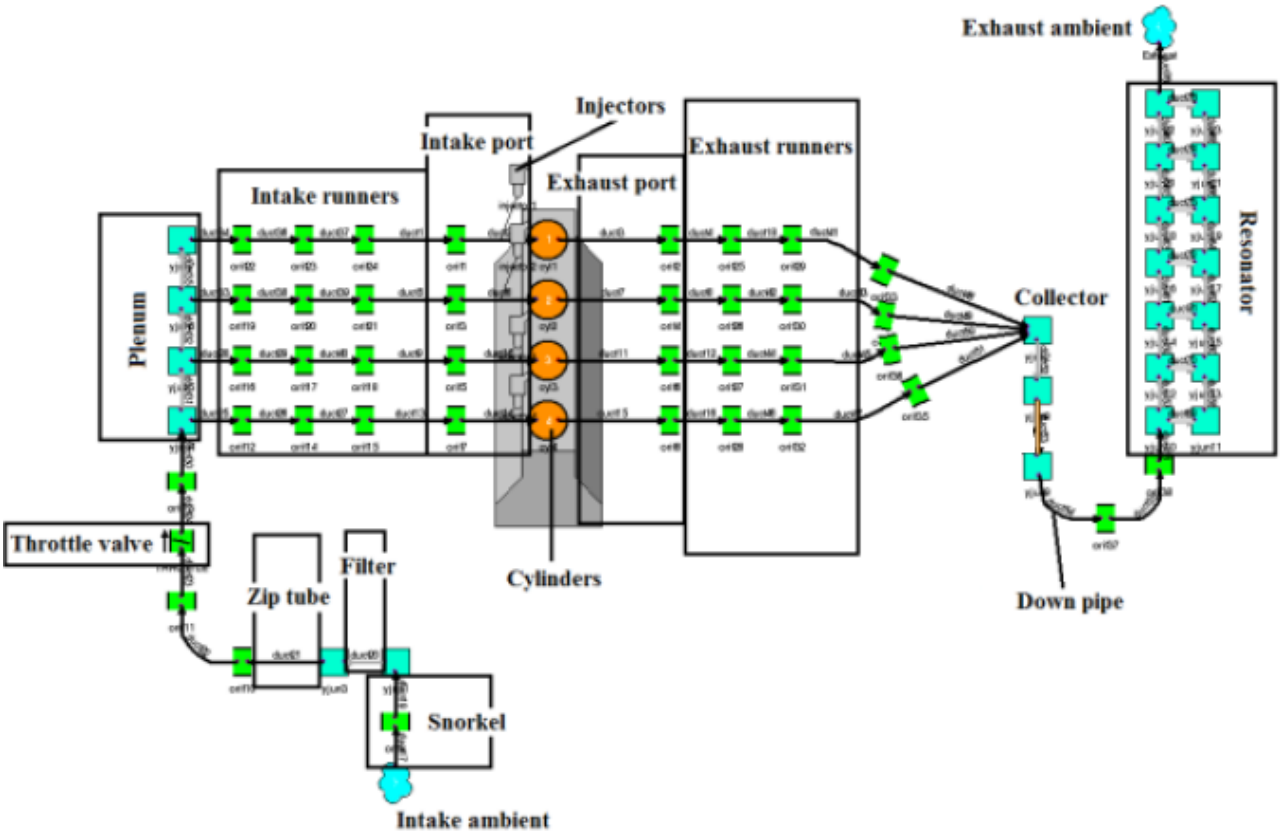

Figure 2. Basics elements of the modelled naturally aspirated gasoline engine

The model of combustion is achieved with calculation of heat release phenomenon regarding in-cylinder pressure trace during the combustion period. SI Wiebe correlational (Eq.10) carried out to identify the rate of fuel mass burned as a function of crankshaft angle [1]:

$$W = 1 - exp\left[-a\left(\frac{\theta-\theta_0}{\mathrm{BDUR}}\right)^{m+1}\right] \quad (10)$$

where W is cumulative burned mass fraction, BDUR (°CA) is combustion duration, θ (°CA) is crank angle and θ_0 (°CA) is start of combustion crank angle and m is Wiebe function exponent.

The basic Woschni correlation, assuming a simple heat flux from confined

combustion gas volume to the engine walls such as cylinder head, cylinder liner, piston face, and valve head, is applied for convective heat transfer (Eq.11). However, Annand heat transfer model [71] is widely used in practical due to more realistic modelling approach in which constant gas velocity assumes equal to the mean piston speed:

$$\mathrm{Q} = \mathrm{h_g} \times \mathrm{A} \times (\mathrm{T_g} - \mathrm{T_w}) \tag{11}$$

where Q (W/m^2) is overall heat loss to the walls, h_g (W/m^2K) is heat transfer coefficient, A (m^2) is heat exposed combustion chamber surface area, T_g (K) is cylinder gas temperature and T_w (K) is cylinder wall temperature.

Annand heat transfer coefficient [71] is given below (Eq.12):

$$h_g = \left(a\left(\frac{\rho\, v_m D}{\mu}\right)^{0.7}\right) \times \frac{k}{D} \tag{12}$$

where a is heat transfer multiplier, ρ (kg/m^3) is gas density, v_m (m/s) is mean piston speed, D (m) is cylinder bore, μ (kg/ms) is dynamic viscosity and k (W/mK) is thermal conductivity.

NO_x prediction based on Zeldovich mechanism is calculated by Arrhenius Equation (Eq.13) relating chemical reaction rate to temperature as given below:

$$\mathrm{NO_x(T)} = \mathrm{A} \times \mathrm{e}^{-\mathrm{E/RT}} \tag{13}$$

where T (K) is absolute burned zone temperature, A is pre-exponent Arrhenius factor, E (kJ/kmol) is activation energy of the reaction and R (kJ/kmolK) is universal gas constant. The pre-exponent Arrhenius factor and activation energy are calculated from experimental rate constants that are measured at different temperatures.

HC emission production is simulated based on post-flame oxidation [71] of unburned

fuel returning to the combustion chamber after combustion (Eq.14):

$$\frac{d[HC]}{dt} = -C_R \times A \times \exp\left(-\frac{E}{RT}\right)[HC]^a[O_2]^b \quad (14)$$

where C_R is calibration constant and O_2 (ppm) is oxygen concentration.

The work from cylinder gases to the piston cannot be transferred without any mechanical losses. The difference between indicated power and brake engine power is defined as a frictional term including friction of rotating engine parts and external auxiliary engine accessories driven by engine crankshaft such as cooling fan, water pump and oil pump. Friction power is very dominant at high speeds resulting in fuel consumption increase [72]. The numerical frictional mean effective pressure (FMEP) is calculated by using Chen-Flynn correlation predicting frictional losses with test cell data correlation. After measuring experimental frictional losses, the coefficients of Chen-Flynn correlation (Eq.15) should be fitted to measure FMEP data appropriate different engine speed and load conditions.

$$FMEP = ACF + BCF(P_{max}) + CCF(rpm \times stroke/2) + QCF(rpm \times stroke/2)^2 \quad (15)$$

where ACF (bar) is frictional pressure constant, BCF is maximum cylinder pressure factor varying with peak cylinder pressure, CCF (Pa/min×m) and QCF ($Pa/min^2/m^2$) are mean piston velocity factors accounting for changes in engine speed.

By using the sub-models above, the engine simulation was carried out at 1-2-3 bar BMEP and 1200-1350-1500-1650-1800 rpm engine speed ranges. BMEP ranges nearly correspond to 14%, 27% and 41% throttle positions for 1, 2 and 3 bar, respectively (Table 2). At 1 bar BMEP, net power levels correspond to 1.83 kW, 2.27 kW and 2.73 kW for 1200 rpm, 1500 rpm and 1800 rpm, respectively. The engine power shifts to different ranges proportional to the load level at given engine speeds.

After the numerical optimisation at these 15 fixed steady state points, the optimised simulation outputs were compared to the test bench experimental data [53,73] and also validated with a reasonably good accuracy.

Table 2. Details of the simulation set-up

Parameter	Value
BMEP (bar)	1-2-3
Engine speed (rpm)	1200-1350-1500-1650-1800
Throttle position (%)	14-27-41

3. Results and Discussion

In this study, the normal engine model is based on architecture in which Woschni combustion model, Annand heat transfer model, Arrhenius NO_x emission model, post flame oxidation HC emission model and Chen-Flynn friction model are considered. The skip cycle engine model is established on models described above and an additional approach called “Net Power Cycle” which can calculate net indicating parameters and brake outputs along a sequential cycle group including a normal cycle and a following skipped cycle with high accuracy verification.

At first stage of numerical analysis, ignition timing optimisation is carried out for both normal operation and skip cycle strategy within each simulation case for equivalent experimental power ranges. The optimised numerical results are validated with the experimental data for both normal cycle and skip cycle. Then the numerical study is extended by combining skip cycle technique and variable valve timing strategy to further eliminate exhaust gas emissions appear as a result of standalone skip cycle

technique. Two variable valve timing strategies are investigated and optimised with regards to reducing hydrocarbon and nitrogen oxide emissions by late exhaust valve opening (LEVO) and early intake valve opening (EIVO) approaches.

3.1. Numerical optimisation of ignition timing

Fuel injection timing and injection pressure are two important engine input parameters providing a fine fuel-air mixture and flame propagation in combustion chamber for direct injection SI engines [74]. However, the effect of injection phenomenon does not play a crucial role on combustion quality, fuel consumption and exhaust pollutants for homogeneous charge port fuel injection (PFI) methodology since lower fuel injection pressure (3-15 bar) and fresh charge are premixing and evaporate before entering into the combustion chamber. In case of cold start, the interaction between air and fuel droplets could affect the engine performance [75]. In this study, the fuel spray effects are neglected due to loaded operating conditions.

The main predictive optimisation parameter is ignition timing which shows relative position of combustion initiation to the compression top dead center (TDC). Spark plug usually ignites the mixture before TDC based on engine operating conditions in order to burn mixture completely. Retarded ignition timing shifts peak cylinder pressure towards the late expansion stroke with lower magnitude and incompleted burning. On the other hand, advanced spark timing causes a fast burning cycle and knock tendency [76]. The optimum ignition timing which gives maximum engine torque, called MBT timing, occurs when magnitude of these two opposing trends (retarding and advancing) just offset each other. Timing which is advanced or retarded from the optimum ignition timing, gives a lower torque value [1].

Executing a detailed engine map (spark advance-load-rpm matrix) through optimisation process on test bench is not comfortable with regards to time and fuel cost for all operation points. Therefore, 2-D interpolation table of spark timing optimisation was obtained depending on average in-cylinder pressure and engine speed conditions as a result steady-state model simulations (see Fig. 4). The numerical calculation allows us to integrate DoE (design of experiment) with "Two-stage" test strategy. In Two-stage model [77], all conditions such as engine speed, load, intake and exhaust settings were kept fixed and just spark timing and throttle valve angle input parameters were manipulated to obtain MBT for optimum spark advance close to TDC as much as possible for the same target engine power. Throttle angle and spark timing independent input parameters were used in a "2-level full factorial experiment" design with all combination settings between either their minimum and maximum values.

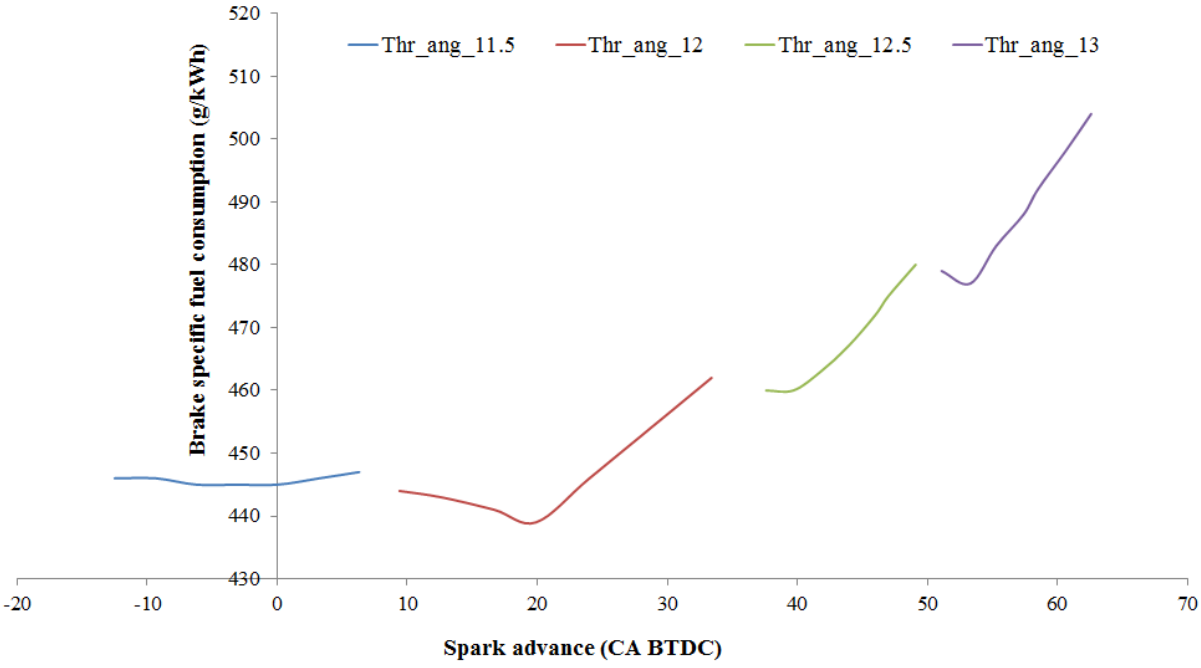

Figure 3. Numerical optimisation of normal engine performance via spark advance (BMEP: 3 bar, 1500 rpm)

Figure 3 shows the impact of different ignition advances on brake specific fuel

366 consumption at 3 bar brake mean effective pressure and 1500 rpm engine speed
367 conditions for normal engine operation. All input parameters except for throttle angle
368 and ignition timing were kept constant. The main goal of numerical optimisation
369 process was to find out minimum spark advance closest to TDC when throttle valve
370 opening enough to reach target torque value. Thanks to four different throttle
371 positions (11.5°-12.0°-12.5° and 13.0°) and twenty-eight different spark timing
372 (varying between -12.5 CA BTDC and 62.5 CA BTDC) and also their combinations,
373 best spark advance point was obtained over four throttle angle curves. As seen in Fig.
374 3, for 41% load level (BMEP=3 bar) and 1500 rpm engine speed, the optimum spark
375 advance was obtained as 19.9 CA BTDC for 12° throttle angle. At 12° throttle angle
376 position, a value of 9.4 CA increase of the spark advance or 7.3 CA retarding from
377 the optimum increases BSFC by about 3.6% and 0.9 % respectively. Compared to
378 optimised combination (12° throttle angle and 19.9 CA BTDC), in case of 12.5 ° or
379 13.0° throttle angle at several spark timings, fuel consumption increases by 6.6% and
380 11.3% on average, respectively. If the throttle is closed to 11.5 ° position, BSFC
381 values increased again and otherwise any spark timing could not reach target torque
382 (for example at 11.5 ° position, BMEP could not be higher than 2.75 bar).
383
384 In Fig. 4, the points indicate the experimental data and solid lines represent extended
385 optimal engine map as a result of DoE for each individual simulation case. As seen in
386 Fig. 4, the spark timing was advanced while the engine speed increases and also
387 retarded as the engine is loaded. For example, at 1500 rpm, the spark advance
388 varies from 24.5 CA to 20.7 CA for 27% and 41% loads, respectively for normal
389 engine operation. At same engine speed, spark advance varies from 18.0 CA to 17.2
390 CA for 27% and 41% loads, respectively for skip cycle strategy.

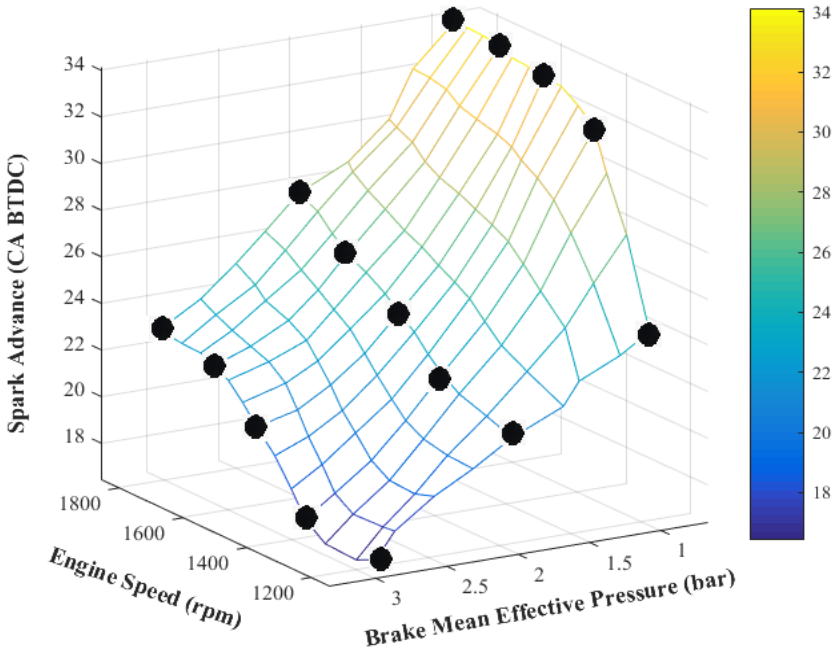

Figure 4. 2-D contour map of optimised spark timing for normal operation

3.2. Model validation with experimental data

This section discusses comparison between optimised numerical results with the engine experimental data for two different engine operating strategies (Figs. 5-12). These are normal engine operation and skip cycle strategy. It is noted that the engine on the test cell is already optimised. For all of the experimental points, intake and exhaust valve timings, valve durations and the stoichiometric AFR values (Table 1) are kept constant. Steady state engine tests are performed at the ranges of part-load (BMEP = 1.0, 2.0 and 3.0 bars) and fixed engine speeds (1200, 1350, 1500, 1650 and 1800 rpm). At each operation point, optimum spark timing is calibrated with regards to maximum brake torque criteria with a throttle valve wide as much as open to allow more fresh intake air into the cylinder. First we validate numerical results with the experimental data for the normal engine.

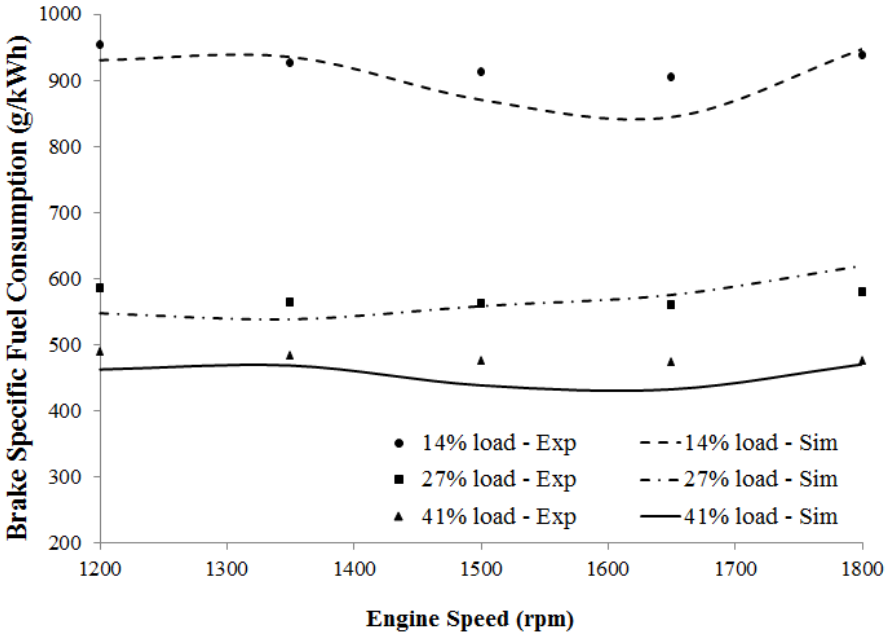

Figure 5. BSFC validation for normal engine operation

Figure 5 shows brake specific fuel consumption comparison between numerical and experimental data at three different load conditions. It is seen that numerical results under predict the experimental data for the low load conditions (at 1500 rpm and 14% load, the prediction error of fuel consumption is about 4.6%). This may happen due to experimental measurement errors of spark advance or throttle position during an engine operation at low load conditions, such as 14%. A prediction error in terms of fuel consumption at a range of 4.6% could be explained by a very small reading error for spark timing or oscillation of engine speed in ±50 rpm range. Nevertheless, the comparison shows good agreement between numerical results and the experimental data at mid-range load conditions.

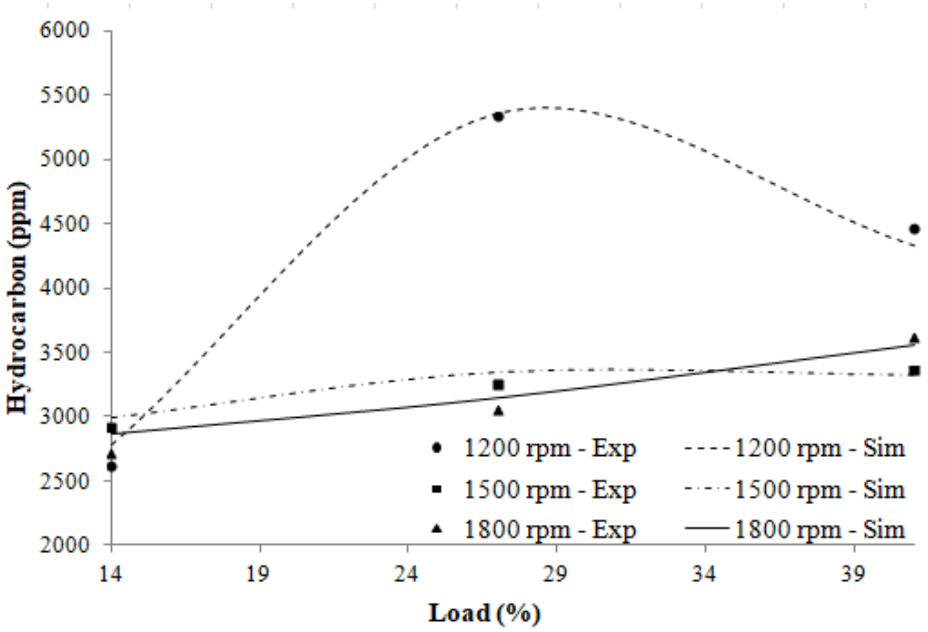

Figure 6. HC Emission validation for normal engine operation

At 3 bar BMEP, HC emission in experiment result is higher than that of simulation results (Fig. 6). This is because of lower combustion velocity in experiment than the simulation and also extension of deflation zone near the chamber wall at expansion process of experimental cycle. This can be further understood from the in-cylinder pressure curve. For example, in Fig. 8, while the pressure rising rate ($dP/d\theta$) in compression process of simulation is equal to the experiment, then it becomes higher near the TDC.

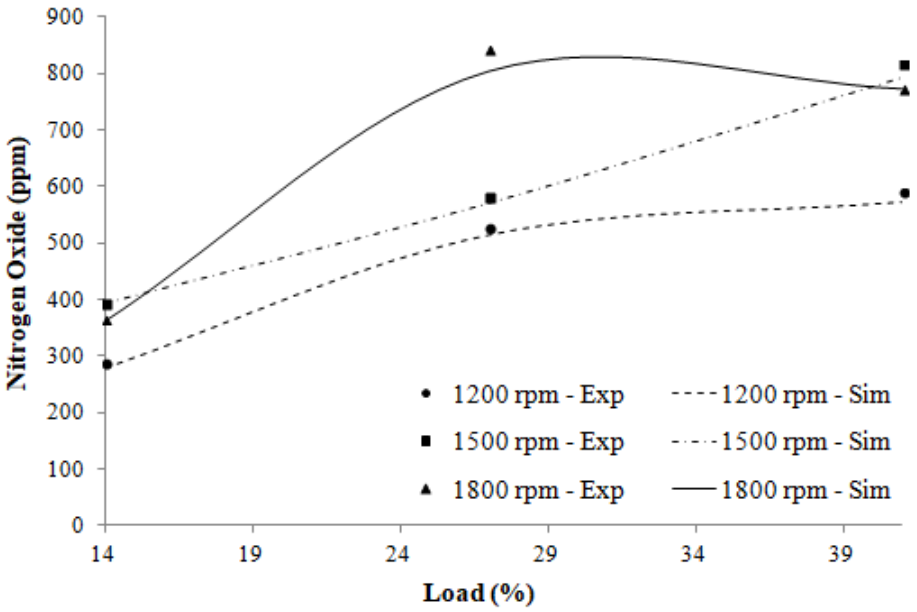

Figure 7. NO_x Emission validation for normal engine operation

At 3 bar BMEP and 1500 rpm range, prediction errors are about 1.1% and 2.9% for HC (Fig. 6) and NO_x (Fig. 7) emissions, respectively. As seen in Fig. 7, NO_x emissions increase while the engine runs at higher speeds. The first reason is relative combustion duration extension as crank angle degrees at high speed ranges. Hence, rate of development and propagation of the premixed engine flame increases due to the higher turbulence level in cylinder. The second one is residual gas fraction reduction (means more fresh oxygen for the next cycle) as speed increases. The last one is higher mean combustion chamber temperature as a result of relative less heat transfer per cycle [1]. However, NO_x emission slightly decreases from 1650 rpm to 1800 rpm at 1 bar and 3 bar BMEP loads (Fig. 7). The possible reason could be due to local chamber temperature decreases as from the speed range where the maximum brake torque occurs. NO_x increases with increasing load because of the same reasons mentioned earlier with respect to increasing speed. On the other hand, HC concentration decreases modestly when the load is increased. As load increases at constant speed, the temperature in expansion and exhaust strokes increase, and the in-cylinder oxidation rate can increase with sufficient oxygen [1].

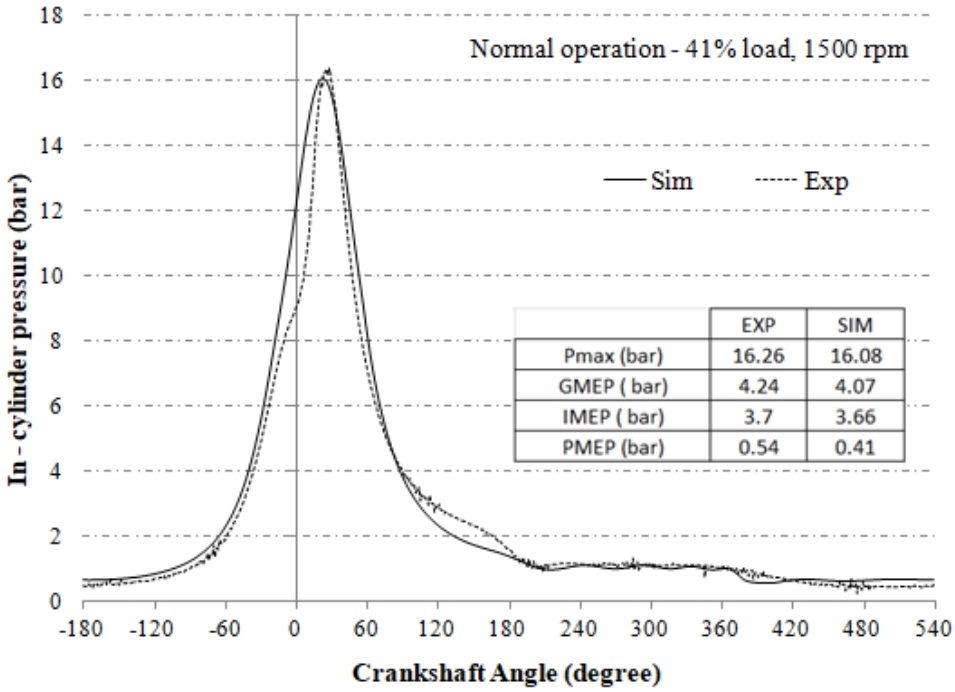

Figure 8. Validation of In-Cylinder pressure curves for normal engine operation at 3 bar BMEP and 1500 rpm engine speed

Figure 8 represents a comparison of in-cylinder pressure curves via crankshaft angle of numerical results and experimental indicating data for 41% load level and 1500 rpm speed range. The graph shows that the pressure curve trace, maximum cylinder pressure value and timing results are very close to the experiments. It is a clear proof for the accuracy of combustion model (Eq.10) which is the key sub-model showing the main characteristics of the cycle modelling.

The model based calibration results show that for an equivalent torque demand value (Brake mean effective pressure: BMEP=1-2-3 bar and engine speed: n=1200-1350-1500-1650-1800 rpm), relative model prediction errors are on average under 2.8%, 0.2% and 1.7% for fuel consumption, HC and NO_x emissions, respectively for normal engine operation. Besides the available model predicts spark advance, maximum cylinder pressure (P_{max}) and volumetric efficiency with an averaged error under 0.8%, 4.9% and 0.4% respectively.

Now, we discuss the comparison of skip cycle engine simulation results with the experimental data. As seen in Figs. 9-12, the proposed model for SCS makes a good agreement with the experimental data. It indicates validation errors under 2.3%, 0.5%, 0.3%, 0.5%, 4.9% and 0.5% on average for fuel consumption, HC, NO_x, spark advance, volumetric efficiency and P_{max}, respectively.

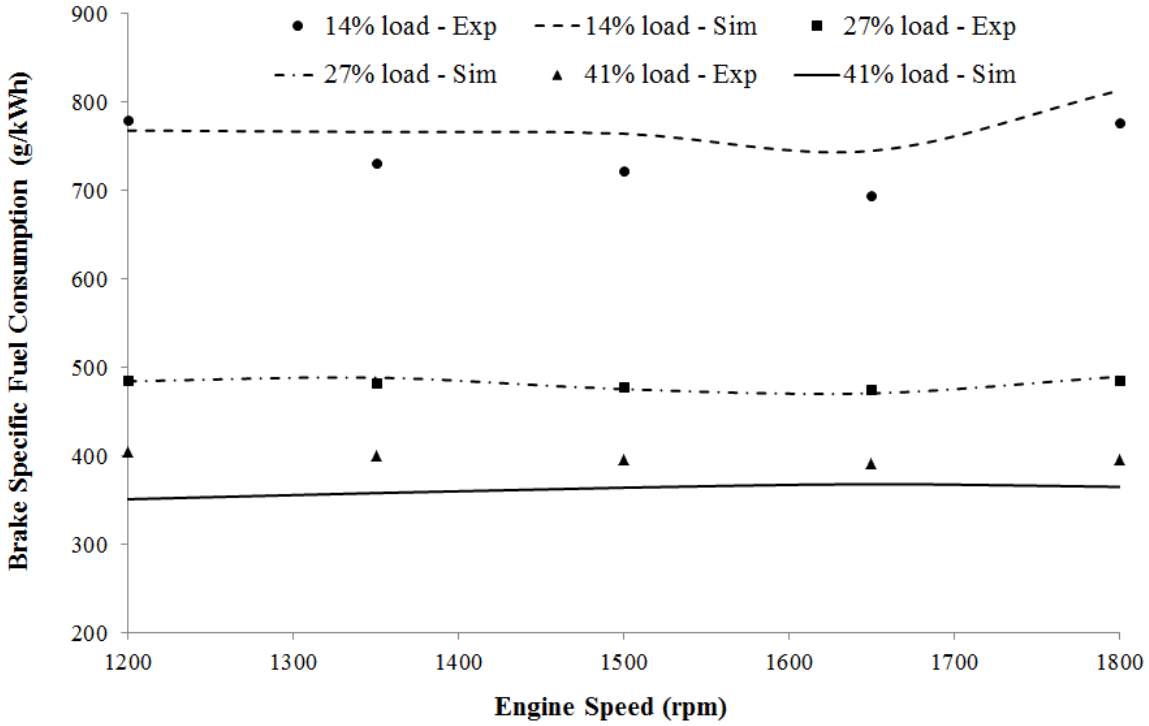

Figure 9. BSFC validation of SCS Strategy

In Fig. 9, brake specific fuel consumption validation of SCS is shown for several operating points. A good agreement provided with 4%, 0.1% and 4.5% prediction errors on average for 1, 2 and 3 bar BMEP load levels, respectively.

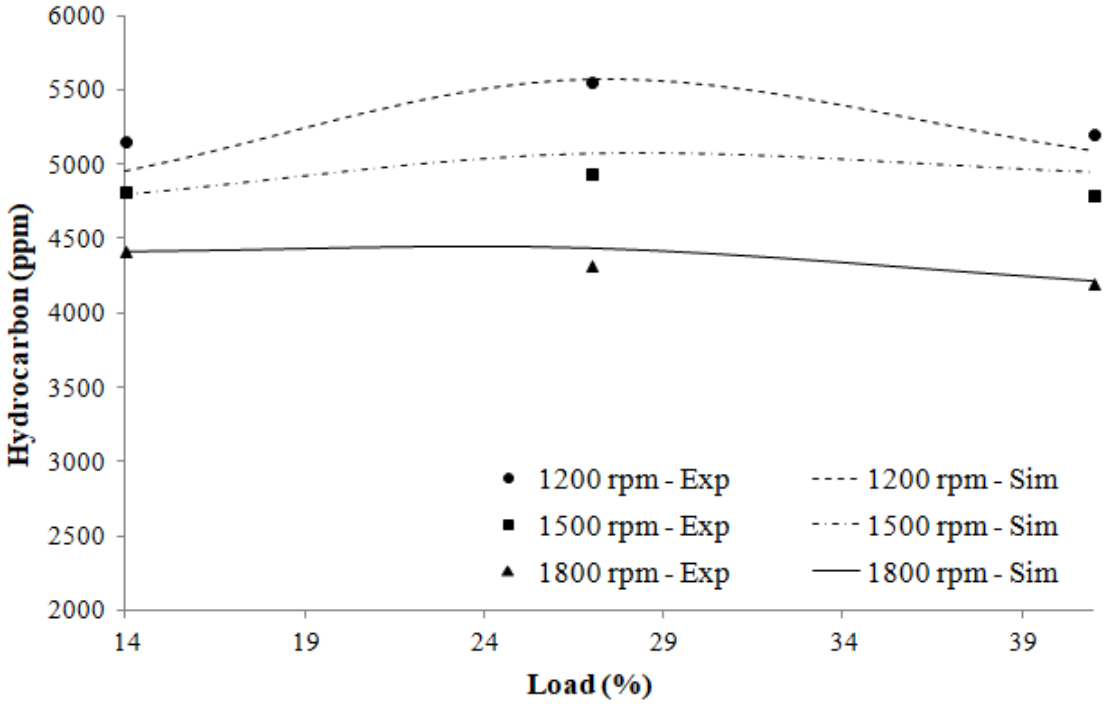

Figure 10. HC Emission validation of SCS Strategy

At 1500 rpm engine speed, hydrocarbon concentration in case of SCS operation has been verified with test bench results in 0.4%, 2.6% and 3.1% approximation for 1, 2 and 3 bar BMEP, respectively (Fig. 10). As expected, HC concentration increases in comparison to normal engine operation (Fig. 6) due to undesired lubrication oil suction to the combustion chamber as a result of excess compression stroke (between 900 CA and 1080 CA) pressure drop in skipped section of SCS operation (Fig. 1). Even though the possible reasons for HC increase could be flame quenching or unburned mixture in crevice cylinder volumes, these two possibilities have not been considered since the same piston, combustion chamber, spark plug and valve geometries are used in skip cycle engine with normal operation. Besides, a better flame development has been reported in skip cycle regime [53]. The post-flame oxidation equation (Eq.14) items and oxidation threshold temperature (600 K) are kept as constant. In order for modelling of HC increase in skip cycle engine, maximum oil film thickness is assumed as good as the radial clearance between

cylinder liner and piston surface (550 μm) at engine geometry. Model based HC emission calibration has been performed by post-flame oxidation equation (Eq.14) and oil film thickness prediction regarding experimental data for each steady-state simulation point (Table 3). As seen in Table 3, oil film becomes thicker when the minimum cylinder pressure is lower at skip cycle strategy. Furthermore, there could be seen an obvious oil film thickness difference between normal and skip cycle engine operations due to undesired oil transfer from crankcase. Even though no measurement recorded for oil consumption, it was observed that crankcase oil level lowered in time more than normal during experiments.

Table 3. Predicted maximum oil film thicknesses at 1500 rpm engine speed condition

	BMEP (bar)	P_{min} (bar)	Max. oil film thickness (μm)
Normal operation	1	0.31	2.5
	2	0.47	20
	3	0.53	16
Skip cycle operation	1	0.092	45
	2	0.075	419
	3	0.064	508

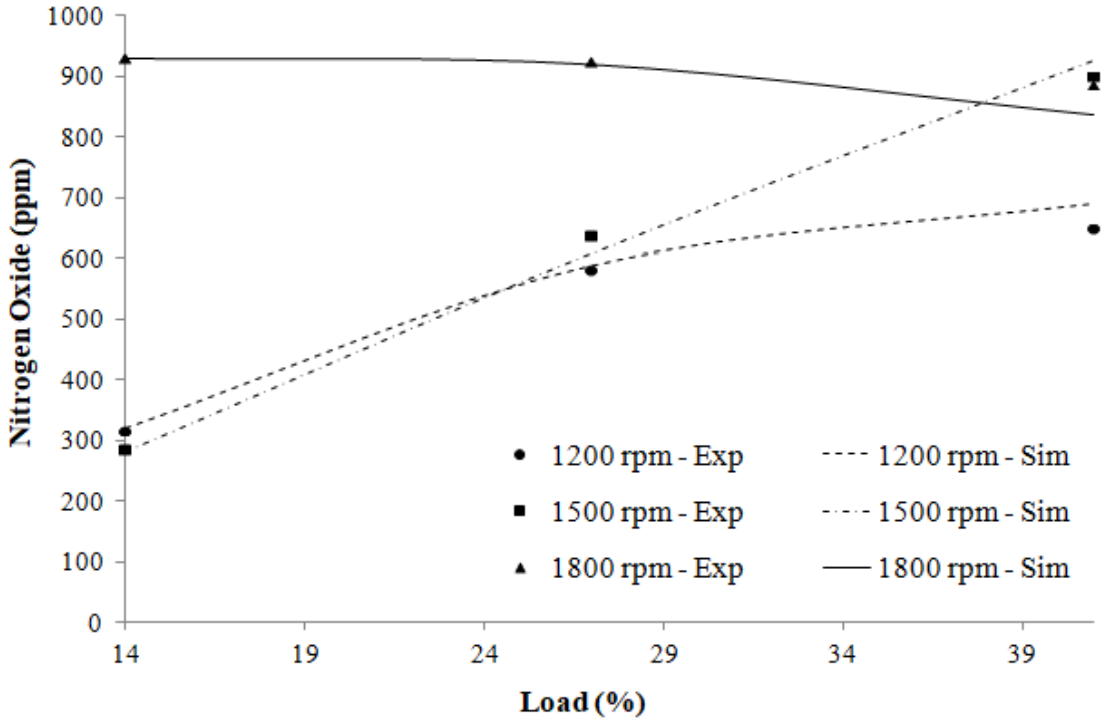

Figure 11. NO_x Emission validation of SCS Strategy

In Fig. 11, nitrogen oxide emission of SCS operation at three different speed ranges is shown. Compared to the experimental results, simulation prediction errors of NO_x are calculated as %1.4, %4.8 and %2.9 at 1500 rpm engine speed for 1, 2 and 3 bar BMEP, respectively. As expected, NOx values increase for SCS operation compared to normal engine operation (Fig. 7) due to higher cylinder pressure and temperature ranges in skip cycle engine. This difference could be evaluated by calibration of pre-exponent Arrhenius factor which is one of the main prediction parameters with burned flame temperature in semi-empirical Arrhenius Equation (Eq.13) against the experimental data. As a nitrogen molecules collision frequency, calibration of pre-exponent Arrhenius factor is a function of temperature, reaction cross-section area and relative orientation of molecules [78]. Calculated pre-exponent Arrhenius factors vary between 1.36 and 0.10 on average at 3 bar BMEP load level for normal and SCS operations, respectively.

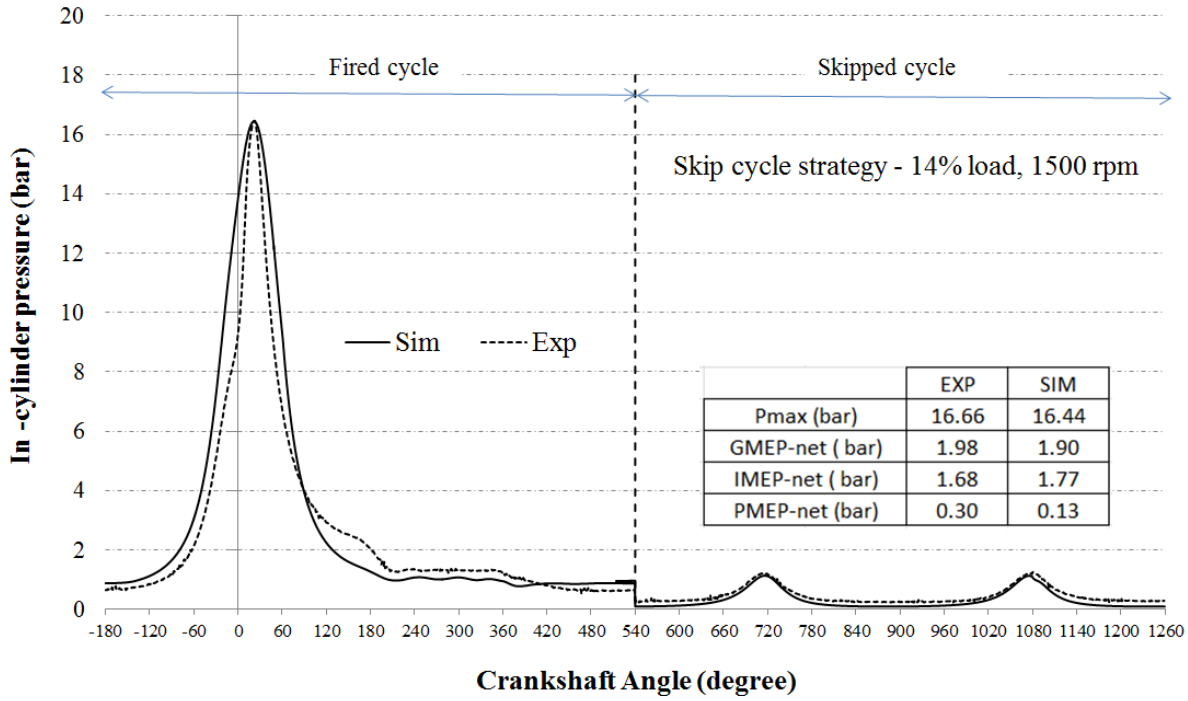

Figure 12. Validation of In-Cylinder pressure curves for SCS Strategy at 1 bar BMEP and 1500 rpm engine speed

Figure 12 shows simulation in-cylinder pressure compatibility with experimental pressure trace at 1 bar BMEP and 1500 rpm conditions. The graph shows that the maximum cylinder pressure value and timing results are very close to the experiments for an equal spark timing and power demand. Even though pressure level at compression stroke starting point (-180 CA) of the fired cycle simulation is higher than experiment one, net gross mean effective and indicated mean effective pressure values point out a good prediction with test data. Consequently, all these results indicate that the proposed mathematical model accurately predicted the indicated parameters, performance and exhaust emissions of the engine and ensured an agreeable compatibility with the experimental data of normal cycle and skip cycle operations.

3.3. Optimisation of VVT for SCS

Despite improvement in better fuel consumption, it is observed that HC and NO_x emissions are increased with SCS. This section studies a way to find a solution to decrease these pollutant emissions by adding a VVT system to the SCS. Depending on physical limitations in current skip cycle mechanism [53], a fully variable valve duration and lift adjustment is very difficult to apply. However, it is believed that retarding or advancing valve timing is sufficient to reduce pollutant emissions, hence reveal a further potential of SCS. Basically, two main valve activation strategies are investigated. First one is early intake valve opening (EIVO) strategy providing a pressure reduction at start of induction process and an increase at rapid burning angle, so that a significant decrease in NO_x emissions. The second strategy is late exhaust valve opening (LEVO) leading a prevention of oil leakage and also HC emission formation regarding with a pressure increase in skipped section of SCS (Fig. 1). Since the valve activation duration is kept fixed and used as in original engine, just intake and exhaust profiles are retarded or advanced relatively to the crankshaft revolution. In order to perform a good matching during optimum EVO and IVO timing determination and general comparison of SCS and SCS&VVT modes, parameters such as brake engine power, spark timing, throttle valve angle, brake specific fuel consumption, pre-exponent Arrhenius factor (A) for NO_x prediction and post-flame oxidation temperature for HC calculation are kept fixed for all simulated test cases.

Possible reason for rising of HC emission in SCS is undesired oil suction from crankcase to the combustion chamber due to extra low vacuum pressure occurred in SCS. Resulting from exhaust valve of fired cycle of SCS is fully closed and just a vacuum gas is remained in compression stroke (between -180 CA and 0 CA of red

curve in Fig. 13) of skip cycle strategy, in-cylinder pressure value dramatically decreases. Hence, the lubricating oil penetrates into combustion chamber more than normal amount. This causes an undesired and thicker oil film profile between liner and piston. At 3 bar BMEP and 1500 rpm SCS operation conditions, 32.8% HC emission increase has been recorded due to lower minimum cylinder pressure compared to normal engine operation (Fig. 13).

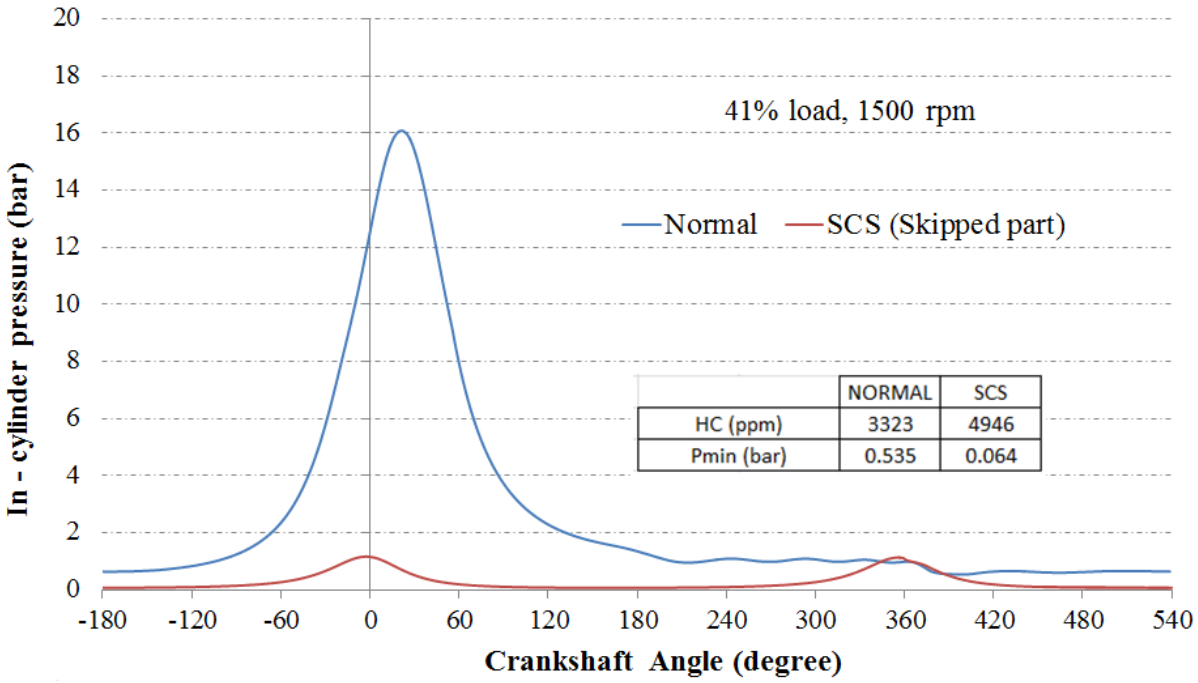

Figure 13. Reason of HC emission increase at SCS

The main reason of increasing NO_x values in SCS case links to higher temperature and pressure levels inside the cylinder due to higher amount of fresh mixture absorbed into the cylinder. As seen in Fig.14, the NOx concentration was increased by 16.9% due to peak temperature increase by 461K in SCS case compared to normal engine case.

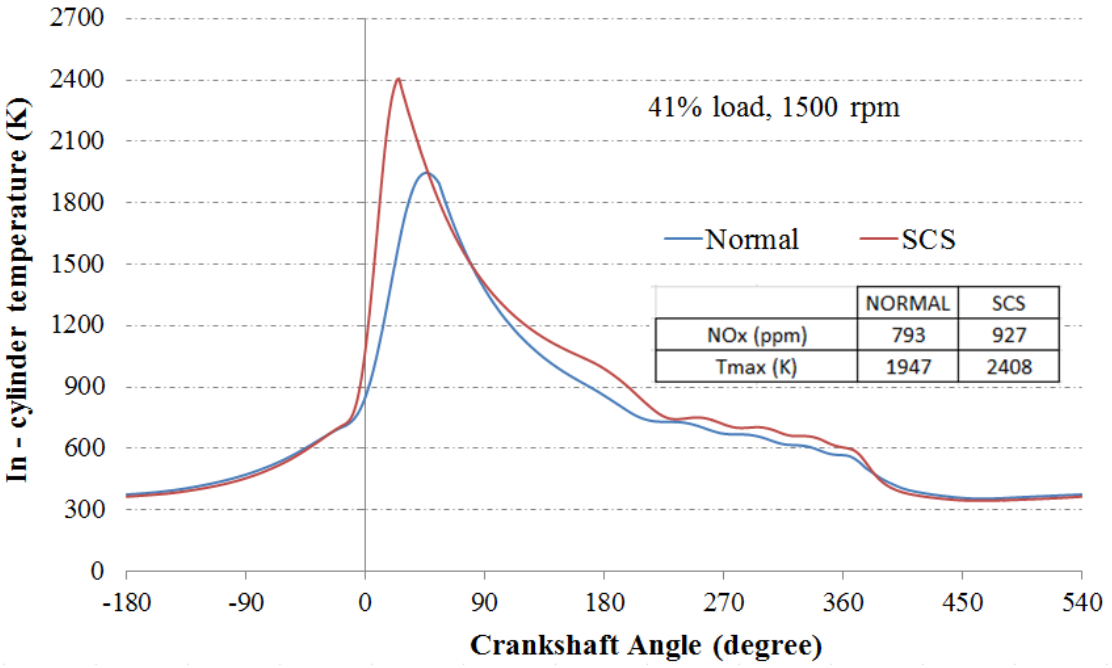

Figure 14. Reason of NO_x emission increase at SCS

A hydraulic oil pressure actuator should be adapted to engine camshaft to control the camshaft position due to the load and engine speed conditions. ECU could regulate oil pressure level to retard or advance cam phasing separately from SCS mechanism.

As indicated in SCS (skipped part) of Fig. 13, the vacuum pressure level is much lower than that of normal operation. This may causes oil leakage to combustion chamber. The pressure limit during intake process of skipped section (red curve in Fig. 13) should be kept above 0.2 bar [45] by trapping exhaust gas retarded in work production section (fired cycle-Fig. 1) of SCS in order to avoid undesired lubrication oil and HC emission. As seen in Fig. 15, minimum cylinder pressure ranges are under 0.1 bar with original exhaust valve opening timing (EVO=140 ATDC of compression) for fired cycle of SCS. This causes a significant increase in HC emissions due to undesired oil suction to the combustion chamber. In case of VVT application on fired section of SCS, when EVO is retarded 50 CA (optimised

EVO=190 ATDC) and exhaust gas trapped in skipped section of SCS and minimum cylinder pressure reaches to 0.2 bar. This also prevents undesired lubrication oil reaches into the cylinder (see Table 4).

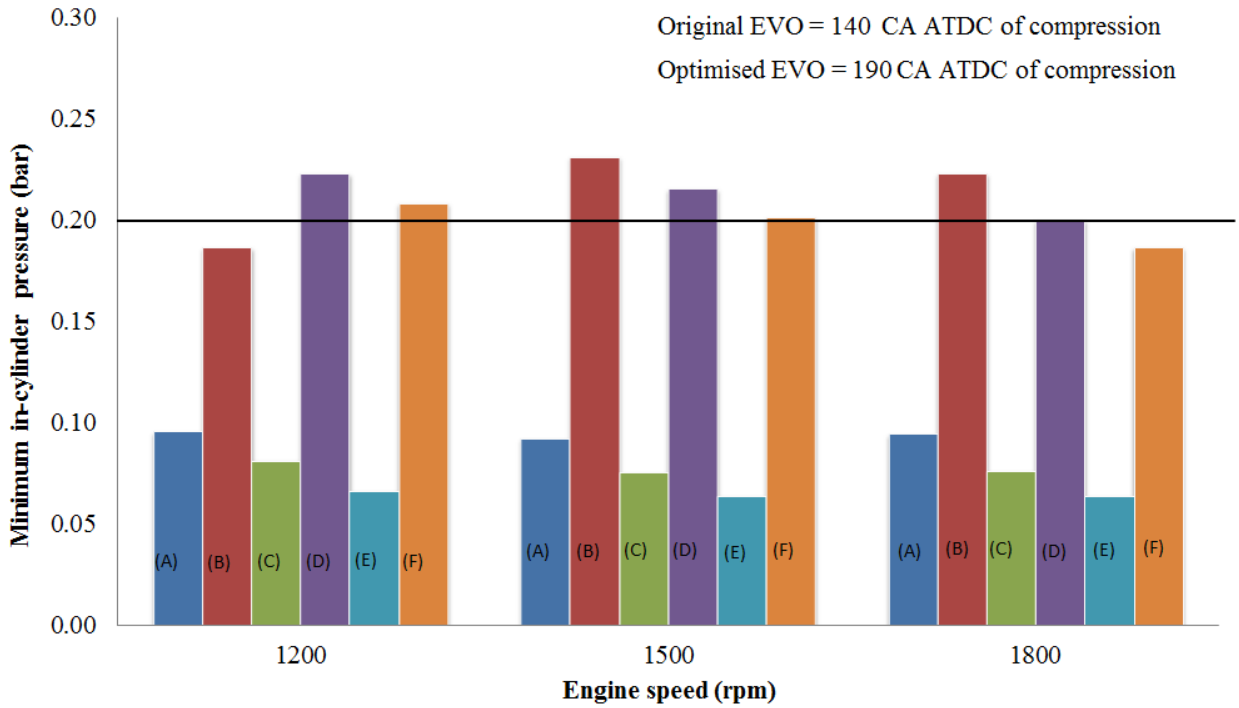

Figure 15. Effect of exhaust valve opening timing on minimum cylinder pressure at different engine conditions. (A): BMEP 1 bar – SCS, (B): BMEP 1 bar – SCS+VVT, (C): BMEP 2 bar – SCS, (D): BMEP 2 bar – SCS+VVT, (E): BMEP 3 bar – SCS, (F): BMEP 3 bar – SCS+VVT

The presence of lubricating oil in the fuel or on the walls of combustion chamber is known to result in an increase in exhaust hydrocarbon levels. Since fuel vapour concentration within the cylinder is close to the inlet manifold concentration during intake and compression, any oil film on the walls will absorb fuel vapour. During combustion, the fuel vapour concentration in the bulk gases goes essentially to zero so the absorbed fuel vapour will desorb from the liquid oil film into the gaseous combustion products. Some of the desorbed vapour fuel will mix with the high

602 temperature combustion products and oxidize. However, desorbed vapour that
603 remains in the cool boundary layer or mixes with the cooler bulk gases at late
604 expansion stroke of the cycle may escape full oxidation and contribute the unburned
605 HC emissions [1]. Experimental and numerical results showed that HC concentration
606 of skip cycle engine increases dramatically due to higher fuel vapour desorption into
607 the combustion gases compared to normal engine operation. Higher vapour
608 increases the of unburned HC emissions regarding higher possibility of non-oxized
609 gas concentration.
610
611 Table 4. Effect of EVO timing on predicted oil film thickness and skipped cycle
612 minimum cylinder pressure ranges with default IVO timing (EVO= 140 CA
613 for SCS and EVO= 190 CA for SCS&VVT)

BMEP (bar)	Speed (rpm)	P_{min} with SCS (bar)	Max. oil film thickness for SCS (μm)	HC (ppm) for SCS	P_{min} with SCS&VVT (bar)	Max. oil film thickness for SCS&VVT (μm)	HC (ppm) for SCS&VVT
1	1200	0.096	130	4954	0.187	3.1	2657
	1500	0.092	45	4795	0.231	3.1	2444
	1800	0.094	129	4436	0.223	3.1	2581
2	1200	0.081	544	5573	0.223	6	3054
	1500	0.075	419	5071	0.216	6	2997
	1800	0.076	359	4436	0.200	6	3103
3	1200	0.066	550	5092	0.208	10	2681
	1500	0.064	508	4946	0.201	10	2701

1800	0.064	432	4210	0.187	10	2801

As a result of higher cylinder pressure during skipped cycle of SCS&VVT operation in comparison to standalone SCS mode, a significant decrease in both oil film thickness on walls and unburned HC emissions could be observed (Table 4). Figure 16 and Table 4 show how HC concentration changed with just 50 CA retarding of exhaust valve opening for fired cycle.

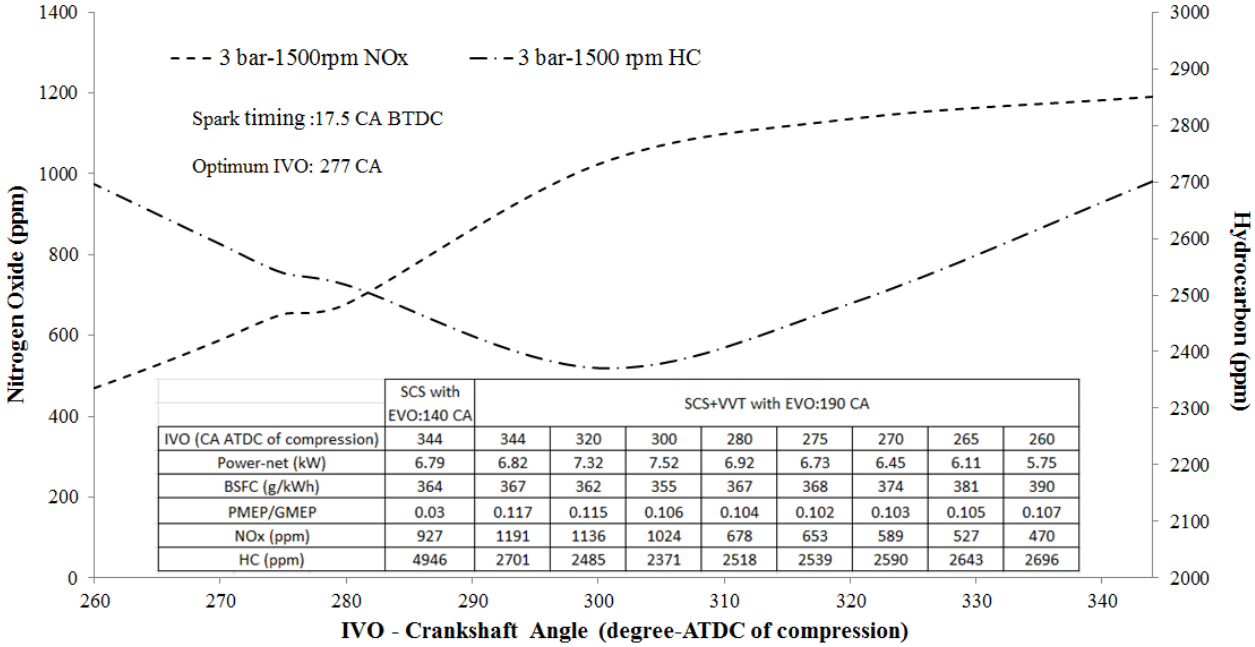

	SCS with EVO:140 CA	SCS+VVT with EVO:190 CA							
IVO (CA ATDC of compression)	344	344	320	300	280	275	270	265	260
Power-net (kW)	6.79	6.82	7.32	7.52	6.92	6.73	6.45	6.11	5.75
BSFC (g/kWh)	364	367	362	355	367	368	374	381	390
PMEP/GMEP	0.03	0.117	0.115	0.106	0.104	0.102	0.103	0.105	0.107
NOx (ppm)	927	1191	1136	1024	678	653	589	527	470
HC (ppm)	4946	2701	2485	2371	2518	2539	2590	2643	2696

Figure 16. Effect of EVO and IVO timing on exhaust emissions at 3 bar BMEP and 1500 rpm

As seen in Fig. 16, at 3 bar BMEP and 1500 rpm condition, after applying late exhaust valve opening, HC emission concentration decreases seriously (from 4946 ppm to 2701 ppm) and NO_x increases slightly due to an increase in cylinder temperature (Fig. 19: maximum temperature changes from 2408 K to 2477 K) and more favourable combustion conditions which occur as a result of more much combustion gas oxidation instead of unburned HC emissions.

By applying an advanced intake valve opening (Fig. 16: from 344 CA ATDC to 277 CA ATDC optimal timing), while nitrogen oxide emissions decrease significantly (Fig. 16: from 1191 ppm to 663 ppm due to dropped pressure at the end of intake process (Fig. 18: from 0.963 bar with SCS to 0.889 bar with EIVO), no important difference is observed at HC concentration (Fig. 16). Even if NO_x concentration decreases continuously with earlier IVO timing (from 277 CA ATDC optimal timing to 260 CA ATDC), engine power becomes insufficient for required level and also 5.6% increase could be observed in fuel consumption. One of the key parameters to determine optimal IVO timing is PMEP/GMEP ratio. Optimal IVO angles correspond to minimum pumping to gross mean effective pressure (PMEP/GMEP) ratio. In Fig. 16, it is shown that minimum PMEP/GMEP ratio occurs between 275 and 280 CA ATDC of compression.

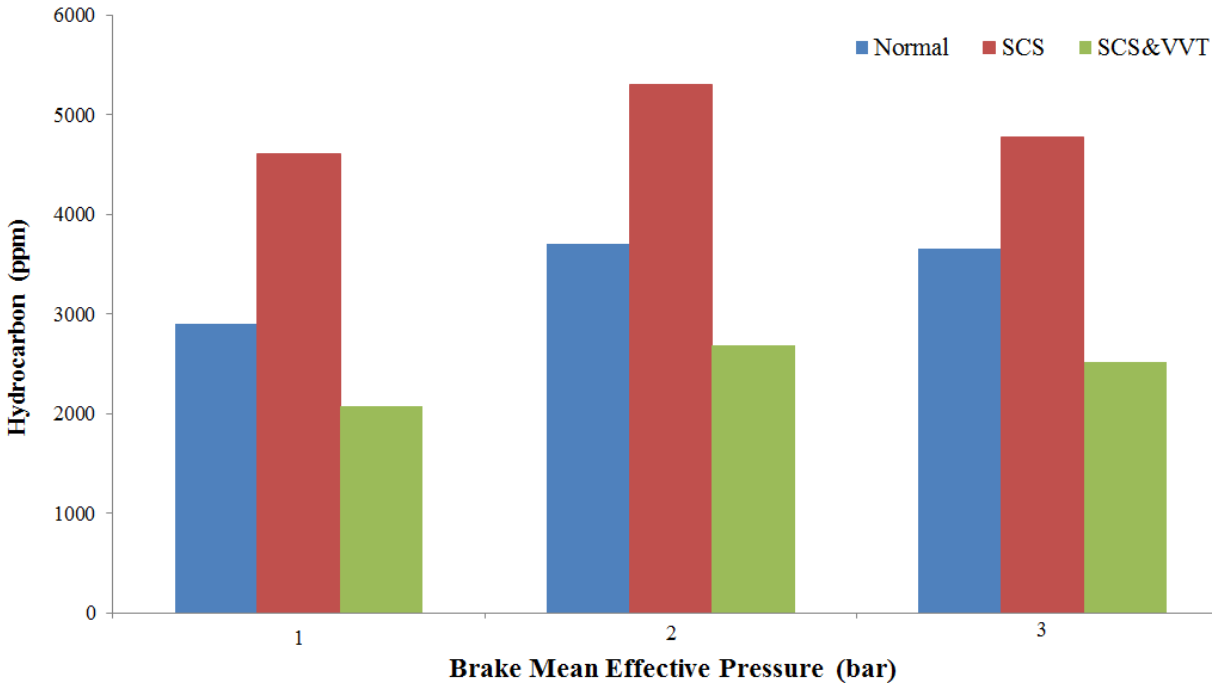

Figure 17. Hydrocarbon emission comparison via BMEP

Compared to SCS operation, it is observed that in SCS&VVT application, HC

concentration decreases by 54.9%, 49.3% and 47.4% at 1, 2 and 3 bar BMEP, respectively (Fig. 17). Increasing ratio of exhaust to inlet pressure increases the fraction of residual gases in cycle fresh charge and thus reduces flame speed and also increases the flame travel [79]. Besides, the pressure at spark timing is very indicative on burning duration (or flame travel period). When the intake valve opens 74 CA earlier (from 344 CA ATDC to 270 CA ATDC) than the original one, cylinder pressure at spark timing changes from 13.19 bar to 12.37 bar (Fig. 18). This also indicates a slower combustion process and retarded heat release curve (CA50 value changes from 12 CA ATDC to 23 CA ATDC).

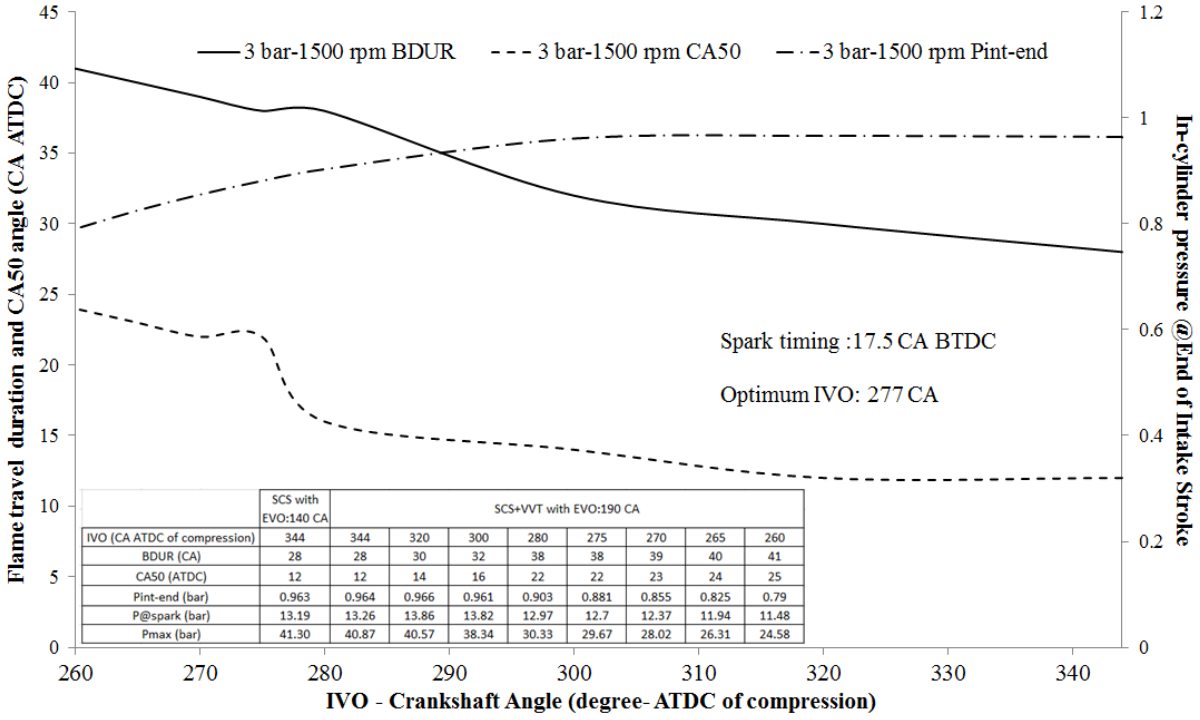

	SCS with EVO:140 CA	SCS+VVT with EVO:190 CA							
IVO (CA ATDC of compression)	344	344	320	300	280	275	270	265	260
BDUR (CA)	28	28	30	32	38	38	39	40	41
CA50 (ATDC)	12	12	14	16	22	22	23	24	25
Pint-end (bar)	0.963	0.964	0.966	0.961	0.903	0.881	0.855	0.825	0.79
P@spark (bar)	13.19	13.26	13.86	13.82	12.97	12.7	12.37	11.94	11.48
Pmax (bar)	41.30	40.87	40.57	38.34	30.33	29.67	28.02	26.31	24.58

Figure 18. Effect of IVO timing on burning angles and intake pressure level

Changes in temperature during combustion process and early part of the expansion stroke are important factors on NO_x formation mechanism (Fig. 19). After exhaust valve opening optimisation, maximum cylinder temperature varies from 2477 K to 2230 K for intake valve opening timing of 344 CA ATDC and 270 CA ATDC, respectively. Besides, maximum in-cylinder pressure decreases from 40.87 bar to

28.02 bar for the same IVO variations. As a result of both temperature and pressure levels in combustion chamber and flame travel period extension, timing of maximum pressure occurs at a further point as CA with regards to combustion top dead center. The retarding of burning duration causes a slower combustion and less NO_x emission compared to original IVO timing. When the intake valve opens 74 CA earlier (from 344 CA ATDC to 270 CA ATDC) than the original one, NO_x changes from 1191 ppm to 589 ppm (Fig. 19).

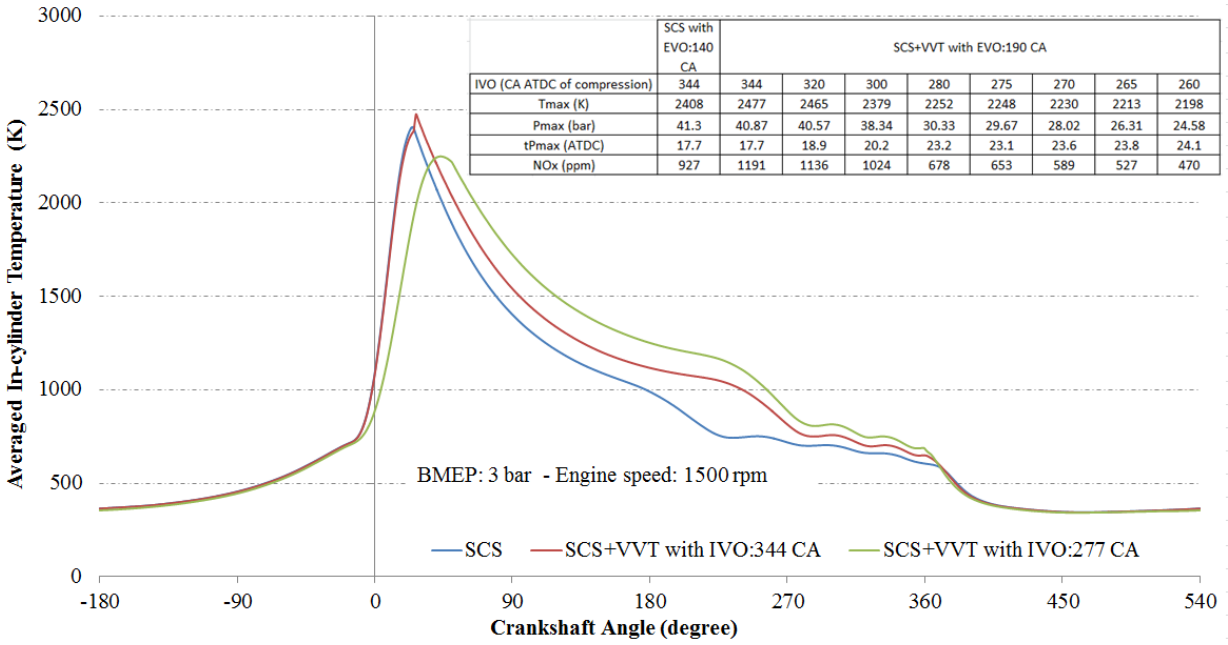

	SCS with EVO:140 CA	SCS+VVT with EVO:190 CA							
IVO (CA ATDC of compression)	344	344	320	300	280	275	270	265	260
Tmax (K)	2408	2477	2465	2379	2252	2248	2230	2213	2198
Pmax (bar)	41.3	40.87	40.57	38.34	30.33	29.67	28.02	26.31	24.58
tPmax (ATDC)	17.7	17.7	18.9	20.2	23.2	23.1	23.6	23.8	24.1
NOx (ppm)	927	1191	1136	1024	678	653	589	527	470

Figure 19. Effect of IVO timing on combustion and early expansion temperature and pressure

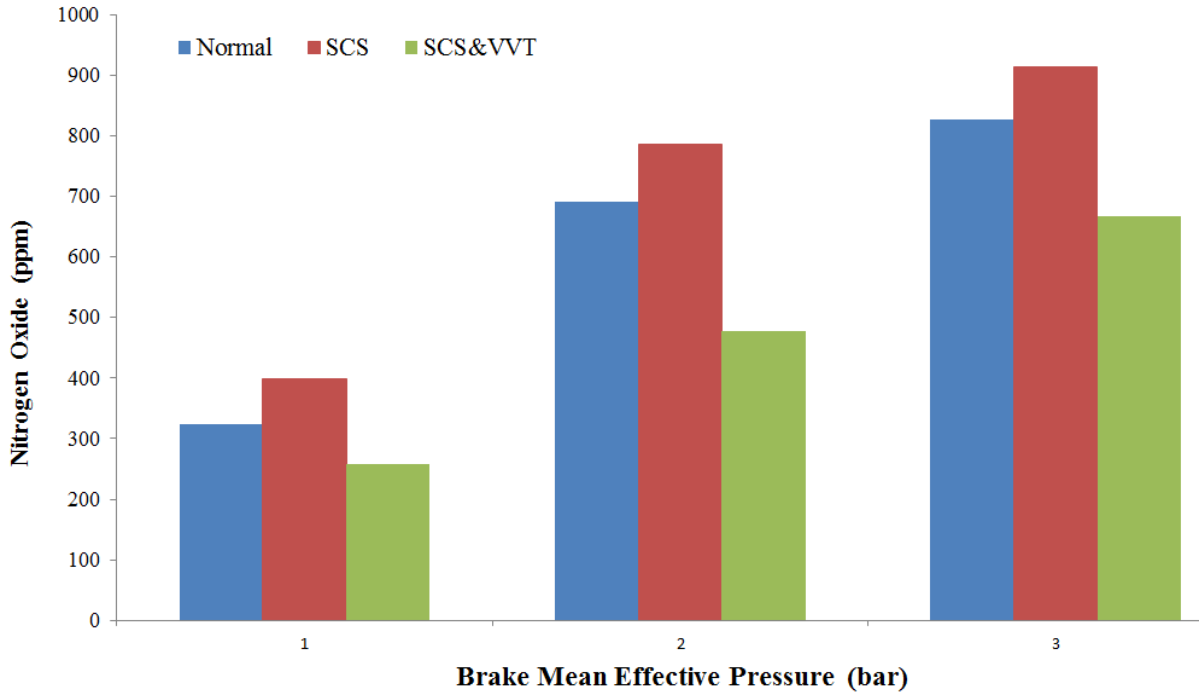

Figure 20. Nitrogen oxide emission comparison via BMEP

Compared to SCS operation, it is observed that in SCS&VVT application, NO_x concentration decreases by 35.1%, 39.4% and 26.8% at 1, 2 and 3 bar BMEP, respectively (Fig. 20). Figure 21 shows a comparison of normal, SCS and SCS&VVT engine operation at low in-cylinder pressure indicating region. The reason of increase in PMEP/GMEP ratio in SCS&VVT is net pumping pressure loss due to late exhaust valve opening as indicated in Fig. 21. The exhaust valve opens after expansion when the piston reaches the bottom dead center (BDC). Hence, the expected pressure drop in SCS&VVT occurs later than in SCS. The characteristic pressure curve of SCS&VVT (green curve in Fig. 21) shows a different pressure trace which causes an additional pumping loss. However, this could not causes an important fuel consumption increase in comparison to SCS operation.

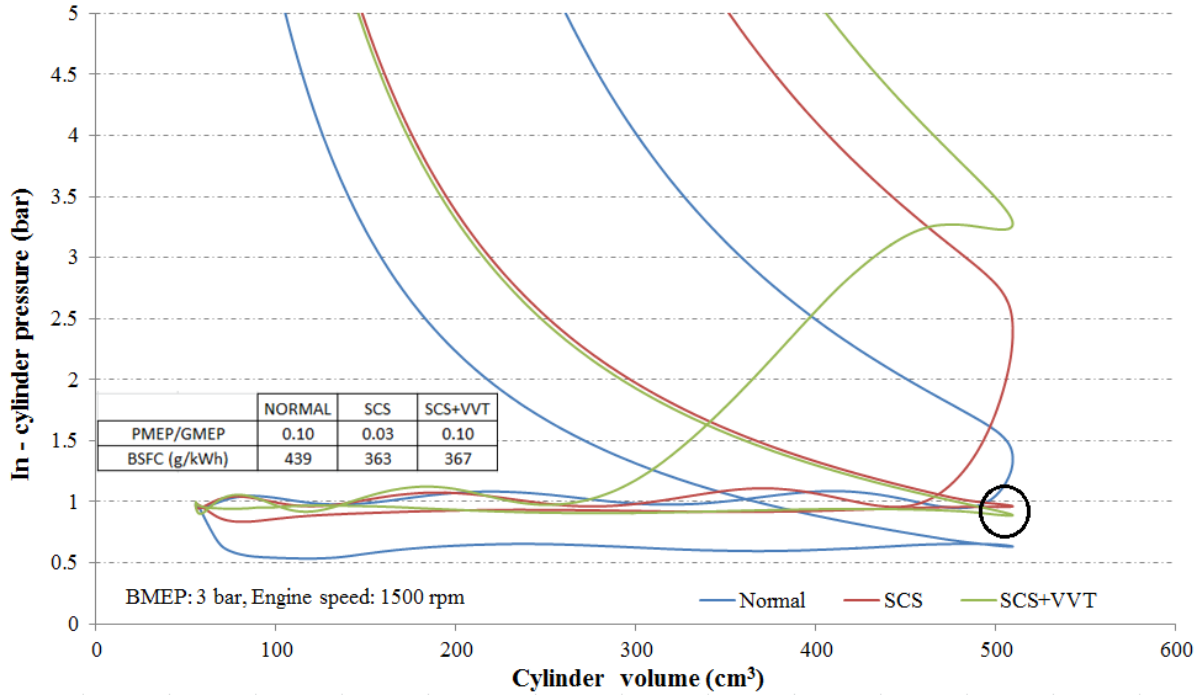

Figure 21. Low pressure indicating comparison of different engine strategies

The other difference between the low pressure indication curves of SCS and SCS&VVT is IVO timing. Because of earlier intake valve opening in SCS&VVT than SCS, in-cylinder pressure drops a little at the end of induction process. This pressure decrease is the key factor of NO_x emission improvement as described before. Furthermore, PMEP/GMEP ratio increases at lower load conditions. As a result of optimisation, intake valve opens earlier at 1 bar BMEP (271 ATDC of compression) in comparison to 3 bar BMEP (280 ATDC of compression).

Figure 22 shows a comparison of normal, SCS and SCS&VVT engine operation at high in-cylinder pressure indicating region. It is seen that maximum pressure range is higher in fired cycle of SCS compared to normal engine operation due to much more fresh charge taken into the combustion chamber. However, maximum cylinder pressure level is again decreased by early IVO action and expanded burning duration in SCS&VVT. Maximum cylinder pressure values are predicted as 16.08 bar, 41.30

bar and 29.95 bar for normal, SCS and SCS&VVT operations, respectively. Due to the expansion of combustion period in SCS&VVT, gross mean effective pressure (GMEP) is higher than in SCS. Gross mean effective pressure ranges of fired cycles are 4.07 bar, 7.79 bar and 8.37 bar for normal, SCS and SCS&VVT, respectively.

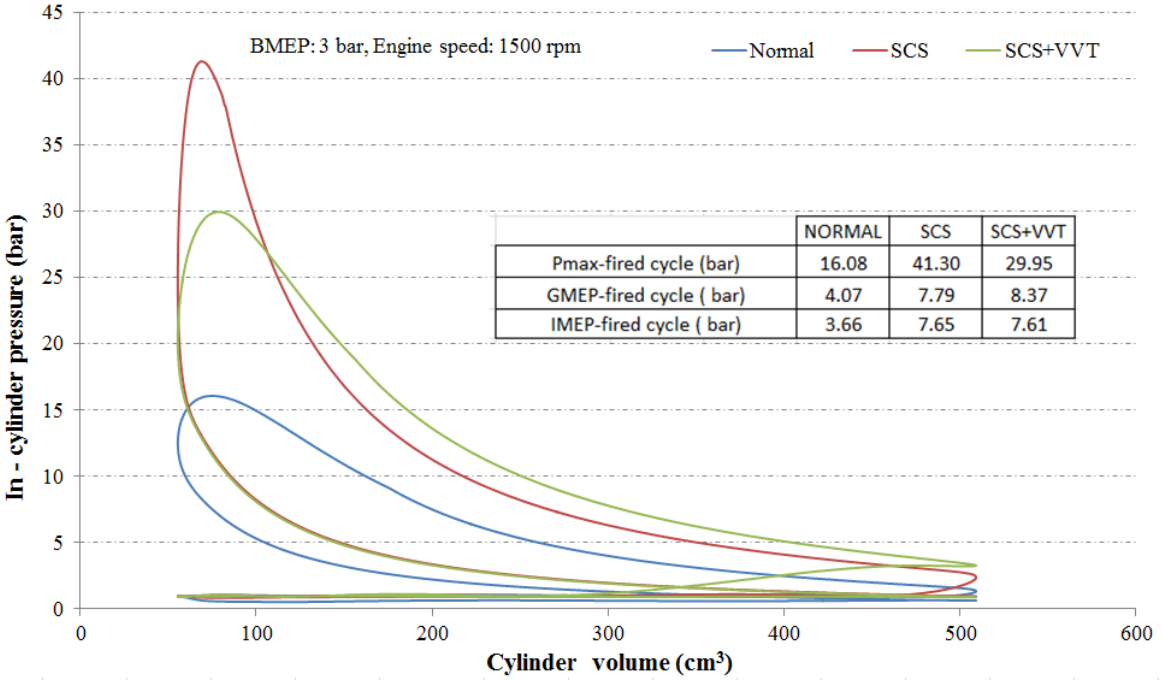

	NORMAL	SCS	SCS+VVT
Pmax-fired cycle (bar)	16.08	41.30	29.95
GMEP-fired cycle (bar)	4.07	7.79	8.37
IMEP-fired cycle (bar)	3.66	7.65	7.61

Figure 22. High pressure indicating comparison of different engine strategies

4. Conclusion

Skip cycle strategy allows a decrease in fuel consumption of gasoline engines through reduced pumping losses at low load engine conditions such as in-city driving or heavy traffic cases. In this study, a detailed numerical investigation has been carried out to investigate the benefits of SCS in achieving lower fuel consumption compared to normal cycle and combination of SCS with variable valve timing strategy in achieving lower exhaust emissions compared to standalone SCS under part-load conditions. Two different variable valve timing strategies were analysed. The numerical computation employed a one-dimensional gas dynamics model based on

717 mean value model approach, Net Power Cycle definition, time dependent fluid
718 governing equations and separated two-zones gas approach for a four-cylinder,
719 water-cooled and port fuel-injected SI engine. The simulations performed at steady
720 state at low load (BMEP: 1-2-3 bar) and low engine speed (1200–1350-1500-1650-
721 1800 rpm) ranges. After numerical spark timing optimisation and validation process of
722 both normal and SCS operations with experimental results, valve timing strategies
723 were integrated into the validated skip cycle engine model. The major findings are
724 summarised as follows:
725 1. As a result of numerical ignition timing optimisation regarding 2-level full factorial
726 experiment design, the spark advance varies from 24.5 CA to 20.7 CA for 1 bar and 2
727 bar BMEP load levels, respectively for normal engine operation at 1500 rpm. At same
728 engine speed, spark advance varies from 18.0 CA to 17.2 CA for 1 bar and 2 bar
729 BMEP load levels, respectively for skip cycle strategy.
730 2. In case of SCS and EIVO (early intake valve opening) application together and
731 valve timing optimisation, NO_x concentration was reduced by 35.1%, 39.4%, 26.8%
732 on average for BMEP load levels of 1, 2 and 3 bar respectively at all engine speed
733 ranges between 1200 and 1800 rpm compared to SCS operation. Early intake valve
734 opening optimisation provided a pressure drop at the end of intake stroke and thus a
735 burning duration expansion and slower combustion process resulting a decrease in
736 cylinder pressure and average temperature and also NO_x emission.
737 3. Late exhaust valve opening (LEVO) decreased HC emission for 54.9%, 49.3% and
738 47.4% on average for BMEP load levels of 1, 2 and 3 bar respectively at all among
739 engine speed ranges between 1200 and 1800 rpm compared to SCS operation. Late
740 exhaust valve timing optimisation provided the minimum in-cylinder pressure level of
741 skipped cycle section of SCS above 0.2 bar in order to prevent undesired lubrication

oil suction to the combustion chamber and also HC production.

4. The addition of variable valve timing strategies to the skip cycle was not led to additional brake specific fuel consumption (BSFC).

Acknowledgments

The first author wishes to thank TUBITAK (Scientific and Technological Research Council of Turkey) 2219 Postdoctoral Research Scholarship Programme for financial support. The authors acknowledge Assistant Professor Doctor Osman Akin Kutlar from Istanbul Technical University for providing experimental data for numerical validation and optimisation.

Nomenclature

SCS	skip cycle strategy	ATDC	after top dead center
NO_x	nitrogen oxide emission	BTDC	before top dead center
HC	unburned hydrocarbon emission	CA50	location of 50% mass fuel burned
N	normal cycle	BDUR	burning duration
S	skipped cycle	ppm	particles per million
F	fired cycle	P_{max}	maximum cylinder pressure
SI	spark ignition	P_{min}	minimum cylinder pressure
MBT	maximum brake torque	cm^3	cubic centimeter
AFR	air-fuel ratio	V	cylinder volume
BSFC	brake specific fuel consumption	K	kelvin
BMEP	brake mean effective pressure	RDE	real driving emission
IMEP	indicated mean effective pressure	CEVC	camless engine valve control
GMEP	gross mean effective pressure	VVT	variable valve timing
PMEP	pumping mean effective pressure	VVL	variable valve lifting
rpm	revolution per minute	EIVO	early intake valve opening
CA	crankshaft angle	LEVO	late exhaust valve opening
TDC	top dead center	DoE	design of experiment

References

[1] Heywood JB. Internal combustion engine fundamentals. USA: Mc Graw-Hill, ISBN 978-0070286375; 1988.

[2] Richard S. Introduction to internal combustion engines. UK: MacMillan, ISBN 978-0230576636; 1999.

[3] Kutlar OA, Arslan H, Calik AT. Methods to improve efficiency of four stroke spark ignition engines at part load. Energy Convers. Manage 2005; 46: 3202-3220. doi.org/10.1016/j.enconman.2005.03.008.

[4] European Commission. Real-driving emissions regulation for passenger and commercial vehicles, https://ec.europa.eu/info/law/better-regulation/initiatives/ares-2016-6339064_en/ [accessed 01 February 2018].

[5] Kutlar OA, Arslan H. Alternative Ignition Systems. In Lackner M. (Ed.). Skip-cycle system for combustion engines (63-84). Verlag ProcessEng Engineering GmbH, ISBN 978-3-902655-05-9; 2009.

[6] Ashok B, Ashok SD, Kumar CR. A review on control system architecture of a SI engine management system. Annual Reviews in Control 2016; 41: 94-118, doi:10.1016/j.arcontrol.2016.04.005.

[7] Liu K, Yang J, Jiang W, Li Y et al. Effect of asynchronous valve timing on combustion characteristic and performance of a high speed SI marine engine with five valves. Energy Convers. Manage 2016; 123: 185-199. doi.org/10.1016/j.enconman.2016.06.042.

[8] Atashkari K, Nariman-Zadeh N, Gölcü M, Khalkhali A et al. Modelling and multi-objective optimization of a variable valve-timing spark-ignition engine using

816 polynomial neural networks and evolutionary algorithms. Energy Convers.
817 Manage 2007; 48: 1029-1041. doi.org/10.1016/j.enconman.2006.07.007.
818 [9] Sher E, Bar-Kohany T. Optimization of variable valve timing for maximizing
819 performance of an unthrottled SI engine-a theoretical study. Energy 2002; 27: 757–
820 775. doi.org/10.1016/S0360-5442(02)00022-1.
821 [10] De Simio L, Gambino M, Iannaccone S, Borrelli L, Gimelli A, Muccillo M.
822 Experimental analysis of a natural gas fueled engine and 1-D simulation of VVT and
823 VVA strategies. SAE technical paper 2013-24-0111; 2013. doi.org/10.4271/2013-24-
824 0111.
825 [11] Gimelli A, Muccillo M, Pennacchia O. Study of a new mechanical variable valve
826 actuation system: Part II - estimation of the actual fuel consumption improvement
827 through one-dimensional fluid dynamic analysis and valve train friction estimation. Int
828 J Eng Res 2015; 16: 762-772. doi.org/10.1177/1468087415604095.
829 [12] Dalla Nora M, Lanzanova TDM, Zhao H. Effects of valve timing, valve lift and
830 exhaust backpressure on performance and gas exchanging of a two-stroke GDI
831 engine with overhead valves. Energy Convers. Manage 2016; 123: 71-83.
832 doi.org/10.1016/j.enconman.2016.05.059.
833 [13] Bonatesta F, Altamore G, Kalsi J, Cary M. Fuel economy analysis of part-load
834 variable camshaft timing strategies in two modern small-capacity spark ignition
835 engines. Appl. Energy 2016; 164: 475-491. doi.org/10.1016/j.apenergy.2015.11.057.
836 [14] Kakaee AH, Mashadi B, Ghajar M. A novel volumetric efficiency model for spark
837 ignition engines equipped with variable valve timing and variable valve lift Part 1:
838 model development. Journal of Automotive Engineering 2017; 231(2): 175-191.
839 doi.org/10.1177/0954407016650545.

[15] Li Y, Khajepour A, Devaud C, Liu K. Power and fuel economy optimizations of gasoline engines using hydraulic variable valve actuation system. Appl. Energy 2017; 206: 577-593. doi.org/10.1016/j.apenergy.2017.08.208.

[16] Venkatesh D, Selvakumar A. A novel design of pneumatic actuator for camless engines. SAE Technical Paper 2016-01-0099; 2016. doi.org/10.4271/2016-01-0099.

[17] Nam K, Choi SB. Development of a camless engine valve actuator system for robust engine valve timing control. Int. J. Veh. Syst. Model. Test 2012; 7.4: 372-389. doi.org/10.1504/IJVSMT.2012.049429.

[18] Mohamed E. Modeling and performance evaluation of an electromechanical valve actuator for a camless IC engine. Int. J. Energy Environ 2012; 3.2: 275-94.

[19] Rioli M, Pivetti G, Ross J, Pietroni A. Pneumatic system for controlling the valves of an internal combustion engine. U.S. Patent No 8,424,499; 2013.

[20] Hoglund A, Carlson U, Von Koenigsegg C. Combustion engine and gas handling system for pneumatic operation of a valve actuator. U.S. Patent Application No 15/025,436; 2016.

[21] Carlson U, Höglund A, Von Koenigsegg C. Internal combustion engine for a vehicle comprising at least one compressor cylinder at least one compressor cylinder connected to a compressed-air tank. U.S. Patent No 8,800,510; 2014.

[22] Rodrigues F, Fernando A, Moreira T et al. E25 stratified torch ignition engine performance, CO_2 emission and combustion analysis. Energy Convers. Manage 2016; 115: 299-307. doi.org/10.1016/j.enconman.2016.02.052.

[23] Zhang B, Ji C, Wang S. Investigation on the lean combustion performance of a hydrogen-enriched n-butanol engine. Energy Convers. Manage 2017; 136: 36-43. doi.org/10.1016/j.enconman.2016.12.065.

[24] Melaika M, Dahlander P. Experimental investigation of methane direct injection with stratified charge combustion in optical SI single cylinder engine. SAE technical paper 2016-01-0797; 2016. doi.org/10.4271/2016-01-0797.

[25] Amrouche F, Erickson Paul A, Varnhagen S, Park Jae W. An experimental study of a hydrogen-enriched ethanol fueled Wankel rotary engine at ultra lean and full load conditions. Energy Convers. Manage 2016; 123: 174-184. doi.org/10.1016/j.enconman.2016.06.034.

[26] Niu R, Yu X, Du Y, Xie H et al. Effect of hydrogen proportion on lean burn performance of a dual fuel SI engine using hydrogen direct-injection. Fuel 2016; 186: 792-799. doi.org/10.1016/j.fuel.2016.09.021.

[27] Li T, Gao Y, Wang J, Chen Z. The Miller cycle effects on improvement of fuel economy in a highly boosted, high compression ratio, direct-injection gasoline engine Energy Convers. Manage 2014; 79: 59-65. doi.org/10.1016/j.enconman.2013.12.022.

[28] Fraser N, Blaxill H, Lumsden G, Bassett M. Challenges for increased efficiency through gasoline engine downsizing. SAE Int J Eng 2009; 2.2009-01-1053: 991-1008. doi.org/10.4271/2009-01-1053.

[29] Tang Q, Fu J, Liu J et al. Comparison and analysis of the effects of various improved turbocharging approaches on gasoline engine transient performances. Appl. Therm. Eng 2016; 93:797-812. doi.org/10.1016/j.applthermaleng.2015.09.063.

[30] Li T, Zheng B, Yin T. Fuel conversion efficiency improvements in a highly boosted spark-ignition engine with ultra-expansion cycle. Energy Convers. Manage 2015; 103:448-58. doi.org/10.1016/j.enconman.2015.06.078.

[31] Li T, Wang B, Zheng B. A comparison between Miller and five-stroke cycles for enabling deeply downsized, highly boosted, SI engines with ultra expansion. Energy Convers. Manage 2016; 123:140-52. doi.org/10.1016/j.enconman.2016.06.038.

[32] Arroyo J, Moreno F, Muñoz M, Monné C. Experimental study of ignition timing and supercharging effects on a gasoline engine fueled with synthetic gases extracted from biogas. Energy Conversion Management 2015 June; 97: pp. 196-211. doi.org/10.1016/j.enconman.2015.03.061.

[33] Isenstadt A, German J, Dorobantu M. Naturally aspirated gasoline engines and cylinder deactivation. International Council on Clean Transportation Working Paper 2016; 12:2016.

[34] Yu S, Ma X, Ma Z, Liu R et al. Experimental and Simulated study on the cylinder deactivation of vehicle gasoline engine. In: Society of Automotive Engineers (SAE)-China Congress 2016; pp. 207-215. doi.org/10.1007/978-981-10-3527-2_19.

[35] Hamid I, Said MFM, Soid SNM, Nasution H. Effect of cylinder deactivation strategies on engine performances using one-dimensional simulation technique. Jurnal teknologi 2016; 78(8-4): 49-55. doi.org/10.11113/jt.v78.9584.

[36] Zainal Abidin SF, Mohd Farid MS, Azhar AA, Mohd AA, and N. I. Arishad. Investigation of performance and fuel economy for cylinder deactivation engine at part load operation. Applied Mechanics and Materials 2016; 819: 443-448. doi.org/10.4028/www.scientific.net/AMM.819.443.

[37] Richardson ES, Soriano BS, Middleton M, Gill M. Efficiency benefits of flexible cylinder deactivation using a novel intake valve system. In: SAE Powertrains, Fuels and Lubricants 2017; 9 pp.

[38] Wilcutts M, Switkes J, Shost M, Tripathi A. Design and benefits of dynamic skip fire strategies for cylinder deactivated engines. SAE Int. J. Engines 2013; 6(2013-01-0359): 278-288. doi.org/10.4271/2013-01-0359.

912 [39] Eisazadeh-Far K, Younkins M. Fuel economy gains through dynamic-skip-fire in
913 SI engines. SAE Technical Paper 2016-01-0672; 2016. doi.org/10.4271/2016-01-
914 0672.
915 [40] Yuksek L, Ozener O, Sandalci T. Cycle-skipping strategies for pumping loss
916 reduction in spark ignition engines: An experimental approach. Energy Convers.
917 Manage 2012; 64: 320-327. doi.org/10.1016/j.enconman.2012.05.025.
918 [41] Wang S, Ji C, Zhang B. Effects of hydrogen addition and cylinder cut-off on
919 combustion and emissions performance of a spark-ignited gasoline engine under a
920 low operating condition. Energy 2010; 35: 4754-4760.
921 doi.org/10.1016/j.energy.2010.09.015.
922 [42] Bech A, Shayler PJ, McGhee M. The effects of cylinder deactivation on the
923 thermal behaviour and performance of a three cylinder spark ignition engine. SAE Int.
924 J. Engines 2016; 9(2016-01-2160): 1999-2009. doi.org/10.4271/2016-01-2160.
925 [43] Kutlar OA, Arslan H, Calik AT. Skip cycle system for spark ignition engines: an
926 experimental investigation of a new type working strategy. Energy Convers. Manage
927 2007; 48: 370-379. doi.org/10.1016/j.enconman.2006.07.004.
928 [44] Saunders RJ, Abdul-Wahab EA. Variable valve closure timing for load control
929 and the Otto Atkinson cycle engine. SAE Technical paper 890677; 1989.
930 doi.org/10.4271/890677.
931 [45] Boggs DL, Hilbert HS, Schechter MM. The Otto–Atkinson cycle engine-fuel
932 economy and emissions results and hardware design. SAE Technical paper 950089;
933 1995. doi.org/10.4271/950089.
934 [46] Goto T, Hatamura K, Takizawa S, Hayama N, et al. Development of V6 Miller
935 cycle gasoline engine. SAE Technical paper 940198; 1994. doi.org/10.4271/940198.

936 [47] Millo F, Mirzaeian M, Luisi S, Doria V et al. Engine displacement modularity for
937 enhancing automotive si engines efficiency at part load. Fuel 2016; 180: 645-652.
938 doi.org/10.1016/j.fuel.2016.04.049.
939 [48] Kuruppu C, Pesiridis A, Rajoo S. Investigation of cylinder deactivation and
940 variable valve actuation on gasoline engine performance. SAE Technical paper
941 2014-01-1170; 2014. doi.org/10.4271/2014-01-1170.
942 [49] Stokes J, Lake TH, Osborne RJ. A gasoline engine concept for improved fuel
943 economy-The Lean Boost system. SAE Technical paper 2000-01-2902; 2000.
944 doi.org/10.4271/2000-01-2902.
945 [50] Lecointe B, Monnier G. Downsizing a gasoline engine using turbocharging with
946 direct injection. SAE Technical paper 2003-01-0542; 2003. doi.org/10.4271/2003-01-
947 0542.
948 [51] Salber W, Wolters P, Esch T, Geiger J, Dilthey J. Synergies of variable valve
949 actuating and direct injection. SAE Technical paper 2002-01-0706; 2002.
950 doi.org/10.4271/2002-01-0706.
951 [52] Hu M, Chang S, Liu L, Xu Y, Xu J. Design and analysis of skip fire valve
952 strategies based on electromagnetic valve train. Appl. Therm. Eng. 2018; 129: 833-
953 840. doi.org/10.1016/j.applthermaleng.2017.10.099.
954 [53] Baykara C, Kutlar OA, Dogru B, Arslan H. Skip cycle method with a valve-control
955 mechanism for spark ignition engines. Energy Convers. Manage 2017; 146: 134-146.
956 doi.org/10.1016/j.enconman.2017.05.016.
957 [54] Feng R, Yang J, Zhang D, Deng B, et al. Experimental study on SI engine fuelled
958 with butanol–gasoline blend and H_2O addition. Energy Convers. Manage 2013; 74:
959 192-200. doi.org/10.1016/j.enconman.2013.05.021.

960 [55] Koç M, Sekmen Y, Topgül T, Yücesu HS. The effects of ethanol-
961 unleaded gasoline blends on engine performance and exhaust emissions in
962 a spark-ignition engine. Renewable Energy 2009; 34(10): 2101-2106.
963 doi.org/10.1016/j.renene.2009.01.018.
964 [56] Cho HM, He BQ. Spark ignition natural gas engines-A review. Energy Convers.
965 Manage 2007; 48(2): 608-618. doi.org/10.1016/j.enconman.2006.05.023.
966 [57] Korakianitis T, Namasivayam AM, Crookes RJ. Natural-gas fueled spark-ignition
967 (SI) and compression-ignition (CI) engine performance and emissions. Prog. Energy
968 Combust. Sci. 2011; 37(1): 89-112. doi.org/10.1016/j.pecs.2010.04.002.
969 [58] Roberts SCE, Mathews RD. Development of an improved ring pack model for
970 hydrocarbon emissions studies. SAE Technical paper 961966; 1996.
971 doi.org/10.4271/961966.
972 [59] Fox JW, Min KD, Cheng WK, Heywood JB. Mixture preparation in a SI engine
973 with port fuel injection during starting and warm-up. SAE Technical paper 922170;
974 1992. doi.org/10.4271/922170.
975 [60] Henning CF, Giles JB. Fuel injection strategies to minimize cold-start HC
976 emissions. SAE Technical paper 970040; 1997. doi.org/10.4271/970040.
977 [61] Cerit M, Ayhan V, Parlak A, Yasar H. Thermal analysis of a partially ceramic
978 coated piston: Effect on cold start HC emission in a spark ignition engine. Appl.
979 Therm. Eng. 2011; 31(2-3): 336-341. doi.org/10.1016/j.applthermaleng.2010.09.015.
980 [62] Rakopoulos DC, Rakopoulos CD, Kakaras EC, Giakoumis EG. Effects of
981 ethanol–diesel fuel blends on the performance and exhaust emissions of heavy duty
982 DI diesel engine. Energy Convers. Manage 2008; 49(11): 3155-3162.
983 doi.org/10.1016/j.enconman.2008.05.023.
984 [63] Cheng WK, Hamrin D, Heywood JB, Hochgreb S et al. An overview of

985 hydrocarbon emissions mechanisms in spark-ignition engines. SAE Technical paper
986 932708; 1993. doi.org/10.4271/932708.
987 [64] Ozcan H, Yamin JA. Performance and emission characteristics of LPG powered
988 four stroke SI engine under variable stroke length and compression ratio. Energy
989 Convers. Manage 2008; 49(5): 1193-1201. doi.org/10.1016/j.enconman.2007.09.004.
990 [65] Al-Baghdadi MAS, Al-Janabi HAS. A prediction study of a spark ignition
991 supercharged hydrogen engine. Energy Convers. Manage 2003; 44(20): 3143-3150.
992 doi.org/10.1016/S0196-8904(03)00127-4.
993 [66] Boam DJ, Clark TA, Hobbs KE. The influence of fuel management on unburnt
994 hydrocarbon emissions during the ECE 15 and US FTP drive cycles. SAE Technical
995 paper 950930; 1995. doi.org/10.4271/950930.
996 [67] Guzzella L, Christopher O. Introduction to Modeling and Control of Internal
997 Combustion Engine Systems. Springer-Verlag Berlin Heidelberg, ISBN 978-3-642-
998 10774-0; 2010.
999 [68] Benedict RP. Fundamentals of pipe flow. USA:Wiley, ISBN 0-471-03375-8; 1980.
1000 [69] Felsch, C., Sloane, T., Han, J., Barths, H. et al., “Numerical Investigation of
1001 Recompression and Fuel Reforming in a SIDI-HCCI Engine,” SAE Technical Paper
1002 2007-01-1878, 2007, doi:10.4271/2007-01-1878.
1003 [70] GT-Power Gamma Technologies Program Help, Version 2012 7.1.
1004 [71] Ricardo Wave User Manual, Version 2016.1.
1005 [72] Abu-Zaid M. Performance of single cylinder, direct injection diesel engine using
1006 water fuel emulsions. Energy Convers. Manage 2004; 45(5): 697-705.
1007 doi.org/10.1016/S0196-8904(03)00179-1.
1008 [73] Dogru B. Skip cycle method investigation at part load conditions of spark ignition
1009 engines. Istanbul Technical University. PhD Thesis; 2015. [in Turkish]

[74] Harada J, Tomita T, Mizuno H, Mashiki Z, et al. Development of direct injection gasoline engine. SAE Technical Paper No. 970540; 1997. doi.org/10.4271/970540.

[75] Zhao FQ, Lai MC, Harrington DL. The spray characteristics of automotive port fuel injection-A critical reviews. SAE Technical Paper No. 950506; 1995. doi.org/10.4271/950506

[76] Ganesan V. Internal combustion engines. India: McGraw Hill Education Pvt Ltd, ISBN 978-1-25-900619-7; 2012.

[77] Isermann R. Engine modeling and control. Berlin: Springers Berlin Heidelberg, ISBN 978-3-642-39933-6; 2014.

[78] Chang R. Physical chemistry for the biosciences. USA: University Science Books, ISBN 1-891389-33-5; 2005.

[79] Taylor CF. The Internal-combustion Engine in Theory and Practice: Combustion, fuels, materials, design (Vol. 2). USA: MIT press, ISBN-13 978-0-262-20052-3; 1985.

Response to reviewers' comments

Manuscript number: ECM-D-18-03419, Energy Conversion and Management

We would like to thanks all three reviewers for their review comments and positive decisions. We also thank the editor for additional comments and recommendations.

We have addressed all comments given by the reviewers and the editor.

Reviewer 1: Reviewer 1 suggested favourable and general comments for the revised version of the manuscript. We would like to thank this reviewer for the comments and addressed his/her comments as follows:

1,Both SCV and VVT performance are analysed with respect to pressure, if possible may give and relate to the power or load.

Answer: The validation of both normal and skip cycle engine with experimental data has been conducted with respect to throttle position (or load) and engine speed. The BMEP levels which represent the related throttle position are indicated in Table 2 titled "Details of simulation set-up". Furthermore, new lines are added into the text in order to give power level information in which the analysis is carried out.

"At 1 bar BMEP, net power levels correspond to 1.83 kW, 2.27 kW and 2.73 kW for 1200 rpm, 1500 rpm and 1800 rpm, respectively. The engine power shifts to different ranges proportional to the load level at given engine speeds"

2. For engine CO_2 emission is a major pollutant, but in your work it is not consider both numerical and experimental results

Answer: CO_2 is a major combustion product and release from the exhaust when you burn hydro-carbon fuel. The combination of skip-cycle strategy and variable valve timing does not influence the major combustion product, but suit well to reduce regulated pollutant emissions such as NOx and HC. This is the problem we have investigated. On the other hand, the averaged difference of CO_2 (%vol) emissions between SCS and normal operation is under 2% due to the experimental results. The CO_2 concentration differs from 13.79 vol% to 14.21 vol% for normal engine case. So there is not a significant difference when it is considered per unit engine work (kg/kWh).

3. How you are validated SCS model with other two models used for NOx and HC emissions

Answer: We have validated numerical results with the experimental data for both normal engine (figure 6 and 7) as well as skip cycle strategy. This has been clearly mentioned at the beginning of section 3.2. Then we combined skip cycle strategy with variable valve timing to further reduce the NOx and HC.

4. Line: 36 not clear reframe the sentence accordingly

Answer: We have revised and strengthened this statement.

5. In general, any simulation model always gives some higher values, but in this work all parameters are minimally only any specific concept or reason

Answer: The modelling results could be over-predicted or under-predicted with the experimental data, depend on the assumption. In our case, we rather have reasonably good comparisons with the experimental data. However, possible reasons for small discrepancy are explained.

6. For journal publication relevant references alone may give -minimize the references if not relevant

Answer: We have considered this comment, but identified that the reference list is very relevant to the SI engine part-load operation, strategies for overcoming emissions at part load operation, numerical modelling and optimisation.

Reviewer 2: Reviewer 2 thinks that paper can be accepted after minor revision. We would like to thank this reviewer and addressed his/her comments as follows:

1. There are number of small grammatical problems in the manuscript. Therefore a carful proof reading is needed.

Answer: We have done a careful proof reading and fixed the small grammatical errors.

2. Abbreviations can only be used after they have been defined and they only need to be defined once.

Answer: We have corrected this issue throughout the manuscript.

3. The format of the References also needs to be fixed, e.g. the style of authors' names of [59], [60] and [63].

Answer: We have corrected this issue throughout the manuscript.

Reviewer 3: Reviewer 3 thinks that the paper can be accepted after some minor corrections. We would like to thank this reviewer and addressed the comments as follows:

1. Fig 2 is an important issue but the resolution must be improved. Much of the internal information is unreadable.

Answer: We have improved the resolution of this figure.

2. How the authors found the activation energy and Arrhenius pre-exponential factor for the described processes evaluated by Equations 13 and 14? How they took into account the factor in-cylinder pressure? In-cylinder pressure is an important factor influencing engine performance and exhausts emissions. Please, include explanation to these in the manuscript.

Answer: We have added a new sentence to clarify this issue. The pre-exponent Arrhenius factor and activation energy are calculated from experimental rate constants that are measured at different temperatures. Since the temperature is depend on in-cylinder pressure, the Arrhenius pre-exponential factor is also influenced by pressure.

3. In line 275 the authors indicated that a validation was developed with a high degree of precision. Nevertheless, very few experimental validation data is used. How this could influence the simulation accuracy?

Answer: We agree with this comment and therefore revised the statement. After the numerical optimisation at these 15 fixed steady state points, the optimised simulation outputs were compared to the test bench experimental data [53,73] and also validated with a reasonably good accuracy.

Editor's comments: We have addressed the editor's comments as follows.

1. Please submit a list or table of changes (or your rebuttal) against each point raised when you upload your revised article and upload this as your 'Response to Reviewers' file/doc - note our system will not allow you to complete the resubmission process without this file.

Answer: We have addressed this comment and provided 'response to reviewers' document'.

2. Also please highlight any revised text using coloured highlighting in a separate word document. This will enable the Editor /Reviewers to identify the amendments and subsequently make faster decisions on the revisions.

Answer: We have highlighted revised texts using red colour in a separate word document.

3. In addition we request one final file, a 'clean' word document of the revised manuscript without any annotations, highlighting or comments, in font 10 or 12 pt with double line spacing.

Answer: We have provided a clean word document of the revised manuscript.

Valve Timing Optimisation of a Spark Ignition Engine with Skip Cycle Strategy

B. Dogru, R. Lot, K.K.J. Ranga Dinesh*

*Corresponding Author, Energy Technology Research group, Faculty of Engineering and the Environment, University of Southampton, Southampton, SO17 1BJ, UK.

Phone: +44 (0)23 8059 2872, email: dinesh.kahanda-koralage@soton.ac.uk

Abstract

Skip cycle strategy (SCS) is a stroke volume modulation method leading to reduction in pumping loss through deactivation of engine valves under part-load conditions. Although SCS achieves a significant fuel economy, it increases regulated pollutant emissions such as nitrogen oxide and unburned hydrocarbon in comparison to normal 4-cycle engine operation. This paper investigated normal cycle strategy, skip cycle strategy as well as combination of skip cycle strategy and variable valve timing strategy for a spark-ignition engine using one-dimensional numerical model. The skip cycle engine was modelled at several steady-state operation points and then optimised at best ignition timing providing maximum brake torque at each simulation case. The numerical results obtained for both normal cycle and skip cycle have been validated against the experimental data. After completing the validation of numerical results with engine test bench data for both normal and skip cycle operations, optimisation of intake and exhaust valve timing profiles have been carried out regarding advancing or retarding camshaft relatively to the crankshaft position. In case of SCS and variable valve timing application together, NO_x concentration was reduced by 35.1%, 39.4%, 26.8% and HC emission was reduced by 54.9%, 49.3% and 47.4% on average for brake mean effective pressure load levels of 1, 2 and 3 bar respectively at all among engine speed ranges between 1200 and 1800 rpm

compared to stand alone SCS strategy. Furthermore, no remarkable additional brake specific fuel consumption was observed for SCS plus variable valve timing strategy compared to stand alone SCS.

Keywords: skip cycle, variable valve timing, fuel economy, unburned hydrocarbon, nitrogen oxide.

1. Introduction

High gas exchange losses and low volumetric efficiency are the main problems effective on fuel consumption and pollutant emissions under urban traffic conditions of spark ignition (SI) engines in which load is conventionally controlled by throttle valve employed between air filter and intake manifold. Due to less fresh charge requirement and the airflow restriction by closer throttle valve position, SI engines are forced to do much more gas exchange work in addition to less power production under part-load conditions [1]. This issue causes poor combustion quality, insufficient combustion speed, and also unexpected further fuel consumption with regards to excessive low indicated efficiency during power cycle at part-load condtions compared to high-lead conditions [2]. In addition, road transport emissions are shown the main source of air pollution and aimed to keep under control by several legislations, policies and regulations [3] (e.g. European Union Directives and Regulations on Motor Vehicles) to ensure a high level environmental protection. In order for adaptation of Euro 6 emission standards to passenger cars and light commercial vehicles in a real driving emission (RDE) test procedure, a new regulation [4] has been reported recently to reflect vehicle emissions along a total trip including urban, rural and motorway route segments better than laboratory testing.

Since all reasons described above, instead of conventional load control based on just throttle valve position, alternative SI engine load control technologies such as variable valve timing (VVT), variable valve lift (VVL), camless engine valve control (CEVC), fuel stratification, turbocharging (or supercharging) and stroke volume modulation strategies have been investigated for two decades to manufacture environment friendly vehicles with a better fuel economy [5]. Thanks to electronic engine control management (EECM) systems which have recently become an essential factor for gasoline engines to perform high engine efficiency and low exhaust emissions while satisfying in driving comfort and road holding issues, these high technology and complex engine solutions are widely used in most of the gasoline engine market [6].

Variable valve timing options such as earlier or later valve opening-closing than default valve profile in terms of rotating camshaft back or forward relatively to the crankshaft, shifting valve duration or valve lifting are very effective on fuel consumption over reducing pumping losses and pollutant emissions over changing in-cylinder states such as pressure and averaged temperature [7-15].

The opinion of camless engines in terms of eliminating camshaft and timing belt allowing valve control by electromagnetic or pneumatic actuators has been afforded for a short time past [16-18]. In this camless concept, an electronically controlled solenoid system allows a fully flexible valve actuation, valve duration shifting and lift adjustment depending on cyclic load and crankshaft speed levels. Although a few engine research and development companies have been working on camless engine prototype experimentation on test bench [19-21], no mass car production has been

presented into market yet due to lack of expected valve activation sensitivity, noise and electrical safety problems.

Fuel stratification method enables a wider throttle valve area and less fuel consumption by supplying a rich mixture near spark plug and a very lean mixture at other regions of combustion chamber [22-26]. Turbocharging and supercharging meet same power requirement with a smaller engine displacement (i.e. engine downsizing) so it offers a better fuel economy and reduced friction losses [27-32]. Stroke volume modulation strategy can be categorised into three groups such as cylinder deactivation (cylinder cut-off), skip fire and skip cycle strategies. Cylinder deactivation can be applied for a cylinder or a group of cylinders permanently during desired operation conditions either by deactivation of intake and exhaust valves to reduce the active stroke volume allowing a reduction in pumping losses as well as heat transfer losses under part-load conditions [33]. A few recent studies have also been reported deactivating a cylinder by means of valve deactivation and combination of spark cut-off and fuel cut-off [34-37]. Skip fire strategy is based on just cutting spark fire in order to deactivate a cylinder depending on driver torque demand [38-39] or skip a power cycle with both ignition and injection disabling [40-42].

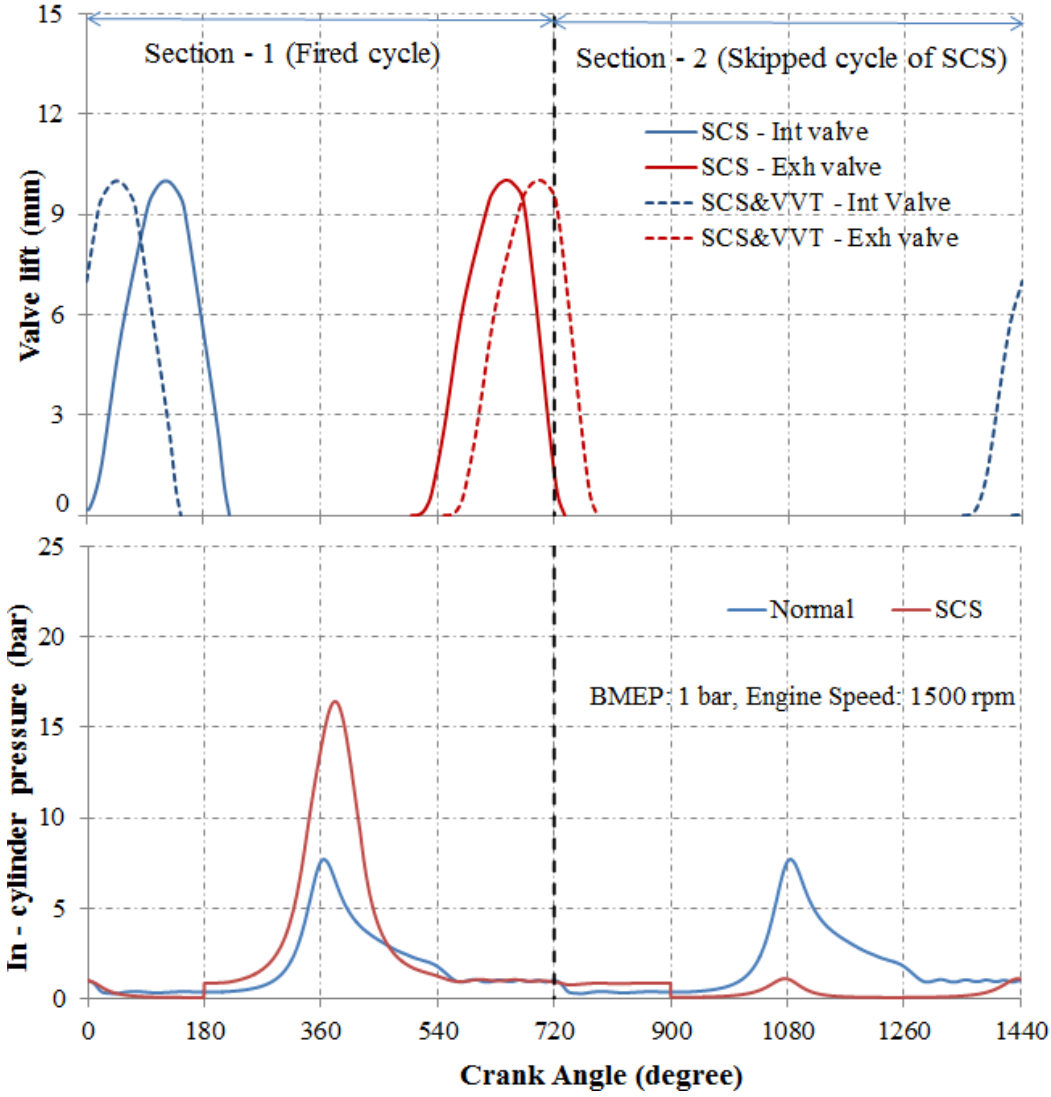

Figure 1. Representation of SCS and proposed further VVT strategies at BMEP: 1 bar and 1500 rpm

Skip cycle strategy (SCS) is another type of stroke volume modulation strategy to vary the power frequency of SI engines under part-load operation conditions [43]. This technique is based on a principle in which valve engagement, fuel supply and spark arc are disabled in several cycles to reduce pumping (throttling) losses therefore to achieve an equivalent power level. In this technique, the fresh charge is increased in sequential cycle as seen in fired cycle section of Fig. 1. However, in contrast to part-load conditions, SCS is not expected to play a major role on fuel

economy at full-load conditions due to lower pumping losses and higher volumetric efficiency as a result of wide open throttle (WOT).

Possible combination selections from among the methods mentioned above could present various advantages in order to overcome efficiency problem of SI engines. The one possible combination studied in the literature was VVT and supercharging combination [44-46]. A few studies were also reported for VVT and cylinder deactivation combination [47, 48]. Other combinations investigated were: supercharging with stratified charge mixture [49]; supercharging with VVT and VVL [50]; cylinder deactivation, VVT and VVL with stratified charge [51]. A recent study reported a camless fully flexible electromagnetic valve train system (without a mechanical valve deactivation) combined with a skip cycle approach with optimum valve timing and lift adjustments to reduce pumping losses [52].

However, combined effect of mechanical skip cycle and variable valve actuation on SI engine performance and emissions has not been investigated so far. Previously, the authors have presented a self-developed novel skip cycle mechanism which has been manufactured to engage or disengage the intake and exhaust poppet valves [53]. Despite achieving significant fuel saving under part-load operation conditions in this experimental SCS investigation, nitrogen oxide (NO_x) concentration could increase due to higher fresh charge and averaged cylinder temperature rise as observed in [54-56], hydrocarbon (HC) emissions in terms of incomplete combustion products could also increase due to undesired oil suction from crankcase to cylinder as mentioned in [57-60], flame quenching on cylinder wall as discussed in [61-63], and deposit of unburned mixtures in crevice cylinder volumes such as piston liner,

valve seat and spark plug thread as discussed in [64-66] in comparison to normal (N) 4-cycle engine operation.

The objective of the present study is to mitigate the unfavourable exhaust gas emissions of a skip cycle SI engine under part-load conditions. Two variable valve timing strategies (EIVO: early intake valve opening, LEVO: late exhaust valve opening) along with skip cycle strategy are investigated for an SI engine using a one-dimensional simulation model. Firstly, the skip cycle strategy was modelled and ignition timing was optimised based on minimum spark advance for maximum brake torque (MBT) at 15 steady-state simulation points including low load (break mean effective pressure, BMEP: 1-2-3 bar) and low engine speed (1200-1350-1500-1650-1800 rpm) ranges. Secondly, the simulation results for both normal engine and SCS were verified with the experimental data for a four cylinder water-cooled naturally aspirated SI engine with 1.8 litre stroke volume and stoichiometric air-fuel ratio (AFR=14.6) in which SCS was carried out. Then intake valve timing and exhaust valve timing were optimised and integrated into the model in a way that the valve duration and the valve lift are kept default in the engine configuration. The comparative results regarding engine performance and engine-out emissions will be presented for normal operation, SCS and SCS with variable valve timing (SCS&VVT) strategies. The findings of this study will help to identify the advantage of combining skip cycle strategy with variable valve timing in achieving lower engine exhaust emissions with better fuel economy.

2. Numerical model architecture

Simulation of normal engine operation and proposed skip cycle strategy was carried out using a one dimensional Ricardo Wave gas dynamics analysis software. Software library is based on physical principles of “Mean Value Model” which assumes all processes and effects are spread out over the engine cycle, all boundary conditions at the beginning of an engine cycle are fixed and the same initial starting conditions are exposed [67]. In order to build up base engine model, predictive engine parameters such as throttle valve position, burning duration (BDUR) and 50% fuel mass burned (CA50) are used to estimate the engine performance at several low BMEP load levels and engine speed ranges. BDUR is rapid burning angle as a crank interval required to burn the bulk of mixture charge and CA50 corresponds to crankshaft angle where half of fuel heat is released due to the combustion. Both are very important for representing combustion curve characteristics [1]. The pre-validation process showed that predicted CA50, BDUR and throttle valve angles using for combustion model calculation are very compatible to experimental test bench data. The nominal engine features at full load condition are given in Table 1.

Table 1. Nominal engine specifications at full load condition

Feature	Value
Displacement	1820 cc
Number of cylinders	4 (in-line)
Bore×Stroke	85×80 mm
Compression ratio	9:1
AFR (Air-fuel ratio)	14.6

Power	27.3 kW@2400 rpm
Torque	108.7 Nm@1600 rpm
BMEP	7.5 bar
Timing of IVO (intake valve opening)	16°CA BTDC
Timing of EVO (exhaust valve opening)	40°CA BBDC
Valve duration	236°CA (for both intake and exhaust)

Modelling of skip cycle strategy needs a full valve deactivation for the skipped cycle and higher fresh mixture for the fired cycle of two sequential cycles (Fig. 1). In this study, a new approach consisting of a fired (F) cycle and a skipped cycle (S) is applied into the simulation model to reflect a “Net Power Cycle” definition derived from these two cycles in order to allow an equivalent power level with a normal (N) operation cycle. Since more fresh charge is inducted to the engine in fired section of two sequential cycles, throttle valve must be opened wider and spark timing must be adjusted closer to compression top dead centre (TDC) due to having a higher cylinder compression pressure and a better flame development. A wider throttle valve position provides a decrease in pumping losses and fuel consumption. In calculation of net power cycle, net cycle power is obtained with extraction of fired cycle power from skipped cycle power (Eq.1). The indicating parameters such as GMEP (gross mean effective pressure) and IMEP (indicated mean effective pressure) are calculated as an average cycle value (Eq. 2 and Eq. 3) to represent a virtual cycle giving target power demand. The net power cycle concept is also referred in experimental data calculations. The equations used for a “Net Power Cycle” are described as following (Eq.1-6):

$$Power_{net} = Power_{cycle-F} - Power_{cycle-S} \quad (1)$$

$$GMEP_{net} = \left(GMEP_{cycle-F} - GMEP_{cycle-S}\right)/2 \quad (2)$$

$$IMEP_{net} = \left(IMEP_{cycle-F} - IMEP_{cycle-S}\right)/2 \quad (3)$$

$$PMEP_{net} = GMEP_{net} - IMEP_{net} \quad (4)$$

$$BMEP_{net} = \frac{1200 \times Power_{net}}{V_h \times n} \quad (5)$$

$$FMEP_{net} = BMEP_{net} - IMEP_{net} \quad (6)$$

where $GMEP_{net}$ (bar) is net gross mean effective pressure, $IMEP_{net}$ (bar) is net indicated mean effective pressure, $PMEP_{net}$ (bar) is net pumping mean effective pressure, V_h (litre) cylinder displacement, n (1/sec) is crankshaft revolution per minute and $FMEP_{net}$ (bar) is net frictional mean effective pressure.

The modelling framework consists of time-dependent governing equations involving the simultaneous of the flow in a duct configuration. By assuming flow varies only in stream wise direction (x-direction), the governing conversation equations of mass (Eq.7), energy (Eq.8) and momentum (Eq.9) of unsteady compressible fluid motion can be written as follows [68]:

$$\frac{\partial \rho}{\partial t} + \frac{\partial}{\partial x}(\rho u_x) = 0 \quad (7)$$

$$\frac{\partial}{\partial t}[\rho h] + \frac{\partial}{\partial x}[\rho u_x h] = \frac{\partial \rho}{\partial t} + u_x \frac{\partial p}{\partial x} + \tau_{xx} \frac{\partial u_x}{\partial x} - \frac{\partial q_x}{\partial x} + \dot{Q} + \dot{W}_{ext} \quad (8)$$

$$u_x \frac{\partial}{\partial x}[\rho u_x] + \frac{\partial}{\partial t}[\rho u_x] = -\frac{\partial p}{\partial x} + \frac{2}{3}\mu\left(2\frac{\partial^2 u_x}{\partial x^2}\right) \quad (9)$$

where ρ (kg/m^3) is fluid density, t (sec) is time, u_x (m/s) is averaged axial velocity, h (J/kg) is enthalpy, p (N/m^2) is pressure, τ_{xx} (N/m^2) is viscous shear stress, q_x (J/m^{2}s) is heat flux, $\dot{Q}$ (J/s) is heat source, $\dot{W_{ext}}$ (J/s) is external work and μ (kg/ms) is dynamic viscosity.

The equations are spatially discretised using a second order finite difference method and the time integration is based on the first order explicit method. The mass equation accounts for changes of in-cylinder mass due to flow through valves and due to fuel injection. The energy equation is based on the first law of thermodynamics and equates the change of internal energy of in-cylinder gases to the sum of enthalpy fluxes in and out of the chamber, heat transfer, and piston work [69].

Since combustion occurs through a flame propagation process, the changes in gas temperature, pressure and density require a separated gas approach in the combustion chamber as burned and unburned regions [1]. The two-zone model is used to capture more details about the chemical processes taking place during the combustion period. Hence, all the sub-models (combustion model, heat transfer model and emission models) are performed by two zones assumption which the mixture is conceptually divided into burned and unburned zones.

Based on mean value model approach, Net Power Cycle definition, time dependent fluid governing equations and separated two-zones gas approach described above , each engine component is modelled by simulation elements such as orifices (joints linking two ducts), throttle valve, ambient (flow termination for intake and exhaust), engine valves, engine cylinders, ducts (connecting orifices or junctions) and Y–junctions (using for modelling spherical volumes representing a compatible geometry with original engine dimensions and configuration). In the proposed simulation; 75 ducts, 38 orifices and 23 Y-junctions are used to discretize large single volume geometry into sub-volumes to show the pulsed characteristics of fluid propagation better than constant as in mean value models [70]. Moreover, 4 injectors, 8 engine

valves, 1 throttle valve, 2 ambients and 4 engine cylinders are integrated into the model (Fig. 2).

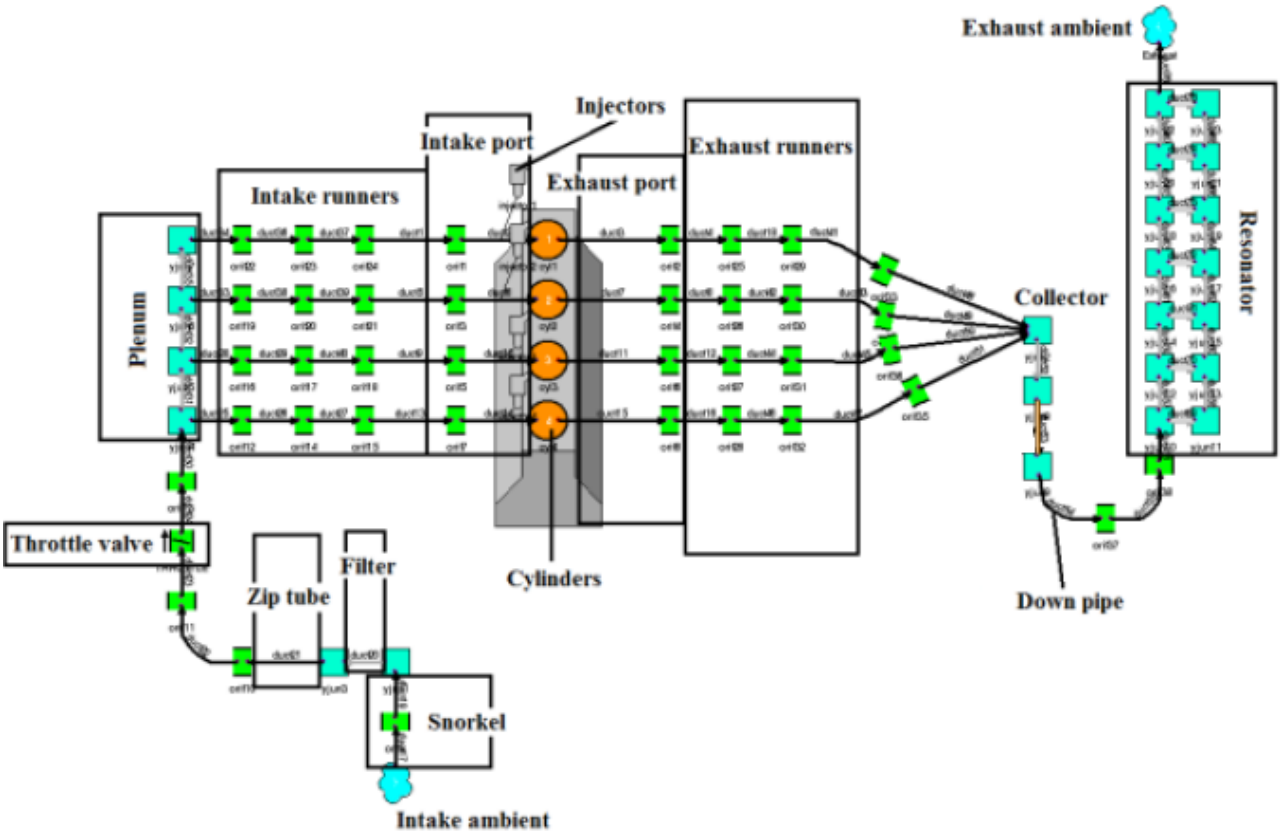

Figure 2. Basics elements of the modelled naturally aspirated gasoline engine

The model of combustion is achieved with calculation of heat release phenomenon regarding in-cylinder pressure trace during the combustion period. SI Wiebe correlational (Eq.10) carried out to identify the rate of fuel mass burned as a function of crankshaft angle [1]:

$$W = 1 - exp\left[-a\left(\frac{\theta-\theta_0}{\mathrm{BDUR}}\right)^{m+1}\right] \quad (10)$$

where W is cumulative burned mass fraction, BDUR (°CA) is combustion duration, θ (°CA) is crank angle and θ_0 (°CA) is start of combustion crank angle and m is Wiebe function exponent.

The basic Woschni correlation, assuming a simple heat flux from confined

combustion gas volume to the engine walls such as cylinder head, cylinder liner, piston face, and valve head, is applied for convective heat transfer (Eq.11). However, Annand heat transfer model [71] is widely used in practical due to more realistic modelling approach in which constant gas velocity assumes equal to the mean piston speed:

$$Q = h_g \times A \times (T_g - T_w) \quad (11)$$

where Q (W/m^2) is overall heat loss to the walls, h_g (W/m^2K) is heat transfer coefficient, A (m^2) is heat exposed combustion chamber surface area, T_g (K) is cylinder gas temperature and T_w (K) is cylinder wall temperature.

Annand heat transfer coefficient [71] is given below (Eq.12):

$$h_g = \left(a\left(\frac{\rho\, v_m D}{\mu}\right)^{0.7}\right) \times \frac{k}{D} \quad (12)$$

where a is heat transfer multiplier, ρ (kg/m^3) is gas density, v_m (m/s) is mean piston speed, D (m) is cylinder bore, μ (kg/ms) is dynamic viscosity and k (W/mK) is thermal conductivity.

NO_x prediction based on Zeldovich mechanism is calculated by Arrhenius Equation (Eq.13) relating chemical reaction rate to temperature as given below:

$$NO_x(T) = A \times e^{-E/RT} \quad (13)$$

where T (K) is absolute burned zone temperature, A is pre-exponent Arrhenius factor, E (kJ/kmol) is activation energy of the reaction and R (kJ/kmolK) is universal gas constant. The pre-exponent Arrhenius factor and activation energy are calculated from experimental rate constants that are measured at different temperatures.

HC emission production is simulated based on post-flame oxidation [71] of unburned

fuel returning to the combustion chamber after combustion (Eq.14):

$$\frac{d[HC]}{dt} = -C_R \times A \times \exp\left(-\frac{E}{RT}\right)[HC]^a[O_2]^b \quad (14)$$

where C_R is calibration constant and O_2 (ppm) is oxygen concentration.

The work from cylinder gases to the piston cannot be transferred without any mechanical losses. The difference between indicated power and brake engine power is defined as a frictional term including friction of rotating engine parts and external auxiliary engine accessories driven by engine crankshaft such as cooling fan, water pump and oil pump. Friction power is very dominant at high speeds resulting in fuel consumption increase [72]. The numerical frictional mean effective pressure (FMEP) is calculated by using Chen-Flynn correlation predicting frictional losses with test cell data correlation. After measuring experimental frictional losses, the coefficients of Chen-Flynn correlation (Eq.15) should be fitted to measure FMEP data appropriate different engine speed and load conditions.

$$FMEP = ACF + BCF(P_{max}) + CCF(rpm \times stroke/2) + QCF(rpm \times stroke/2)^2 \quad (15)$$

where ACF (bar) is frictional pressure constant, BCF is maximum cylinder pressure factor varying with peak cylinder pressure, CCF (Pa/min×m) and QCF ($Pa/min^2/m^2$) are mean piston velocity factors accounting for changes in engine speed.

By using the sub-models above, the engine simulation was carried out at 1-2-3 bar BMEP and 1200-1350-1500-1650-1800 rpm engine speed ranges. BMEP ranges nearly correspond to 14%, 27% and 41% throttle positions for 1, 2 and 3 bar, respectively (Table 2). At 1 bar BMEP, net power levels correspond to 1.83 kW, 2.27 kW and 2.73 kW for 1200 rpm, 1500 rpm and 1800 rpm, respectively. The engine power shifts to different ranges proportional to the load level at given engine speeds.

After the numerical optimisation at these 15 fixed steady state points, the optimised simulation outputs were compared to the test bench experimental data [53,73] and also validated with a reasonably good accuracy.

Table 2. Details of the simulation set-up

Parameter	Value
BMEP (bar)	1-2-3
Engine speed (rpm)	1200-1350-1500-1650-1800
Throttle position (%)	14-27-41

3. Results and Discussion

In this study, the normal engine model is based on architecture in which Woschni combustion model, Annand heat transfer model, Arrhenius NO_x emission model, post flame oxidation HC emission model and Chen-Flynn friction model are considered. The skip cycle engine model is established on models described above and an additional approach called “Net Power Cycle” which can calculate net indicating parameters and brake outputs along a sequential cycle group including a normal cycle and a following skipped cycle with high accuracy verification.

At first stage of numerical analysis, ignition timing optimisation is carried out for both normal operation and skip cycle strategy within each simulation case for equivalent experimental power ranges. The optimised numerical results are validated with the experimental data for both normal cycle and skip cycle. Then the numerical study is extended by combining skip cycle technique and variable valve timing strategy to further eliminate exhaust gas emissions appear as a result of standalone skip cycle

technique. Two variable valve timing strategies are investigated and optimised with regards to reducing hydrocarbon and nitrogen oxide emissions by late exhaust valve opening (LEVO) and early intake valve opening (EIVO) approaches.

3.1. Numerical optimisation of ignition timing

Fuel injection timing and injection pressure are two important engine input parameters providing a fine fuel-air mixture and flame propagation in combustion chamber for direct injection SI engines [74]. However, the effect of injection phenomenon does not play a crucial role on combustion quality, fuel consumption and exhaust pollutants for homogeneous charge port fuel injection (PFI) methodology since lower fuel injection pressure (3-15 bar) and fresh charge are premixing and evaporate before entering into the combustion chamber. In case of cold start, the interaction between air and fuel droplets could affect the engine performance [75]. In this study, the fuel spray effects are neglected due to loaded operating conditions.

The main predictive optimisation parameter is ignition timing which shows relative position of combustion initiation to the compression top dead center (TDC). Spark plug usually ignites the mixture before TDC based on engine operating conditions in order to burn mixture completely. Retarded ignition timing shifts peak cylinder pressure towards the late expansion stroke with lower magnitude and incompleted burning. On the other hand, advanced spark timing causes a fast burning cycle and knock tendency [76]. The optimum ignition timing which gives maximum engine torque, called MBT timing, occurs when magnitude of these two opposing trends (retarding and advancing) just offset each other. Timing which is advanced or retarded from the optimum ignition timing, gives a lower torque value [1].

Executing a detailed engine map (spark advance-load-rpm matrix) through optimisation process on test bench is not comfortable with regards to time and fuel cost for all operation points. Therefore, 2-D interpolation table of spark timing optimisation was obtained depending on average in-cylinder pressure and engine speed conditions as a result steady-state model simulations (see Fig. 4). The numerical calculation allows us to integrate DoE (design of experiment) with "Two-stage" test strategy. In Two-stage model [77], all conditions such as engine speed, load, intake and exhaust settings were kept fixed and just spark timing and throttle valve angle input parameters were manipulated to obtain MBT for optimum spark advance close to TDC as much as possible for the same target engine power. Throttle angle and spark timing independent input parameters were used in a "2-level full factorial experiment" design with all combination settings between either their minimum and maximum values.

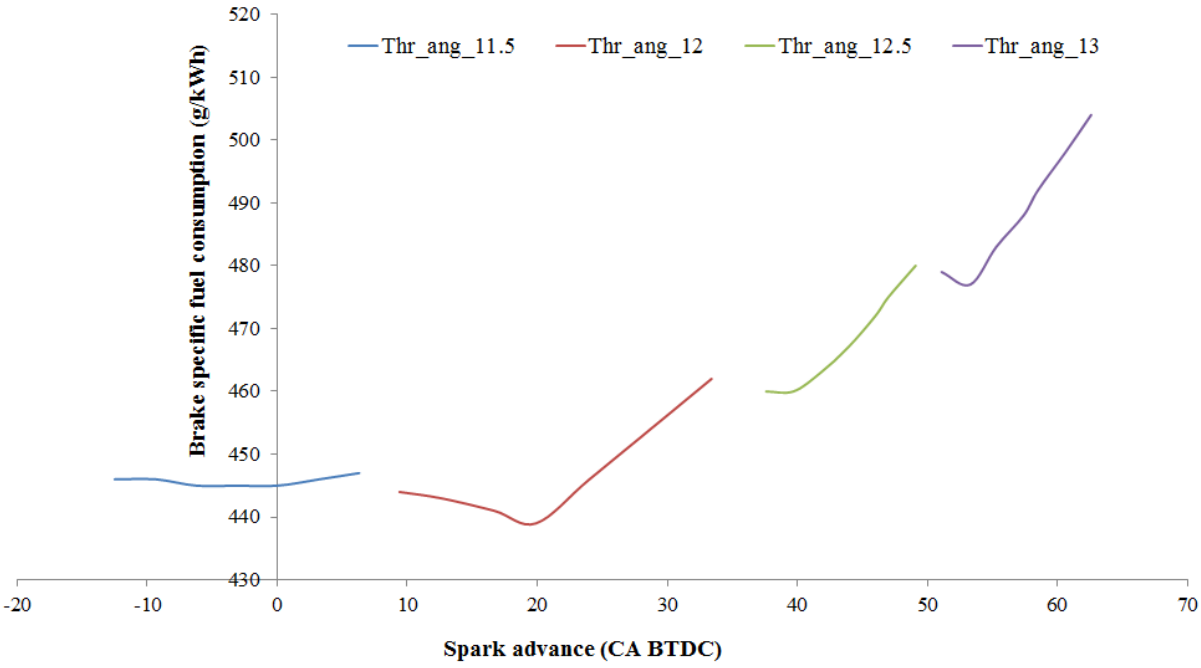

Figure 3. Numerical optimisation of normal engine performance via spark advance (BMEP: 3 bar, 1500 rpm)

Figure 3 shows the impact of different ignition advances on brake specific fuel consumption at 3 bar brake mean effective pressure and 1500 rpm engine speed conditions for normal engine operation. All input parameters except for throttle angle and ignition timing were kept constant. The main goal of numerical optimisation process was to find out minimum spark advance closest to TDC when throttle valve opening enough to reach target torque value. Thanks to four different throttle positions (11.5°-12.0°-12.5° and 13.0°) and twenty-eight different spark timing (varying between -12.5 CA BTDC and 62.5 CA BTDC) and also their combinations, best spark advance point was obtained over four throttle angle curves. As seen in Fig. 3, for 41% load level (BMEP=3 bar) and 1500 rpm engine speed, the optimum spark advance was obtained as 19.9 CA BTDC for 12° throttle angle. At 12° throttle angle position, a value of 9.4 CA increase of the spark advance or 7.3 CA retarding from the optimum increases BSFC by about 3.6% and 0.9 % respectively. Compared to optimised combination (12° throttle angle and 19.9 CA BTDC), in case of 12.5 ° or 13.0° throttle angle at several spark timings, fuel consumption increases by 6.6% and 11.3% on average, respectively. If the throttle is closed to 11.5 ° position, BSFC values increased again and otherwise any spark timing could not reach target torque (for example at 11.5 ° position, BMEP could not be higher than 2.75 bar).

In Fig. 4, the points indicate the experimental data and solid lines represent extended optimal engine map as a result of DoE for each individual simulation case. As seen in Fig. 4, the spark timing was advanced while the engine speed increases and also retarded as the engine is loaded. For example, at 1500 rpm, the spark advance varies from 24.5 CA to 20.7 CA for 27% and 41% loads, respectively for normal engine operation. At same engine speed, spark advance varies from 18.0 CA to 17.2

CA for 27% and 41% loads, respectively for skip cycle strategy.

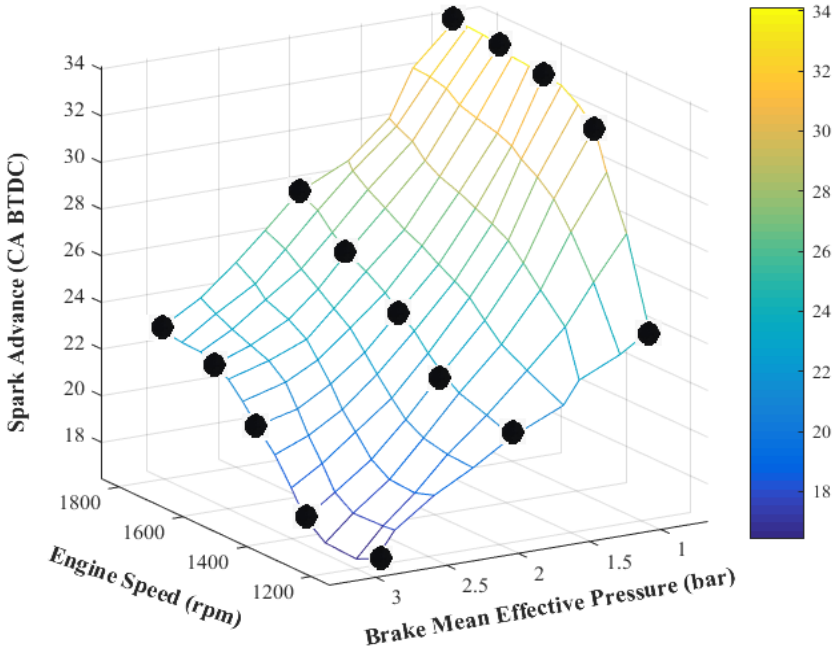

Figure 4. 2-D contour map of optimised spark timing for normal operation

3.2. Model validation with experimental data

This section discusses comparison between optimised numerical results with the engine experimental data for two different engine operating strategies (Figs. 5-12). These are normal engine operation and skip cycle strategy. It is noted that the engine on the test cell is already optimised. For all of the experimental points, intake and exhaust valve timings, valve durations and the stoichiometric AFR values (Table 1) are kept constant. Steady state engine tests are performed at the ranges of part-load (BMEP = 1.0, 2.0 and 3.0 bars) and fixed engine speeds (1200, 1350, 1500, 1650 and 1800 rpm). At each operation point, optimum spark timing is calibrated with regards to maximum brake torque criteria with a throttle valve wide as much as open to allow more fresh intake air into the cylinder. First we validate numerical results with the experimental data for the normal engine.

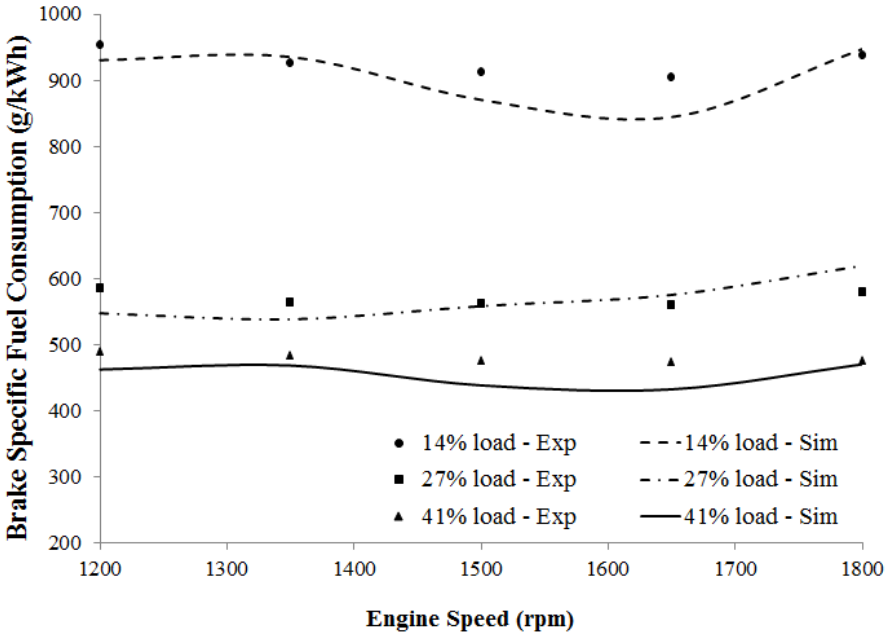

Figure 5. BSFC validation for normal engine operation

Figure 5 shows brake specific fuel consumption comparison between numerical and experimental data at three different load conditions. It is seen that numerical results under predict the experimental data for the low load conditions (at 1500 rpm and 14% load, the prediction error of fuel consumption is about 4.6%). This may happen due to experimental measurement errors of spark advance or throttle position during an engine operation at low load conditions, such as 14%. A prediction error in terms of fuel consumption at a range of 4.6% could be explained by a very small reading error for spark timing or oscillation of engine speed in ±50 rpm range. Nevertheless, the comparison shows good agreement between numerical results and the experimental data at mid-range load conditions.

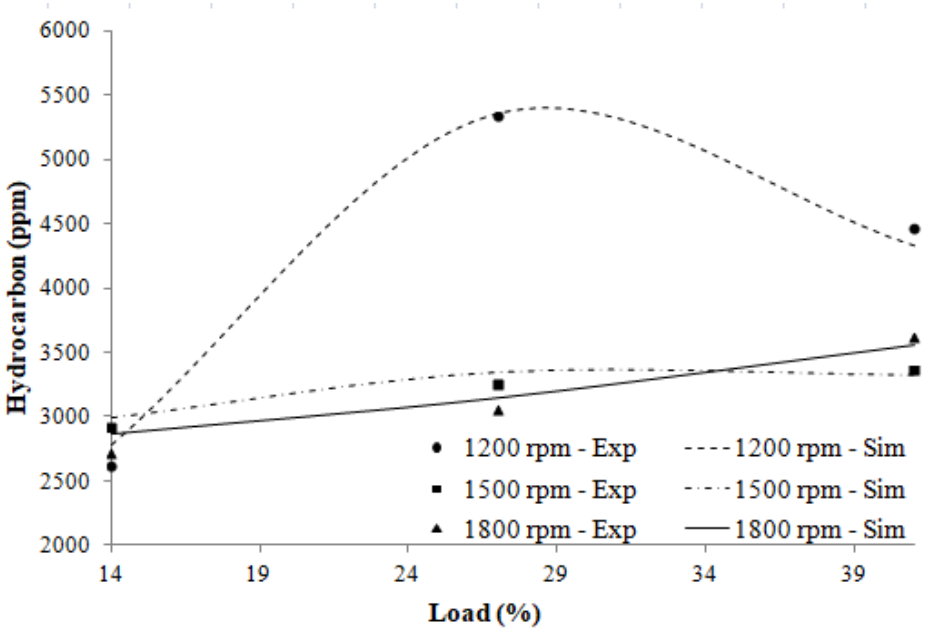

Figure 6. HC Emission validation for normal engine operation

At 3 bar BMEP, HC emission in experiment result is higher than that of simulation results (Fig. 6). This is because of lower combustion velocity in experiment than the simulation and also extension of deflation zone near the chamber wall at expansion process of experimental cycle. This can be further understood from the in-cylinder pressure curve. For example, in Fig. 8, while the pressure rising rate ($dP/d\theta$) in compression process of simulation is equal to the experiment, then it becomes higher near the TDC.

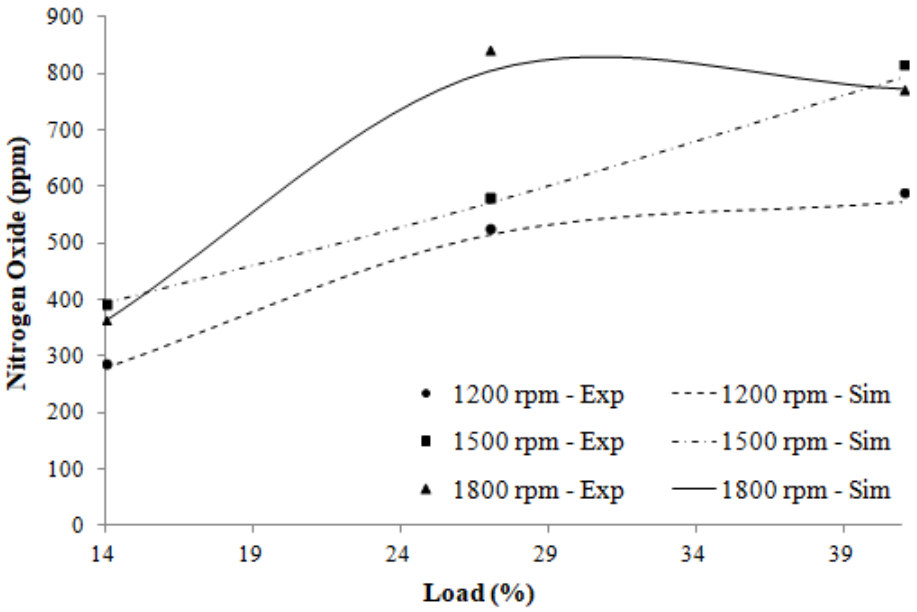

Figure 7. NO_x Emission validation for normal engine operation

At 3 bar BMEP and 1500 rpm range, prediction errors are about 1.1% and 2.9% for HC (Fig. 6) and NO_x (Fig. 7) emissions, respectively. As seen in Fig. 7, NO_x emissions increase while the engine runs at higher speeds. The first reason is relative combustion duration extension as crank angle degrees at high speed ranges. Hence, rate of development and propagation of the premixed engine flame increases due to the higher turbulence level in cylinder. The second one is residual gas fraction reduction (means more fresh oxygen for the next cycle) as speed increases. The last one is higher mean combustion chamber temperature as a result of relative less heat transfer per cycle [1]. However, NO_x emission slightly decreases from 1650 rpm to 1800 rpm at 1 bar and 3 bar BMEP loads (Fig. 7). The possible reason could be due to local chamber temperature decreases as from the speed range where the maximum brake torque occurs. NO_x increases with increasing load because of the same reasons mentioned earlier with respect to increasing speed. On the other hand, HC concentration decreases modestly when the load is increased. As load increases at constant speed, the temperature in expansion and exhaust strokes increase, and the in-cylinder oxidation rate can increase with sufficient oxygen [1].

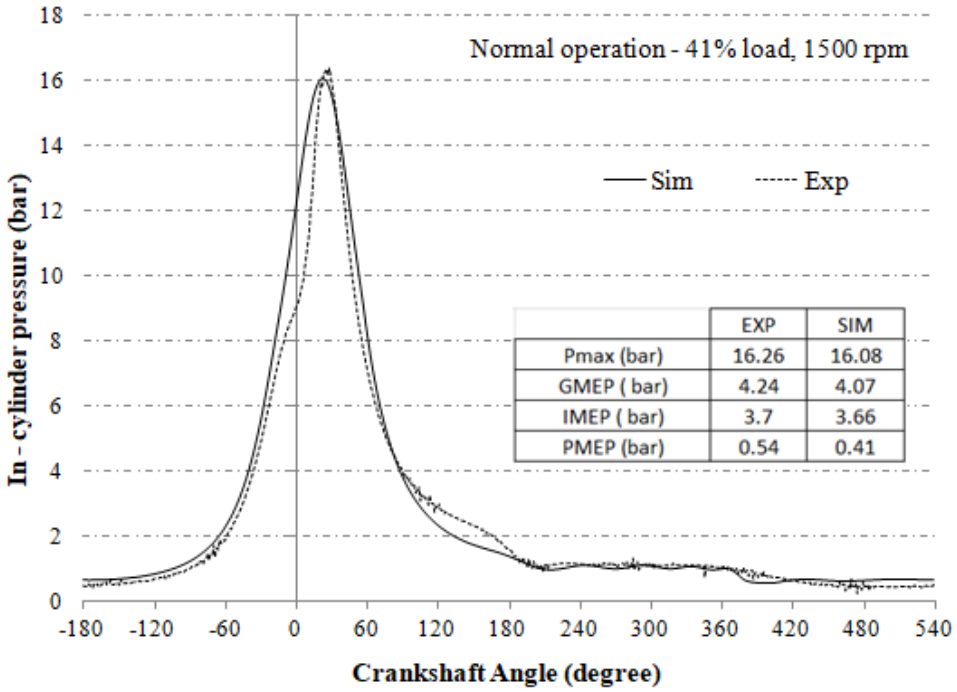

Figure 8. Validation of In-Cylinder pressure curves for normal engine operation at 3 bar BMEP and 1500 rpm engine speed

Figure 8 represents a comparison of in-cylinder pressure curves via crankshaft angle of numerical results and experimental indicating data for 41% load level and 1500 rpm speed range. The graph shows that the pressure curve trace, maximum cylinder pressure value and timing results are very close to the experiments. It is a clear proof for the accuracy of combustion model (Eq.10) which is the key sub-model showing the main characteristics of the cycle modelling.

The model based calibration results show that for an equivalent torque demand value (Brake mean effective pressure: BMEP=1-2-3 bar and engine speed: n=1200-1350-1500-1650-1800 rpm), relative model prediction errors are on average under 2.8%, 0.2% and 1.7% for fuel consumption, HC and NO_x emissions, respectively for normal engine operation. Besides the available model predicts spark advance, maximum cylinder pressure (P_{max}) and volumetric efficiency with an averaged error under 0.8%, 4.9% and 0.4% respectively.

Now, we discuss the comparison of skip cycle engine simulation results with the experimental data. As seen in Figs. 9-12, the proposed model for SCS makes a good agreement with the experimental data. It indicates validation errors under 2.3%, 0.5%, 0.3%, 0.5%, 4.9% and 0.5% on average for fuel consumption, HC, NO_x, spark advance, volumetric efficiency and P_{max}, respectively.

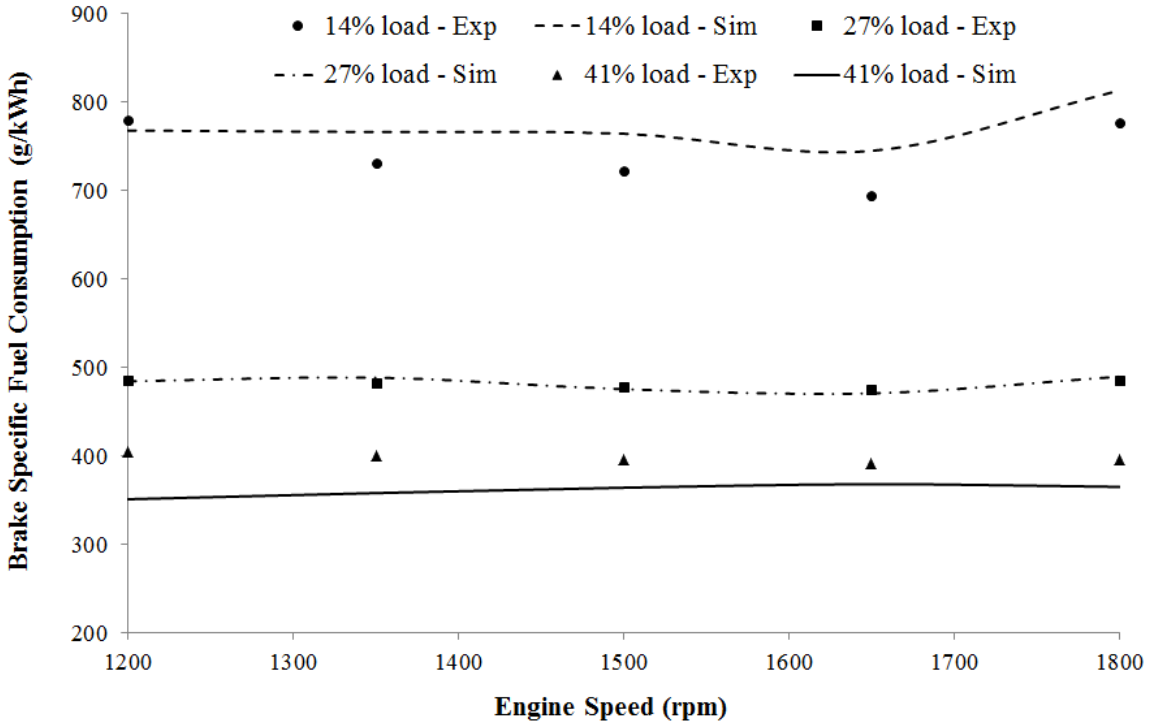

Figure 9. BSFC validation of SCS Strategy

In Fig. 9, brake specific fuel consumption validation of SCS is shown for several operating points. A good agreement provided with 4%, 0.1% and 4.5% prediction errors on average for 1, 2 and 3 bar BMEP load levels, respectively.

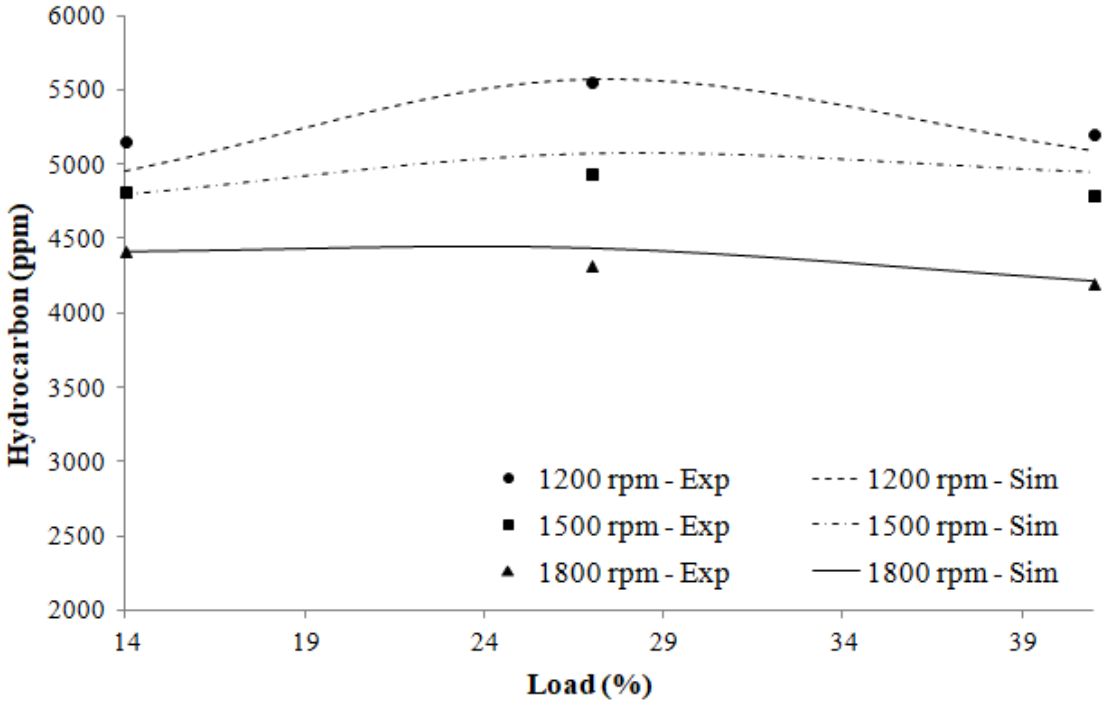

Figure 10. HC Emission validation of SCS Strategy

At 1500 rpm engine speed, hydrocarbon concentration in case of SCS operation has been verified with test bench results in 0.4%, 2.6% and 3.1% approximation for 1, 2 and 3 bar BMEP, respectively (Fig. 10). As expected, HC concentration increases in comparison to normal engine operation (Fig. 6) due to undesired lubrication oil suction to the combustion chamber as a result of excess compression stroke (between 900 CA and 1080 CA) pressure drop in skipped section of SCS operation (Fig. 1). Even though the possible reasons for HC increase could be flame quenching or unburned mixture in crevice cylinder volumes, these two possibilities have not been considered since the same piston, combustion chamber, spark plug and valve geometries are used in skip cycle engine with normal operation. Besides, a better flame development has been reported in skip cycle regime [53]. The post-flame oxidation equation (Eq.14) items and oxidation threshold temperature (600 K) are kept as constant. In order for modelling of HC increase in skip cycle engine, maximum oil film thickness is assumed as good as the radial clearance between

cylinder liner and piston surface (550 μm) at engine geometry. Model based HC emission calibration has been performed by post-flame oxidation equation (Eq.14) and oil film thickness prediction regarding experimental data for each steady-state simulation point (Table 3). As seen in Table 3, oil film becomes thicker when the minimum cylinder pressure is lower at skip cycle strategy. Furthermore, there could be seen an obvious oil film thickness difference between normal and skip cycle engine operations due to undesired oil transfer from crankcase. Even though no measurement recorded for oil consumption, it was observed that crankcase oil level lowered in time more than normal during experiments.

Table 3. Predicted maximum oil film thicknesses at 1500 rpm engine speed condition

	BMEP (bar)	P_{min} (bar)	Max. oil film thickness (μm)
Normal operation	1	0.31	2.5
	2	0.47	20
	3	0.53	16
Skip cycle operation	1	0.092	45
	2	0.075	419
	3	0.064	508

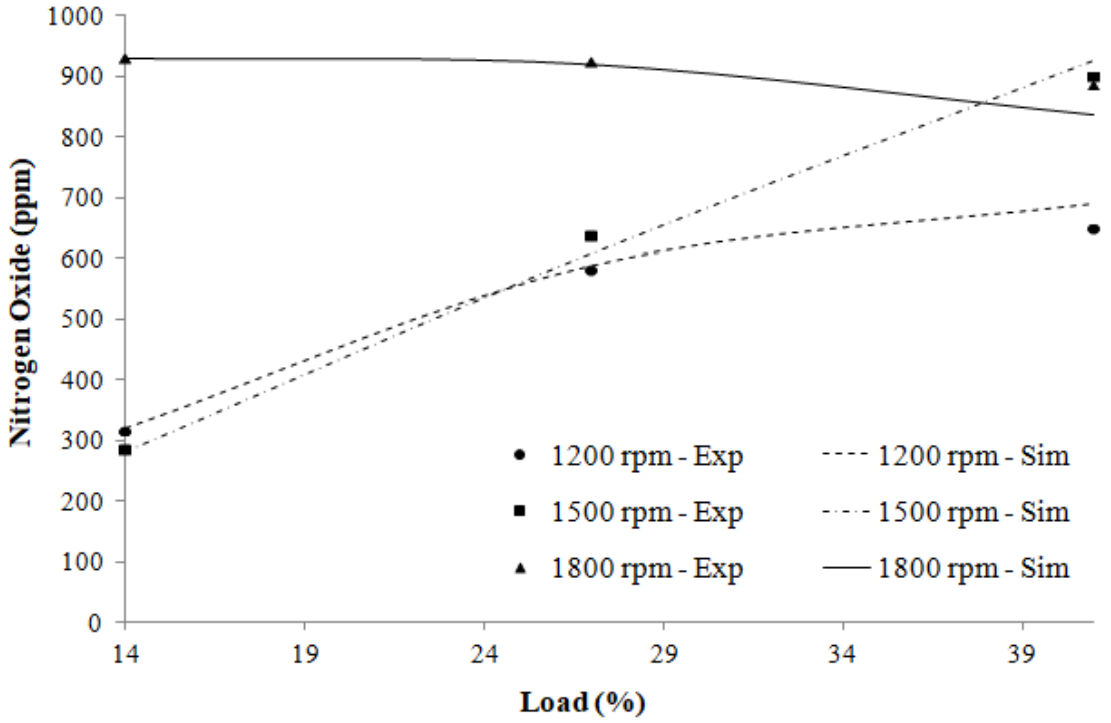

Figure 11. NO_x Emission validation of SCS Strategy

In Fig. 11, nitrogen oxide emission of SCS operation at three different speed ranges is shown. Compared to the experimental results, simulation prediction errors of NO_x are calculated as %1.4, %4.8 and %2.9 at 1500 rpm engine speed for 1, 2 and 3 bar BMEP, respectively. As expected, NOx values increase for SCS operation compared to normal engine operation (Fig. 7) due to higher cylinder pressure and temperature ranges in skip cycle engine. This difference could be evaluated by calibration of pre-exponent Arrhenius factor which is one of the main prediction parameters with burned flame temperature in semi-empirical Arrhenius Equation (Eq.13) against the experimental data. As a nitrogen molecules collision frequency, calibration of pre-exponent Arrhenius factor is a function of temperature, reaction cross-section area and relative orientation of molecules [78]. Calculated pre-exponent Arrhenius factors vary between 1.36 and 0.10 on average at 3 bar BMEP load level for normal and SCS operations, respectively.

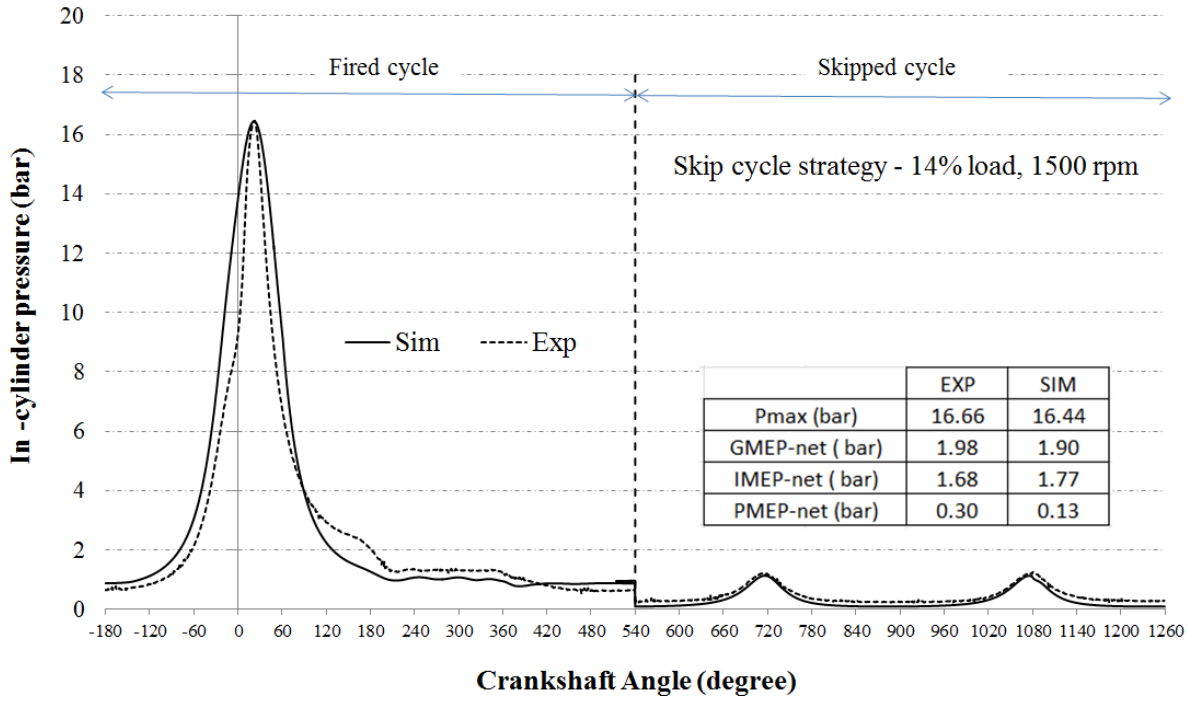

Figure 12. Validation of In-Cylinder pressure curves for SCS Strategy at 1 bar BMEP and 1500 rpm engine speed

Figure 12 shows simulation in-cylinder pressure compatibility with experimental pressure trace at 1 bar BMEP and 1500 rpm conditions. The graph shows that the maximum cylinder pressure value and timing results are very close to the experiments for an equal spark timing and power demand. Even though pressure level at compression stroke starting point (-180 CA) of the fired cycle simulation is higher than experiment one, net gross mean effective and indicated mean effective pressure values point out a good prediction with test data. Consequently, all these results indicate that the proposed mathematical model accurately predicted the indicated parameters, performance and exhaust emissions of the engine and ensured an agreeable compatibility with the experimental data of normal cycle and skip cycle operations.

3.3. Optimisation of VVT for SCS

Despite improvement in better fuel consumption, it is observed that HC and NO_x emissions are increased with SCS. This section studies a way to find a solution to decrease these pollutant emissions by adding a VVT system to the SCS. Depending on physical limitations in current skip cycle mechanism [53], a fully variable valve duration and lift adjustment is very difficult to apply. However, it is believed that retarding or advancing valve timing is sufficient to reduce pollutant emissions, hence reveal a further potential of SCS. Basically, two main valve activation strategies are investigated. First one is early intake valve opening (EIVO) strategy providing a pressure reduction at start of induction process and an increase at rapid burning angle, so that a significant decrease in NO_x emissions. The second strategy is late exhaust valve opening (LEVO) leading a prevention of oil leakage and also HC emission formation regarding with a pressure increase in skipped section of SCS (Fig. 1). Since the valve activation duration is kept fixed and used as in original engine, just intake and exhaust profiles are retarded or advanced relatively to the crankshaft revolution. In order to perform a good matching during optimum EVO and IVO timing determination and general comparison of SCS and SCS&VVT modes, parameters such as brake engine power, spark timing, throttle valve angle, brake specific fuel consumption, pre-exponent Arrhenius factor (A) for NO_x prediction and post-flame oxidation temperature for HC calculation are kept fixed for all simulated test cases.

Possible reason for rising of HC emission in SCS is undesired oil suction from crankcase to the combustion chamber due to extra low vacuum pressure occurred in SCS. Resulting from exhaust valve of fired cycle of SCS is fully closed and just a vacuum gas is remained in compression stroke (between -180 CA and 0 CA of red

curve in Fig. 13) of skip cycle strategy, in-cylinder pressure value dramatically decreases. Hence, the lubricating oil penetrates into combustion chamber more than normal amount. This causes an undesired and thicker oil film profile between liner and piston. At 3 bar BMEP and 1500 rpm SCS operation conditions, 32.8% HC emission increase has been recorded due to lower minimum cylinder pressure compared to normal engine operation (Fig. 13).

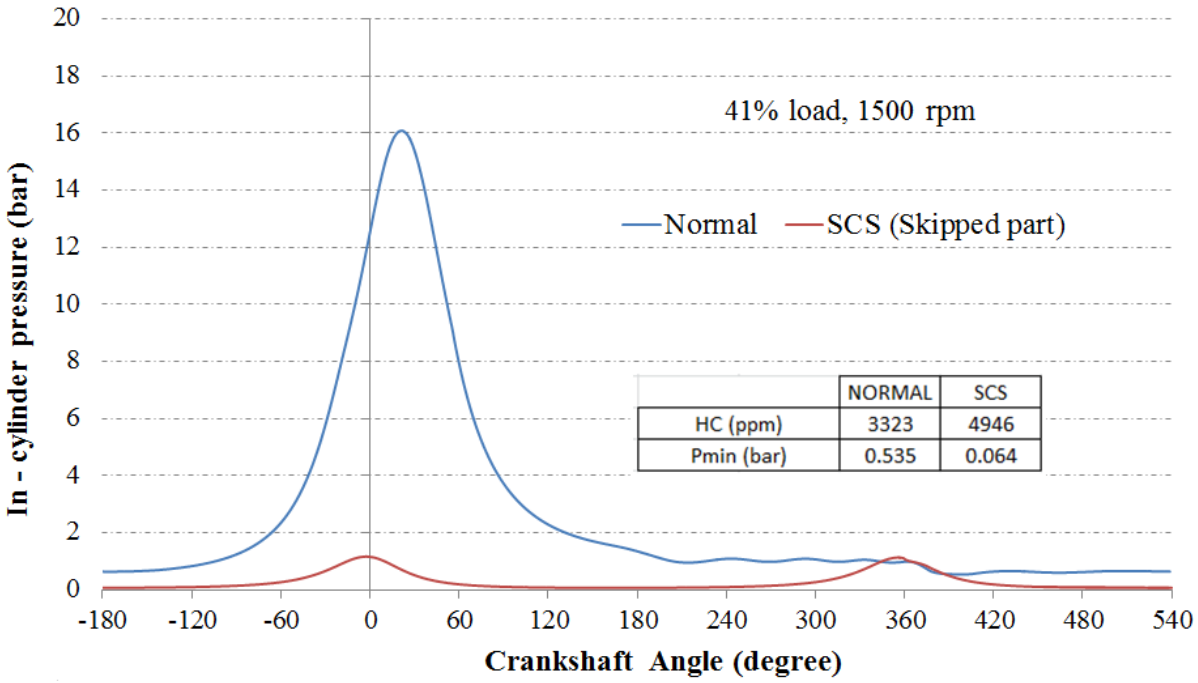

Figure 13. Reason of HC emission increase at SCS

The main reason of increasing NO_x values in SCS case links to higher temperature and pressure levels inside the cylinder due to higher amount of fresh mixture absorbed into the cylinder. As seen in Fig.14, the NOx concentration was increased by 16.9% due to peak temperature increase by 461K in SCS case compared to normal engine case.

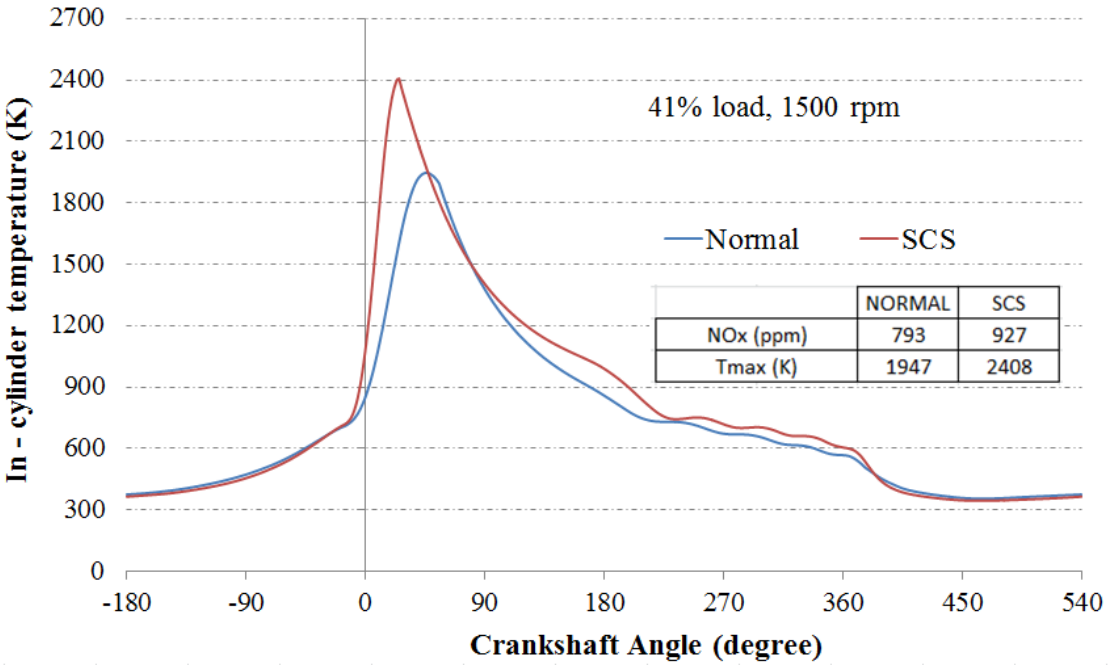

Figure 14. Reason of NO_x emission increase at SCS

A hydraulic oil pressure actuator should be adapted to engine camshaft to control the camshaft position due to the load and engine speed conditions. ECU could regulate oil pressure level to retard or advance cam phasing separately from SCS mechanism.

As indicated in SCS (skipped part) of Fig. 13, the vacuum pressure level is much lower than that of normal operation. This may causes oil leakage to combustion chamber. The pressure limit during intake process of skipped section (red curve in Fig. 13) should be kept above 0.2 bar [45] by trapping exhaust gas retarded in work production section (fired cycle-Fig. 1) of SCS in order to avoid undesired lubrication oil and HC emission. As seen in Fig. 15, minimum cylinder pressure ranges are under 0.1 bar with original exhaust valve opening timing (EVO=140 ATDC of compression) for fired cycle of SCS. This causes a significant increase in HC emissions due to undesired oil suction to the combustion chamber. In case of VVT application on fired section of SCS, when EVO is retarded 50 CA (optimised

EVO=190 ATDC) and exhaust gas trapped in skipped section of SCS and minimum cylinder pressure reaches to 0.2 bar. This also prevents undesired lubrication oil reaches into the cylinder (see Table 4).

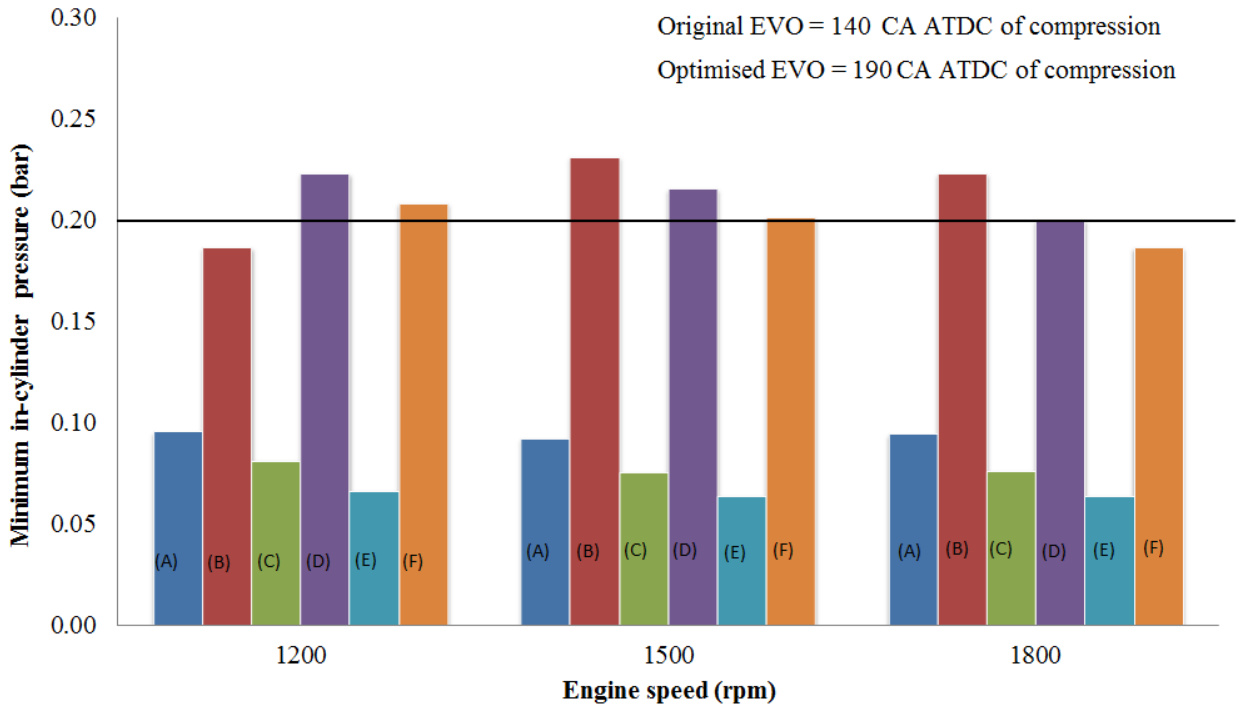

Figure 15. Effect of exhaust valve opening timing on minimum cylinder pressure at different engine conditions. (A): BMEP 1 bar – SCS, (B): BMEP 1 bar – SCS+VVT, (C): BMEP 2 bar – SCS, (D): BMEP 2 bar – SCS+VVT, (E): BMEP 3 bar – SCS, (F): BMEP 3 bar – SCS+VVT

The presence of lubricating oil in the fuel or on the walls of combustion chamber is known to result in an increase in exhaust hydrocarbon levels. Since fuel vapour concentration within the cylinder is close to the inlet manifold concentration during intake and compression, any oil film on the walls will absorb fuel vapour. During combustion, the fuel vapour concentration in the bulk gases goes essentially to zero so the absorbed fuel vapour will desorb from the liquid oil film into the gaseous combustion products. Some of the desorbed vapour fuel will mix with the high

603 temperature combustion products and oxidize. However, desorbed vapour that
604 remains in the cool boundary layer or mixes with the cooler bulk gases at late
605 expansion stroke of the cycle may escape full oxidation and contribute the unburned
606 HC emissions [1]. Experimental and numerical results showed that HC concentration
607 of skip cycle engine increases dramatically due to higher fuel vapour desorption into
608 the combustion gases compared to normal engine operation. Higher vapour
609 increases the of unburned HC emissions regarding higher possibility of non-oxized
610 gas concentration.
611
612 Table 4. Effect of EVO timing on predicted oil film thickness and skipped cycle
613 minimum cylinder pressure ranges with default IVO timing (EVO= 140 CA
614 for SCS and EVO= 190 CA for SCS&VVT)

BMEP (bar)	Speed (rpm)	P_{min} with SCS (bar)	Max. oil film thickness for SCS (μm)	HC (ppm) for SCS	P_{min} with SCS&VVT (bar)	Max. oil film thickness for SCS&VVT (μm)	HC (ppm) for SCS&VVT
1	1200	0.096	130	4954	0.187	3.1	2657
	1500	0.092	45	4795	0.231	3.1	2444
	1800	0.094	129	4436	0.223	3.1	2581
2	1200	0.081	544	5573	0.223	6	3054
	1500	0.075	419	5071	0.216	6	2997
	1800	0.076	359	4436	0.200	6	3103
3	1200	0.066	550	5092	0.208	10	2681
	1500	0.064	508	4946	0.201	10	2701

1800	0.064	432	4210	0.187	10	2801

As a result of higher cylinder pressure during skipped cycle of SCS&VVT operation in comparison to standalone SCS mode, a significant decrease in both oil film thickness on walls and unburned HC emissions could be observed (Table 4). Figure 16 and Table 4 show how HC concentration changed with just 50 CA retarding of exhaust valve opening for fired cycle.

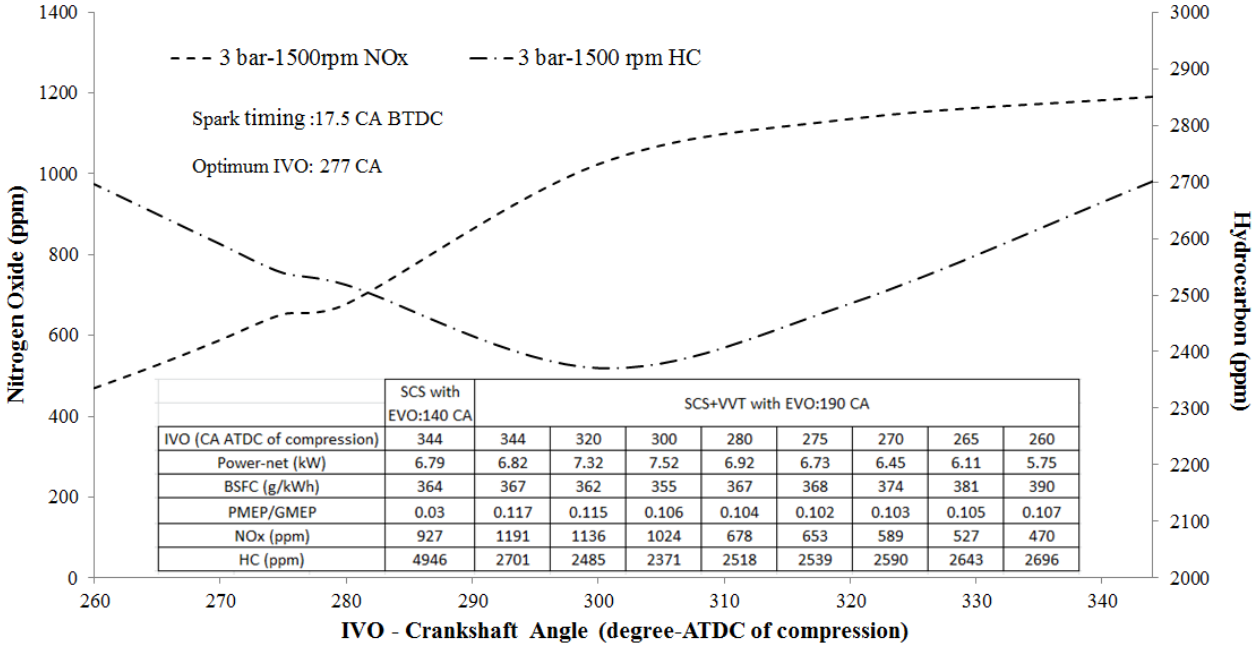

	SCS with EVO:140 CA	SCS+VVT with EVO:190 CA							
IVO (CA ATDC of compression)	344	344	320	300	280	275	270	265	260
Power-net (kW)	6.79	6.82	7.32	7.52	6.92	6.73	6.45	6.11	5.75
BSFC (g/kWh)	364	367	362	355	367	368	374	381	390
PMEP/GMEP	0.03	0.117	0.115	0.106	0.104	0.102	0.103	0.105	0.107
NOx (ppm)	927	1191	1136	1024	678	653	589	527	470
HC (ppm)	4946	2701	2485	2371	2518	2539	2590	2643	2696

Figure 16. Effect of EVO and IVO timing on exhaust emissions at 3 bar BMEP and 1500 rpm

As seen in Fig. 16, at 3 bar BMEP and 1500 rpm condition, after applying late exhaust valve opening, HC emission concentration decreases seriously (from 4946 ppm to 2701 ppm) and NO_x increases slightly due to an increase in cylinder temperature (Fig. 19: maximum temperature changes from 2408 K to 2477 K) and more favourable combustion conditions which occur as a result of more much combustion gas oxidation instead of unburned HC emissions.

By applying an advanced intake valve opening (Fig. 16: from 344 CA ATDC to 277 CA ATDC optimal timing), while nitrogen oxide emissions decrease significantly (Fig. 16: from 1191 ppm to 663 ppm due to dropped pressure at the end of intake process (Fig. 18: from 0.963 bar with SCS to 0.889 bar with EIVO), no important difference is observed at HC concentration (Fig. 16). Even if NO_x concentration decreases continuously with earlier IVO timing (from 277 CA ATDC optimal timing to 260 CA ATDC), engine power becomes insufficient for required level and also 5.6% increase could be observed in fuel consumption. One of the key parameters to determine optimal IVO timing is PMEP/GMEP ratio. Optimal IVO angles correspond to minimum pumping to gross mean effective pressure (PMEP/GMEP) ratio. In Fig. 16, it is shown that minimum PMEP/GMEP ratio occurs between 275 and 280 CA ATDC of compression.

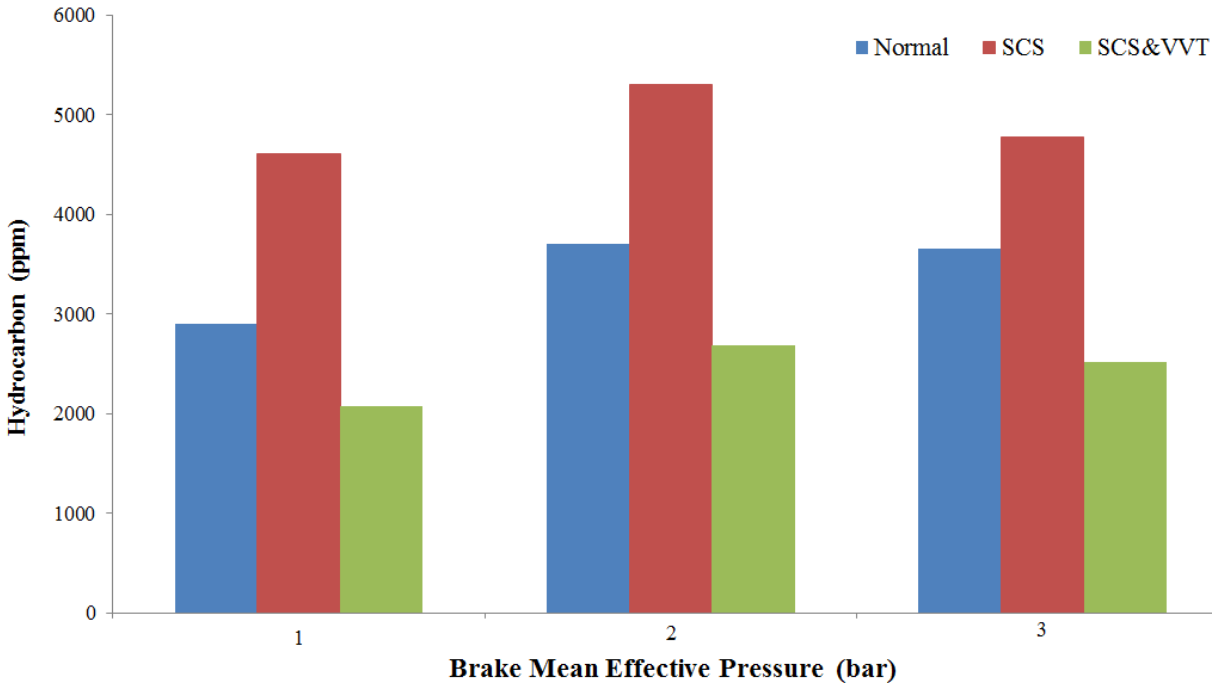

Figure 17. Hydrocarbon emission comparison via BMEP

Compared to SCS operation, it is observed that in SCS&VVT application, HC

concentration decreases by 54.9%, 49.3% and 47.4% at 1, 2 and 3 bar BMEP, respectively (Fig. 17). Increasing ratio of exhaust to inlet pressure increases the fraction of residual gases in cycle fresh charge and thus reduces flame speed and also increases the flame travel [79]. Besides, the pressure at spark timing is very indicative on burning duration (or flame travel period). When the intake valve opens 74 CA earlier (from 344 CA ATDC to 270 CA ATDC) than the original one, cylinder pressure at spark timing changes from 13.19 bar to 12.37 bar (Fig. 18). This also indicates a slower combustion process and retarded heat release curve (CA50 value changes from 12 CA ATDC to 23 CA ATDC).

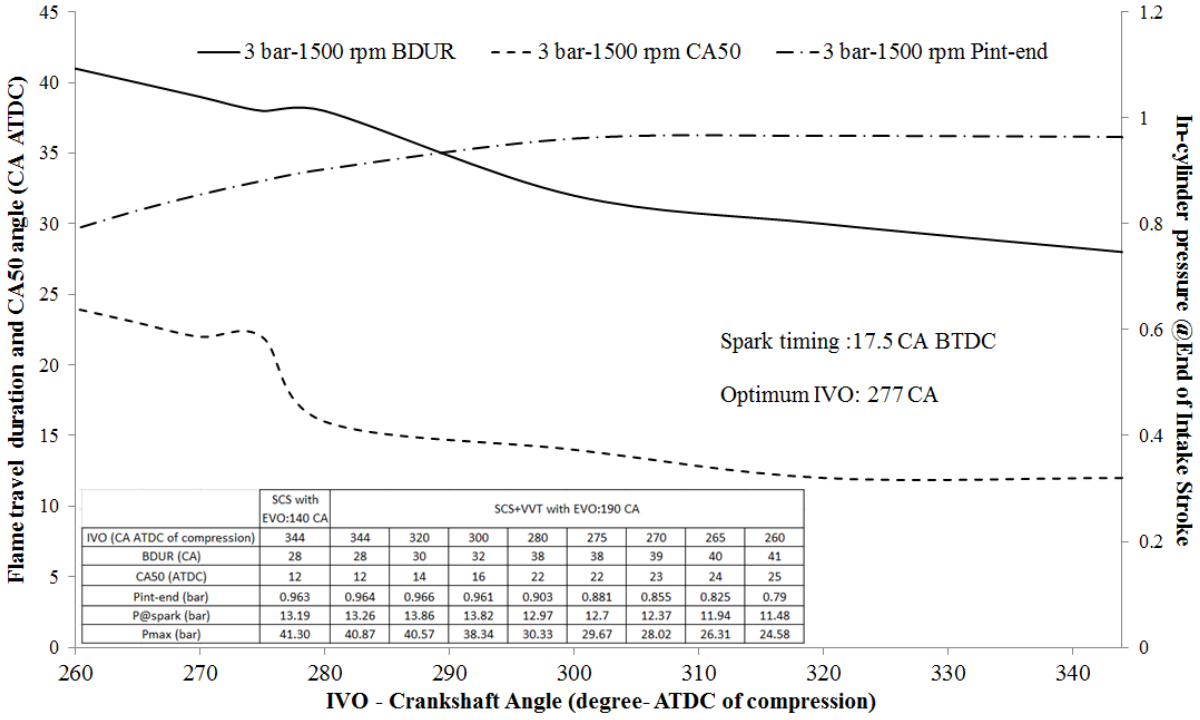

	SCS with EVO:140 CA	SCS+VVT with EVO:190 CA							
IVO (CA ATDC of compression)	344	344	320	300	280	275	270	265	260
BDUR (CA)	28	28	30	32	38	38	39	40	41
CA50 (ATDC)	12	12	14	16	22	22	23	24	25
Pint-end (bar)	0.963	0.964	0.966	0.961	0.903	0.881	0.855	0.825	0.79
P@spark (bar)	13.19	13.26	13.86	13.82	12.97	12.7	12.37	11.94	11.48
Pmax (bar)	41.30	40.87	40.57	38.34	30.33	29.67	28.02	26.31	24.58

Figure 18. Effect of IVO timing on burning angles and intake pressure level

Changes in temperature during combustion process and early part of the expansion stroke are important factors on NO_x formation mechanism (Fig. 19). After exhaust valve opening optimisation, maximum cylinder temperature varies from 2477 K to 2230 K for intake valve opening timing of 344 CA ATDC and 270 CA ATDC, respectively. Besides, maximum in-cylinder pressure decreases from 40.87 bar to

28.02 bar for the same IVO variations. As a result of both temperature and pressure levels in combustion chamber and flame travel period extension, timing of maximum pressure occurs at a further point as CA with regards to combustion top dead center. The retarding of burning duration causes a slower combustion and less NO_x emission compared to original IVO timing. When the intake valve opens 74 CA earlier (from 344 CA ATDC to 270 CA ATDC) than the original one, NO_x changes from 1191 ppm to 589 ppm (Fig. 19).

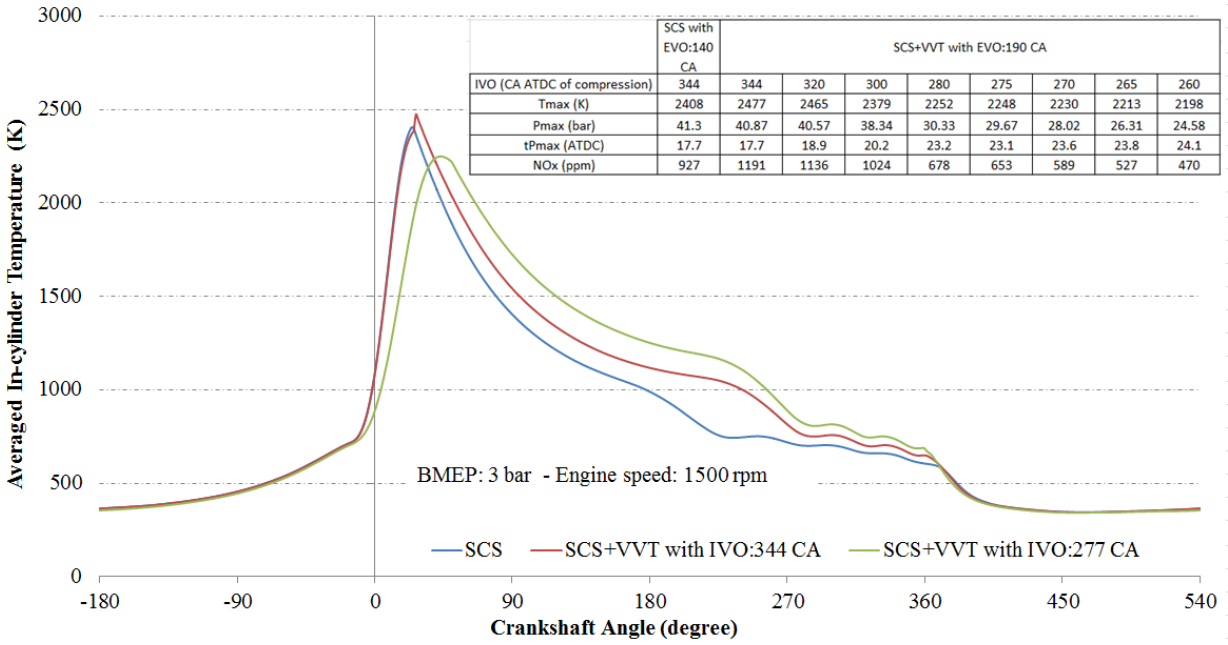

	SCS with EVO:140 CA	SCS+VVT with EVO:190 CA							
IVO (CA ATDC of compression)	344	344	320	300	280	275	270	265	260
Tmax (K)	2408	2477	2465	2379	2252	2248	2230	2213	2198
Pmax (bar)	41.3	40.87	40.57	38.34	30.33	29.67	28.02	26.31	24.58
tPmax (ATDC)	17.7	17.7	18.9	20.2	23.2	23.1	23.6	23.8	24.1
NOx (ppm)	927	1191	1136	1024	678	653	589	527	470

Figure 19. Effect of IVO timing on combustion and early expansion temperature and pressure

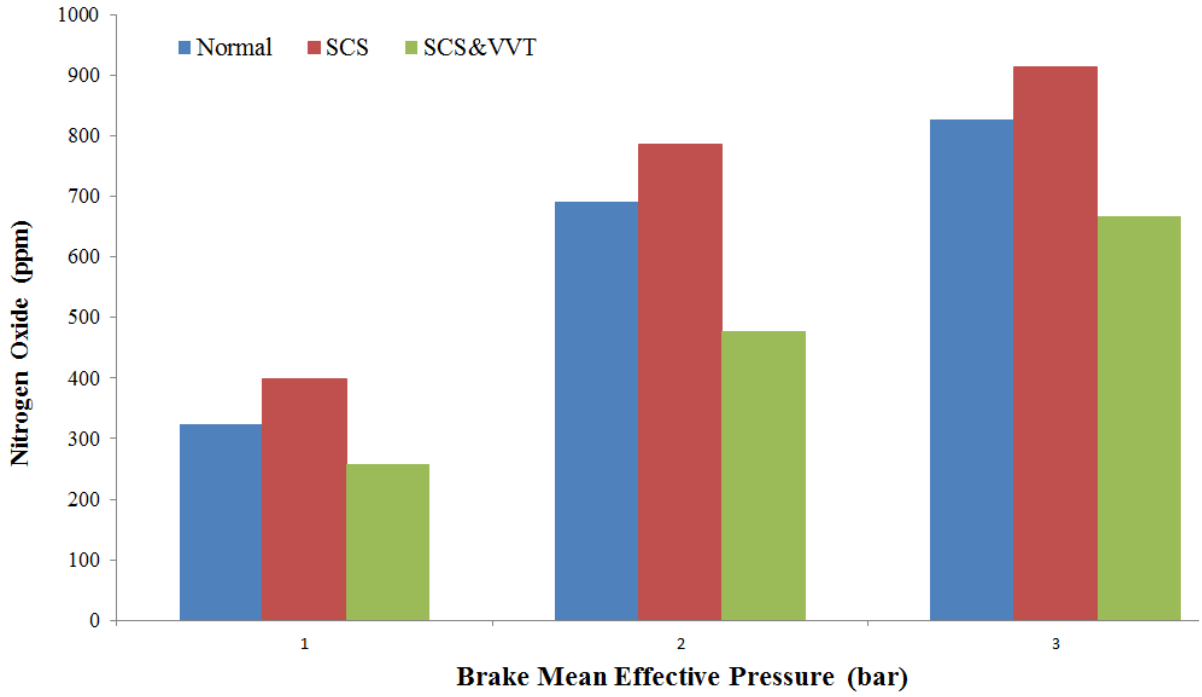

Figure 20. Nitrogen oxide emission comparison via BMEP

Compared to SCS operation, it is observed that in SCS&VVT application, NO_x concentration decreases by 35.1%, 39.4% and 26.8% at 1, 2 and 3 bar BMEP, respectively (Fig. 20). Figure 21 shows a comparison of normal, SCS and SCS&VVT engine operation at low in-cylinder pressure indicating region. The reason of increase in PMEP/GMEP ratio in SCS&VVT is net pumping pressure loss due to late exhaust valve opening as indicated in Fig. 21. The exhaust valve opens after expansion when the piston reaches the bottom dead center (BDC). Hence, the expected pressure drop in SCS&VVT occurs later than in SCS. The characteristic pressure curve of SCS&VVT (green curve in Fig. 21) shows a different pressure trace which causes an additional pumping loss. However, this could not causes an important fuel consumption increase in comparison to SCS operation.

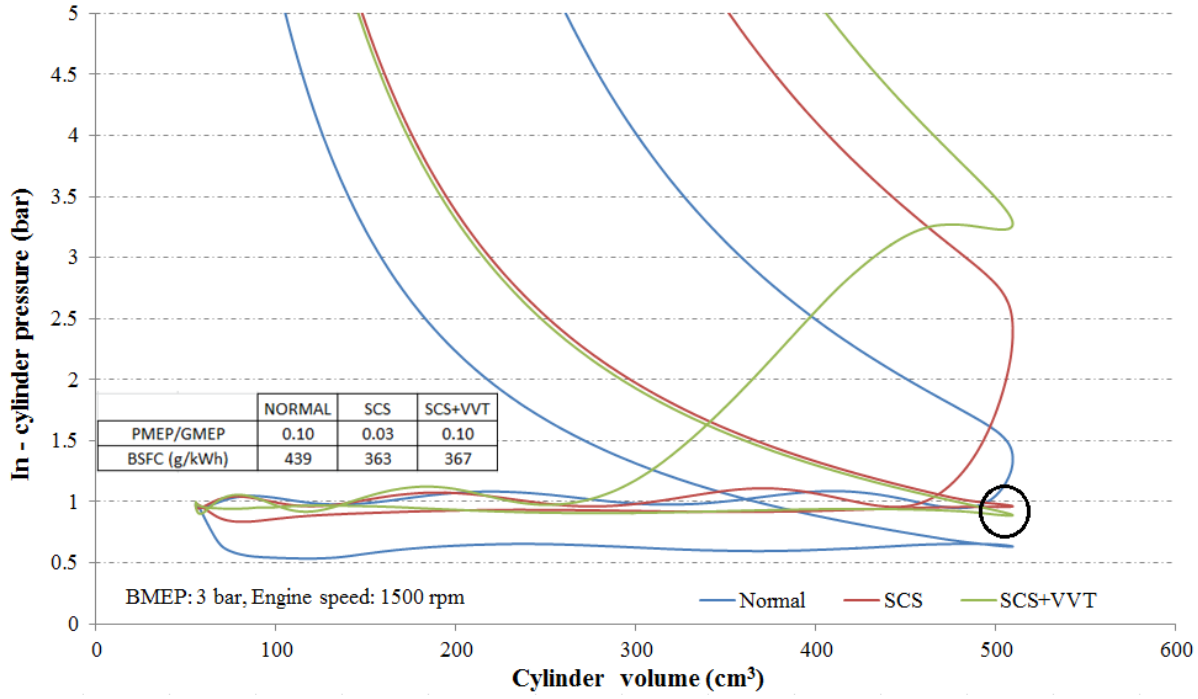

686

687 Figure 21. Low pressure indicating comparison of different engine strategies

688 The other difference between the low pressure indication curves of SCS and
689 SCS&VVT is IVO timing. Because of earlier intake valve opening in SCS&VVT than
690 SCS, in-cylinder pressure drops a little at the end of induction process. This pressure
691 decrease is the key factor of NO_x emission improvement as described before.
692 Furthermore, PMEP/GMEP ratio increases at lower load conditions. As a result of
693 optimisation, intake valve opens earlier at 1 bar BMEP (271 ATDC of compression) in
694 comparison to 3 bar BMEP (280 ATDC of compression).

695

696 Figure 22 shows a comparison of normal, SCS and SCS&VVT engine operation at
697 high in-cylinder pressure indicating region. It is seen that maximum pressure range is
698 higher in fired cycle of SCS compared to normal engine operation due to much more
699 fresh charge taken into the combustion chamber. However, maximum cylinder
700 pressure level is again decreased by early IVO action and expanded burning duration
701 in SCS&VVT. Maximum cylinder pressure values are predicted as 16.08 bar, 41.30

bar and 29.95 bar for normal, SCS and SCS&VVT operations, respectively. Due to the expansion of combustion period in SCS&VVT, gross mean effective pressure (GMEP) is higher than in SCS. Gross mean effective pressure ranges of fired cycles are 4.07 bar, 7.79 bar and 8.37 bar for normal, SCS and SCS&VVT, respectively.

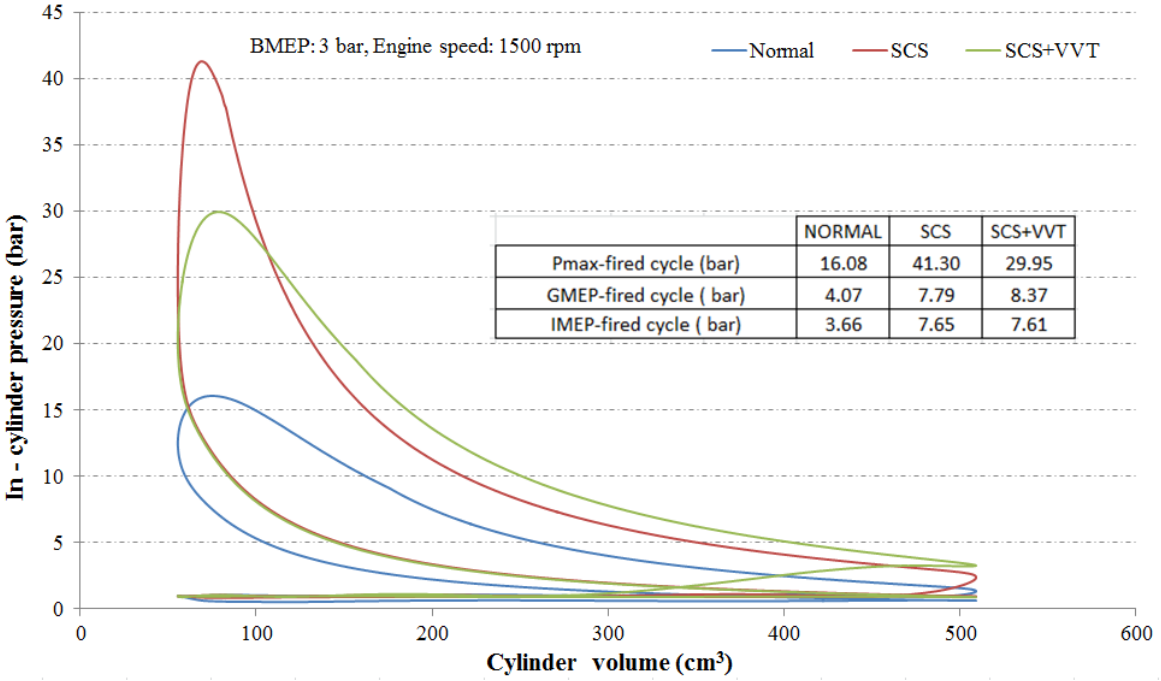

Figure 22. High pressure indicating comparison of different engine strategies

4. Conclusion

Skip cycle strategy allows a decrease in fuel consumption of gasoline engines through reduced pumping losses at low load engine conditions such as in-city driving or heavy traffic cases. In this study, a detailed numerical investigation has been carried out to investigate the benefits of SCS in achieving lower fuel consumption compared to normal cycle and combination of SCS with variable valve timing strategy in achieving lower exhaust emissions compared to standalone SCS under part-load conditions. Two different variable valve timing strategies were analysed. The numerical computation employed a one-dimensional gas dynamics model based on

718 mean value model approach, Net Power Cycle definition, time dependent fluid
719 governing equations and separated two-zones gas approach for a four-cylinder,
720 water-cooled and port fuel-injected SI engine. The simulations performed at steady
721 state at low load (BMEP: 1-2-3 bar) and low engine speed (1200–1350-1500-1650-
722 1800 rpm) ranges. After numerical spark timing optimisation and validation process of
723 both normal and SCS operations with experimental results, valve timing strategies
724 were integrated into the validated skip cycle engine model. The major findings are
725 summarised as follows:
726 1. As a result of numerical ignition timing optimisation regarding 2-level full factorial
727 experiment design, the spark advance varies from 24.5 CA to 20.7 CA for 1 bar and 2
728 bar BMEP load levels, respectively for normal engine operation at 1500 rpm. At same
729 engine speed, spark advance varies from 18.0 CA to 17.2 CA for 1 bar and 2 bar
730 BMEP load levels, respectively for skip cycle strategy.
731 2. In case of SCS and EIVO (early intake valve opening) application together and
732 valve timing optimisation, NO_x concentration was reduced by 35.1%, 39.4%, 26.8%
733 on average for BMEP load levels of 1, 2 and 3 bar respectively at all engine speed
734 ranges between 1200 and 1800 rpm compared to SCS operation. Early intake valve
735 opening optimisation provided a pressure drop at the end of intake stroke and thus a
736 burning duration expansion and slower combustion process resulting a decrease in
737 cylinder pressure and average temperature and also NO_x emission.
738 3. Late exhaust valve opening (LEVO) decreased HC emission for 54.9%, 49.3% and
739 47.4% on average for BMEP load levels of 1, 2 and 3 bar respectively at all among
740 engine speed ranges between 1200 and 1800 rpm compared to SCS operation. Late
741 exhaust valve timing optimisation provided the minimum in-cylinder pressure level of
742 skipped cycle section of SCS above 0.2 bar in order to prevent undesired lubrication

oil suction to the combustion chamber and also HC production.

4. The addition of variable valve timing strategies to the skip cycle was not led to additional brake specific fuel consumption (BSFC).

Acknowledgments

The first author wishes to thank TUBITAK (Scientific and Technological Research Council of Turkey) 2219 Postdoctoral Research Scholarship Programme for financial support. The authors acknowledge Assistant Professor Doctor Osman Akin Kutlar from Istanbul Technical University for providing experimental data for numerical validation and optimisation.

Nomenclature

SCS	skip cycle strategy	ATDC	after top dead center
NO_x	nitrogen oxide emission	BTDC	before top dead center
HC	unburned hydrocarbon emission	CA50	location of 50% mass fuel burned
N	normal cycle	BDUR	burning duration
S	skipped cycle	ppm	particles per million
F	fired cycle	P_{max}	maximum cylinder pressure
SI	spark ignition	P_{min}	minimum cylinder pressure
MBT	maximum brake torque	cm^3	cubic centimeter
AFR	air-fuel ratio	V	cylinder volume
BSFC	brake specific fuel consumption	K	kelvin
BMEP	brake mean effective pressure	RDE	real driving emission
IMEP	indicated mean effective pressure	CEVC	camless engine valve control
GMEP	gross mean effective pressure	VVT	variable valve timing
PMEP	pumping mean effective pressure	VVL	variable valve lifting
rpm	revolution per minute	EIVO	early intake valve opening
CA	crankshaft angle	LEVO	late exhaust valve opening
TDC	top dead center	DoE	design of experiment

References

[1] Heywood JB. Internal combustion engine fundamentals. USA: Mc Graw-Hill, ISBN 978-0070286375; 1988.

[2] Richard S. Introduction to internal combustion engines. UK: MacMillan, ISBN 978-0230576636; 1999.

[3] Kutlar OA, Arslan H, Calik AT. Methods to improve efficiency of four stroke spark ignition engines at part load. Energy Convers. Manage 2005; 46: 3202-3220. doi.org/10.1016/j.enconman.2005.03.008.

[4] European Commission. Real-driving emissions regulation for passenger and commercial vehicles, https://ec.europa.eu/info/law/better-regulation/initiatives/ares-2016-6339064_en/ [accessed 01 February 2018].

[5] Kutlar OA, Arslan H. Alternative Ignition Systems. In Lackner M. (Ed.). Skip-cycle system for combustion engines (63-84). Verlag ProcessEng Engineering GmbH, ISBN 978-3-902655-05-9; 2009.

[6] Ashok B, Ashok SD, Kumar CR. A review on control system architecture of a SI engine management system. Annual Reviews in Control 2016; 41: 94-118, doi:10.1016/j.arcontrol.2016.04.005.

[7] Liu K, Yang J, Jiang W, Li Y et al. Effect of asynchronous valve timing on combustion characteristic and performance of a high speed SI marine engine with five valves. Energy Convers. Manage 2016; 123: 185-199. doi.org/10.1016/j.enconman.2016.06.042.

[8] Atashkari K, Nariman-Zadeh N, Gölcü M, Khalkhali A et al. Modelling and multi-objective optimization of a variable valve-timing spark-ignition engine using

817 polynomial neural networks and evolutionary algorithms. Energy Convers.
818 Manage 2007; 48: 1029-1041. doi.org/10.1016/j.enconman.2006.07.007.
819 [9] Sher E, Bar-Kohany T. Optimization of variable valve timing for maximizing
820 performance of an unthrottled SI engine-a theoretical study. Energy 2002; 27: 757–
821 775. doi.org/10.1016/S0360-5442(02)00022-1.
822 [10] De Simio L, Gambino M, Iannaccone S, Borrelli L, Gimelli A, Muccillo M.
823 Experimental analysis of a natural gas fueled engine and 1-D simulation of VVT and
824 VVA strategies. SAE technical paper 2013-24-0111; 2013. doi.org/10.4271/2013-24-
825 0111.
826 [11] Gimelli A, Muccillo M, Pennacchia O. Study of a new mechanical variable valve
827 actuation system: Part II - estimation of the actual fuel consumption improvement
828 through one-dimensional fluid dynamic analysis and valve train friction estimation. Int
829 J Eng Res 2015; 16: 762-772. doi.org/10.1177/1468087415604095.
830 [12] Dalla Nora M, Lanzanova TDM, Zhao H. Effects of valve timing, valve lift and
831 exhaust backpressure on performance and gas exchanging of a two-stroke GDI
832 engine with overhead valves. Energy Convers. Manage 2016; 123: 71-83.
833 doi.org/10.1016/j.enconman.2016.05.059.
834 [13] Bonatesta F, Altamore G, Kalsi J, Cary M. Fuel economy analysis of part-load
835 variable camshaft timing strategies in two modern small-capacity spark ignition
836 engines. Appl. Energy 2016; 164: 475-491. doi.org/10.1016/j.apenergy.2015.11.057.
837 [14] Kakaee AH, Mashadi B, Ghajar M. A novel volumetric efficiency model for spark
838 ignition engines equipped with variable valve timing and variable valve lift Part 1:
839 model development. Journal of Automotive Engineering 2017; 231(2): 175-191.
840 doi.org/10.1177/0954407016650545.

[15] Li Y, Khajepour A, Devaud C, Liu K. Power and fuel economy optimizations of gasoline engines using hydraulic variable valve actuation system. Appl. Energy 2017; 206: 577-593. doi.org/10.1016/j.apenergy.2017.08.208.

[16] Venkatesh D, Selvakumar A. A novel design of pneumatic actuator for camless engines. SAE Technical Paper 2016-01-0099; 2016. doi.org/10.4271/2016-01-0099.

[17] Nam K, Choi SB. Development of a camless engine valve actuator system for robust engine valve timing control. Int. J. Veh. Syst. Model. Test 2012; 7.4: 372-389. doi.org/10.1504/IJVSMT.2012.049429.

[18] Mohamed E. Modeling and performance evaluation of an electromechanical valve actuator for a camless IC engine. Int. J. Energy Environ 2012; 3.2: 275-94.

[19] Rioli M, Pivetti G, Ross J, Pietroni A. Pneumatic system for controlling the valves of an internal combustion engine. U.S. Patent No 8,424,499; 2013.

[20] Hoglund A, Carlson U, Von Koenigsegg C. Combustion engine and gas handling system for pneumatic operation of a valve actuator. U.S. Patent Application No 15/025,436; 2016.

[21] Carlson U, Höglund A, Von Koenigsegg C. Internal combustion engine for a vehicle comprising at least one compressor cylinder at least one compressor cylinder connected to a compressed-air tank. U.S. Patent No 8,800,510; 2014.

[22] Rodrigues F, Fernando A, Moreira T et al. E25 stratified torch ignition engine performance, CO_2 emission and combustion analysis. Energy Convers. Manage 2016; 115: 299-307. doi.org/10.1016/j.enconman.2016.02.052.

[23] Zhang B, Ji C, Wang S. Investigation on the lean combustion performance of a hydrogen-enriched n-butanol engine. Energy Convers. Manage 2017; 136: 36-43. doi.org/10.1016/j.enconman.2016.12.065.

865 [24] Melaika M, Dahlander P. Experimental investigation of methane direct injection
866 with stratified charge combustion in optical SI single cylinder engine. SAE technical
867 paper 2016-01-0797; 2016. doi.org/10.4271/2016-01-0797.
868 [25] Amrouche F, Erickson Paul A, Varnhagen S, Park Jae W. An experimental
869 study of a hydrogen-enriched ethanol fueled Wankel rotary engine at ultra lean and
870 full load conditions. Energy Convers. Manage 2016; 123: 174-184.
871 doi.org/10.1016/j.enconman.2016.06.034.
872 [26] Niu R, Yu X, Du Y, Xie H et al. Effect of hydrogen proportion on lean burn
873 performance of a dual fuel SI engine using hydrogen direct-injection. Fuel 2016; 186:
874 792-799. doi.org/10.1016/j.fuel.2016.09.021.
875 [27] Li T, Gao Y, Wang J, Chen Z. The Miller cycle effects on improvement of fuel
876 economy in a highly boosted, high compression ratio, direct-injection gasoline engine
877 Energy Convers. Manage 2014; 79: 59-65. doi.org/10.1016/j.enconman.2013.12.022.
878 [28] Fraser N, Blaxill H, Lumsden G, Bassett M. Challenges for increased efficiency
879 through gasoline engine downsizing. SAE Int J Eng 2009; 2.2009-01-1053: 991-1008.
880 doi.org/10.4271/2009-01-1053.
881 [29] Tang Q, Fu J, Liu J et al. Comparison and analysis of the effects of various
882 improved turbocharging approaches on gasoline engine transient performances. Appl.
883 Therm. Eng 2016; 93:797-812. doi.org/10.1016/j.applthermaleng.2015.09.063.
884 [30] Li T, Zheng B, Yin T. Fuel conversion efficiency improvements in a highly
885 boosted spark-ignition engine with ultra-expansion cycle. Energy Convers. Manage
886 2015; 103:448-58. doi.org/10.1016/j.enconman.2015.06.078.
887 [31] Li T, Wang B, Zheng B. A comparison between Miller and five-stroke cycles for
888 enabling deeply downsized, highly boosted, SI engines with ultra expansion. Energy
889 Convers. Manage 2016; 123:140-52. doi.org/10.1016/j.enconman.2016.06.038.

890 [32] Arroyo J, Moreno F, Muñoz M, Monné C. Experimental study of ignition timing
891 and supercharging effects on a gasoline engine fueled with synthetic gases extracted
892 from biogas. Energy Conversion Management 2015 June; 97: pp. 196-211.
893 doi.org/10.1016/j.enconman.2015.03.061.
894 [33] Isenstadt A, German J, Dorobantu M. Naturally aspirated gasoline engines and
895 cylinder deactivation. International Council on Clean Transportation Working Paper
896 2016; 12:2016.
897 [34] Yu S, Ma X, Ma Z, Liu R et al. Experimental and Simulated study on the cylinder
898 deactivation of vehicle gasoline engine. In: Society of Automotive Engineers (SAE)-
899 China Congress 2016; pp. 207-215. doi.org/10.1007/978-981-10-3527-2_19.
900 [35] Hamid I, Said MFM, Soid SNM, Nasution H. Effect of cylinder deactivation
901 strategies on engine performances using one-dimensional simulation
902 technique. Jurnal teknologi 2016; 78(8-4): 49-55. doi.org/10.11113/jt.v78.9584.
903 [36] Zainal Abidin SF, Mohd Farid MS, Azhar AA, Mohd AA, and N. I. Arishad.
904 Investigation of performance and fuel economy for cylinder deactivation engine at
905 part load operation. Applied Mechanics and Materials 2016; 819: 443-448.
906 doi.org/10.4028/www.scientific.net/AMM.819.443.
907 [37] Richardson ES, Soriano BS, Middleton M, Gill M. Efficiency benefits of flexible
908 cylinder deactivation using a novel intake valve system. In: SAE Powertrains, Fuels
909 and Lubricants 2017; 9 pp.
910 [38] Wilcutts M, Switkes J, Shost M, Tripathi A. Design and benefits of dynamic skip
911 fire strategies for cylinder deactivated engines. SAE Int. J. Engines 2013; 6(2013-01-
912 0359): 278-288. doi.org/10.4271/2013-01-0359.

913 [39] Eisazadeh-Far K, Younkins M. Fuel economy gains through dynamic-skip-fire in
914 SI engines. SAE Technical Paper 2016-01-0672; 2016. doi.org/10.4271/2016-01-
915 0672.
916 [40] Yuksek L, Ozener O, Sandalci T. Cycle-skipping strategies for pumping loss
917 reduction in spark ignition engines: An experimental approach. Energy Convers.
918 Manage 2012; 64: 320-327. doi.org/10.1016/j.enconman.2012.05.025.
919 [41] Wang S, Ji C, Zhang B. Effects of hydrogen addition and cylinder cut-off on
920 combustion and emissions performance of a spark-ignited gasoline engine under a
921 low operating condition. Energy 2010; 35: 4754-4760.
922 doi.org/10.1016/j.energy.2010.09.015.
923 [42] Bech A, Shayler PJ, McGhee M. The effects of cylinder deactivation on the
924 thermal behaviour and performance of a three cylinder spark ignition engine. SAE Int.
925 J. Engines 2016; 9(2016-01-2160): 1999-2009. doi.org/10.4271/2016-01-2160.
926 [43] Kutlar OA, Arslan H, Calik AT. Skip cycle system for spark ignition engines: an
927 experimental investigation of a new type working strategy. Energy Convers. Manage
928 2007; 48: 370-379. doi.org/10.1016/j.enconman.2006.07.004.
929 [44] Saunders RJ, Abdul-Wahab EA. Variable valve closure timing for load control
930 and the Otto Atkinson cycle engine. SAE Technical paper 890677; 1989.
931 doi.org/10.4271/890677.
932 [45] Boggs DL, Hilbert HS, Schechter MM. The Otto–Atkinson cycle engine-fuel
933 economy and emissions results and hardware design. SAE Technical paper 950089;
934 1995. doi.org/10.4271/950089.
935 [46] Goto T, Hatamura K, Takizawa S, Hayama N, et al. Development of V6 Miller
936 cycle gasoline engine. SAE Technical paper 940198; 1994. doi.org/10.4271/940198.

[47] Millo F, Mirzaeian M, Luisi S, Doria V et al. Engine displacement modularity for enhancing automotive si engines efficiency at part load. Fuel 2016; 180: 645-652. doi.org/10.1016/j.fuel.2016.04.049.

[48] Kuruppu C, Pesiridis A, Rajoo S. Investigation of cylinder deactivation and variable valve actuation on gasoline engine performance. SAE Technical paper 2014-01-1170; 2014. doi.org/10.4271/2014-01-1170.

[49] Stokes J, Lake TH, Osborne RJ. A gasoline engine concept for improved fuel economy-The Lean Boost system. SAE Technical paper 2000-01-2902; 2000. doi.org/10.4271/2000-01-2902.

[50] Lecointe B, Monnier G. Downsizing a gasoline engine using turbocharging with direct injection. SAE Technical paper 2003-01-0542; 2003. doi.org/10.4271/2003-01-0542.

[51] Salber W, Wolters P, Esch T, Geiger J, Dilthey J. Synergies of variable valve actuating and direct injection. SAE Technical paper 2002-01-0706; 2002. doi.org/10.4271/2002-01-0706.

[52] Hu M, Chang S, Liu L, Xu Y, Xu J. Design and analysis of skip fire valve strategies based on electromagnetic valve train. Appl. Therm. Eng. 2018; 129: 833-840. doi.org/10.1016/j.applthermaleng.2017.10.099.

[53] Baykara C, Kutlar OA, Dogru B, Arslan H. Skip cycle method with a valve-control mechanism for spark ignition engines. Energy Convers. Manage 2017; 146: 134-146. doi.org/10.1016/j.enconman.2017.05.016.

[54] Feng R, Yang J, Zhang D, Deng B, et al. Experimental study on SI engine fuelled with butanol–gasoline blend and H_2O addition. Energy Convers. Manage 2013; 74: 192-200. doi.org/10.1016/j.enconman.2013.05.021.

961 [55] Koç M, Sekmen Y, Topgül T, Yücesu HS. The effects of ethanol-
962 unleaded gasoline blends on engine performance and exhaust emissions in
963 a spark-ignition engine. Renewable Energy 2009; 34(10): 2101-2106.
964 doi.org/10.1016/j.renene.2009.01.018.
965 [56] Cho HM, He BQ. Spark ignition natural gas engines-A review. Energy Convers.
966 Manage 2007; 48(2): 608-618. doi.org/10.1016/j.enconman.2006.05.023.
967 [57] Korakianitis T, Namasivayam AM, Crookes RJ. Natural-gas fueled spark-ignition
968 (SI) and compression-ignition (CI) engine performance and emissions. Prog. Energy
969 Combust. Sci. 2011; 37(1): 89-112. doi.org/10.1016/j.pecs.2010.04.002.
970 [58] Roberts SCE, Mathews RD. Development of an improved ring pack model for
971 hydrocarbon emissions studies. SAE Technical paper 961966; 1996.
972 doi.org/10.4271/961966.
973 [59] Fox JW, Min KD, Cheng WK, Heywood JB. Mixture preparation in a SI engine
974 with port fuel injection during starting and warm-up. SAE Technical paper 922170;
975 1992. doi.org/10.4271/922170.
976 [60] Henning CF, Giles JB. Fuel injection strategies to minimize cold-start HC
977 emissions. SAE Technical paper 970040; 1997. doi.org/10.4271/970040.
978 [61] Cerit M, Ayhan V, Parlak A, Yasar H. Thermal analysis of a partially ceramic
979 coated piston: Effect on cold start HC emission in a spark ignition engine. Appl.
980 Therm. Eng. 2011; 31(2-3): 336-341. doi.org/10.1016/j.applthermaleng.2010.09.015.
981 [62] Rakopoulos DC, Rakopoulos CD, Kakaras EC, Giakoumis EG. Effects of
982 ethanol–diesel fuel blends on the performance and exhaust emissions of heavy duty
983 DI diesel engine. Energy Convers. Manage 2008; 49(11): 3155-3162.
984 doi.org/10.1016/j.enconman.2008.05.023.
985 [63] Cheng WK, Hamrin D, Heywood JB, Hochgreb S et al. An overview of

986 hydrocarbon emissions mechanisms in spark-ignition engines. SAE Technical paper
987 932708; 1993. doi.org/10.4271/932708.
988 [64] Ozcan H, Yamin JA. Performance and emission characteristics of LPG powered
989 four stroke SI engine under variable stroke length and compression ratio. Energy
990 Convers. Manage 2008; 49(5): 1193-1201. doi.org/10.1016/j.enconman.2007.09.004.
991 [65] Al-Baghdadi MAS, Al-Janabi HAS. A prediction study of a spark ignition
992 supercharged hydrogen engine. Energy Convers. Manage 2003; 44(20): 3143-3150.
993 doi.org/10.1016/S0196-8904(03)00127-4.
994 [66] Boam DJ, Clark TA, Hobbs KE. The influence of fuel management on unburnt
995 hydrocarbon emissions during the ECE 15 and US FTP drive cycles. SAE Technical
996 paper 950930; 1995. doi.org/10.4271/950930.
997 [67] Guzzella L, Christopher O. Introduction to Modeling and Control of Internal
998 Combustion Engine Systems. Springer-Verlag Berlin Heidelberg, ISBN 978-3-642-
999 10774-0; 2010.
1000 [68] Benedict RP. Fundamentals of pipe flow. USA:Wiley, ISBN 0-471-03375-8; 1980.
1001 [69] Felsch, C., Sloane, T., Han, J., Barths, H. et al., “Numerical Investigation of
1002 Recompression and Fuel Reforming in a SIDI-HCCI Engine,” SAE Technical Paper
1003 2007-01-1878, 2007, doi:10.4271/2007-01-1878.
1004 [70] GT-Power Gamma Technologies Program Help, Version 2012 7.1.
1005 [71] Ricardo Wave User Manual, Version 2016.1.
1006 [72] Abu-Zaid M. Performance of single cylinder, direct injection diesel engine using
1007 water fuel emulsions. Energy Convers. Manage 2004; 45(5): 697-705.
1008 doi.org/10.1016/S0196-8904(03)00179-1.
1009 [73] Dogru B. Skip cycle method investigation at part load conditions of spark ignition
1010 engines. Istanbul Technical University. PhD Thesis; 2015. [in Turkish]

1011 [74] Harada J, Tomita T, Mizuno H, Mashiki Z, et al. Development of direct injection
1012 gasoline engine. SAE Technical Paper No. 970540; 1997. doi.org/10.4271/970540.
1013 [75] Zhao FQ, Lai MC, Harrington DL. The spray characteristics of automotive port
1014 fuel injection-A critical reviews. SAE Technical Paper No. 950506; 1995.
1015 doi.org/10.4271/950506
1016 [76] Ganesan V. Internal combustion engines. India: McGraw Hill Education Pvt Ltd,
1017 ISBN 978-1-25-900619-7; 2012.
1018 [77] Isermann R. Engine modeling and control. Berlin: Springers Berlin Heidelberg,
1019 ISBN 978-3-642-39933-6; 2014.
1020 [78] Chang R. Physical chemistry for the biosciences. USA: University Science Books,
1021 ISBN 1-891389-33-5; 2005.
1022 [79] Taylor CF. The Internal-combustion Engine in Theory and Practice: Combustion,
1023 fuels, materials, design (Vol. 2). USA: MIT press, ISBN-13 978-0-262-20052-3; 1985.